

8-1-2022

## Dissolution and Electrochemical Recovery of UO<sub>2</sub>, UO<sub>3</sub>, and U<sub>3</sub>O<sub>8</sub> in Ionic Liquids

Katherine Iolani Thornock Luebke

Follow this and additional works at: <https://digitalscholarship.unlv.edu/thesesdissertations>



Part of the [Analytical Chemistry Commons](#), and the [Inorganic Chemistry Commons](#)

---

### Repository Citation

Luebke, Katherine Iolani Thornock, "Dissolution and Electrochemical Recovery of UO<sub>2</sub>, UO<sub>3</sub>, and U<sub>3</sub>O<sub>8</sub> in Ionic Liquids" (2022). *UNLV Theses, Dissertations, Professional Papers, and Capstones*. 4515.  
<http://dx.doi.org/10.34917/33690289>

This Dissertation is protected by copyright and/or related rights. It has been brought to you by Digital Scholarship@UNLV with permission from the rights-holder(s). You are free to use this Dissertation in any way that is permitted by the copyright and related rights legislation that applies to your use. For other uses you need to obtain permission from the rights-holder(s) directly, unless additional rights are indicated by a Creative Commons license in the record and/or on the work itself.

This Dissertation has been accepted for inclusion in UNLV Theses, Dissertations, Professional Papers, and Capstones by an authorized administrator of Digital Scholarship@UNLV. For more information, please contact [digitalscholarship@unlv.edu](mailto:digitalscholarship@unlv.edu).

DISSOLUTION AND ELECTROCHEMICAL RECOVERY OF  
UO<sub>2</sub>, UO<sub>3</sub>, AND U<sub>3</sub>O<sub>8</sub> IN IONIC LIQUIDS

By

Katherine Iolani Thornock Luebke

Bachelor of Science – Chemistry  
Boise State University  
2014

A dissertation submitted in partial fulfillment  
of the requirements for the

Doctor of Philosophy - Radiochemistry

Department of Chemistry and Biochemistry  
College of Sciences  
The Graduate College

University of Nevada, Las Vegas  
August 2022

Copyright 2022 Katherine Luebke

All Rights Reserved

**Dissertation Approval**

The Graduate College  
The University of Nevada, Las Vegas

May 5, 2022

This dissertation prepared by

Katherine Iolani Thornock Luebke

entitled

Dissolution and Electrochemical Recovery of UO<sub>2</sub>, UO<sub>3</sub>, and U<sub>3</sub>O<sub>8</sub> in Ionic Liquids

is approved in partial fulfillment of the requirements for the degree of

Doctor of Philosophy – Radiochemistry  
Department of Chemistry and Biochemistry

David Hatchett, Ph.D.  
*Examination Committee Chair*

Kenneth Czerwinski, Ph.D.  
*Examination Committee Member*

Frederic Poineau, Ph.D.  
*Examination Committee Member*

William Culbreth, Ph.D.  
*Graduate College Faculty Representative*

Kathryn Hausbeck Korgan, Ph.D.  
*Vice Provost for Graduate Education &  
Dean of the Graduate College*

## Abstract

This research explores a novel method of increasing the solubility of uranium oxides and other actinide oxides in room temperature ionic liquids (IL) using direct dissolution. The goal is to further expand our knowledge of actinide dissolution and possible nuclear fuel cycle material applications using ionic liquids. The novelty of the methods is focused on the use of oxidizing gas generated using air passed through an ozone generator. While examples of dissolution exist in IL using acidic functionalized ionic liquids, the solubility of all possible oxide species was not demonstrated. Also, the addition of aqueous acid to IL containing actinide oxides has been successfully demonstrated. However, the presence of large concentrations of water and secondary acid species complicates both the speciation and recovery of the actinides electrochemically using IL systems. Thus the direct dissolution of  $U_3O_8$ ,  $UO_2$ , and  $UO_3$  with air-generated oxidizing gas was evaluated separately in n-trimethyl-n-butylammonium bis(trifluoromethanesulfonyl)imide  $[Me_3NnBu][TFSI]$  without acid functionalization or addition of secondary species such as HTFSI. These soluble species for each compound were analyzed spectroscopically and characterized electrochemically with the goal of recovering the actinide materials at the electrode surface. Methods including cyclic voltammetry, bulk deposition, and pulse deposition electrochemical techniques were utilized to obtain uranium deposits at the electrode surface. These deposits were then analyzed by scanning electron microscopy and x-ray diffraction. These same processes and instrumental analyses were then applied to a mixture of uranium oxides. The goal of this dissertation work is to provide a robust pathway for the recovery of oxide material similar to spent fuel, and to provide comparison to modern techniques of nuclear material separation and recovery. This method will show that uranium oxides, regardless of molecular form, can be dissolved and recovered using the same methods to create a

consistent procedure that can contribute to technological advances or waste-reducing alternative processes in the nuclear fuel cycle. This dissertation hypothesizes a pathway to directly dissolve uranium oxides with minimal outside contaminants in a manner that allows for spectroscopic and electrochemical analysis, ultimately resulting in the recovery of uranium oxide.

## Acknowledgements

I wish to thank the NSSC for funding and support throughout my graduate school career. This material is based upon work supported by the Department of Energy National Nuclear Security Administration through the Nuclear Science and Security Consortium under Award Number(s) DE-NA0003180 and/or DE-NA0000979.

Disclaimer: This report was prepared as an account of work sponsored by an agency of the United States Government. Neither the United States Government nor any agency thereof, nor any of their employees, makes any warranty, express or implied, or assumes any legal liability or responsibility for the accuracy, completeness, or usefulness of any information, apparatus, product, or process disclosed, or represents that its use would not infringe privately owned rights. Reference herein to any specific commercial product, process, or service by trade name, trademark, manufacturer, or otherwise does not necessarily constitute or imply its endorsement, recommendation, or favoring by the United States Government or any agency thereof. The views and opinions of authors expressed herein do not necessarily state or reflect those of the United States Government or any agency thereof.

I'd like to thank my advisor and mentor, Dr. David Hatchett, for all of his support, knowledge, encouragement, and patience. I'd also like to thank my other committee members, Dr. Ken Czerwinski, Dr. Frederic Poineau, and Dr. William Culbreth, for their support and advice. Thank you all for shaping my dissertation into a superior work.

I'm grateful as well to my lab mates Cassara Higgins and Phillip Hammer, as well as my year mate James Louis-Jean for always being there for me. I wish you all continued success in

your endeavors. For support in and out of the lab, I owe thanks to Julie Bertoia, Trevor Lowe, Kelly Seeley, and Wendee Johns.

Finally, I wish to thank my family for their love. To my parents Curtis and Annette Thornock for instilling my curiosity, to my sister Brittany who makes me feel like a rock star, and more than anything to my husband Brock, without whom this wouldn't have been possible. My last thank you is to my daughter Felicity. I wrote this while I grew you – may you both have a great impact.



## Table of Contents

Abstract .....	iii
Acknowledgements .....	v
Table of Contents .....	vii
List of Figures .....	x
Chapter 1 .....	1
1.1 Motivation .....	1
1.2 Fuel Cycle .....	2
1.3 Nuclear Waste and Storage .....	5
1.4 Standard PUREX Separations .....	7
1.5 Ionic Solvent Systems .....	9
1.6 Properties of ionic liquids .....	11
1.7 Conclusion .....	16
Chapter 2 .....	17
Abstract .....	17
2.1 Synthesis of Uranium Oxides with Trace $^{233}\text{U}$ .....	17
2.2 Dissolution of Uranium Oxide Powders in n-trimethyl-n-butylammonium bis(trifluoromethanesulfonyl)imide ([Me <sub>3</sub> NnBu][TFSI]) .....	21
2.3 Instrumental Analysis of Dissolved Uranyl Samples .....	31
2.4 Electrochemical Analysis .....	35
2.5 Solids Analysis Techniques .....	41
Chapter 3 .....	43

Abstract .....	43
3.1 Introduction.....	43
3.2 Materials .....	47
Results and Discussion .....	47
3.3 Synthesis and Dissolution.....	47
3.4 Powder X-Ray Diffraction.....	50
3.5 Liquid Scintillation Analysis .....	52
3.6 UV-Vis.....	54
3.7 Electrochemical Analysis.....	58
3.8 Scanning Electron Microscopy and Energy Dispersive X-Ray Spectroscopy (SEM/EDX) .....	64
Conclusion .....	68
Chapter 4.....	70
Abstract.....	70
4.1 Introduction.....	70
4.2 Materials .....	72
Results and Discussion .....	72
4.3 Synthesis and Dissolution.....	72
4.4 PXRD.....	73
4.5 LSC .....	75
4.6 UV-Visible spectroscopy .....	77
4.7 Electrochemical Analysis.....	79
4.8 SEM/EDX.....	83

Conclusion .....	88
Chapter 5.....	89
Abstract.....	89
5.1 Introduction.....	89
5.2 Materials .....	91
Results and Discussion .....	91
5.3 PXRD.....	92
5.4 LSC .....	93
5.5 UV-Visible spectroscopy .....	96
5.6 Electrochemical Analysis.....	100
5.7 SEM/EDX.....	105
5.8 Conclusion .....	110
Chapter 6: Conclusions .....	112
References.....	116
Curriculum Vitae.....	120

## List of Figures

Figure 1: An infographic of the nuclear fuel cycle from mining natural uranium to fuel production, and then reprocessing for either disposal or reuse.....	4
Figure 2: Pathway of a PUREX stream showing different extraction lines. ....	8
Figure 3: Electrochemical windows of aqueous (0.1 M H <sub>2</sub> O <sub>4</sub> ) and ionic liquid ([Me <sub>3</sub> NnBu][TFSI]) solutions with various electrodes.....	15
Figure 4: Ozone Concentration (top) and Ozone Production (bottom) in dry air flow .....	23
Figure 5: Internal Schematic of a Cary6000 UV-Vis Spectrophotometer <sup>51</sup> .....	33
Figure 6: Voltage change over time, and the resulting voltammogram showing a typical current response <sup>13</sup> .....	37
Figure 7: a) PXRD pattern of U <sub>3</sub> O <sub>8</sub> and b) the same pattern with software matched identity. ....	51
Figure 8: LSC showing dissolution over time of U <sub>3</sub> O <sub>8</sub> in activity (cpm/g), left, and percent dissolution of each sample, right. ....	52
Figure 9: The reaction rate of the U <sub>3</sub> O <sub>8</sub> dissolution over time. ....	53
Figure 10: Qualitative molecular orbital diagram for the bonding in the free uranyl ion. <sup>75</sup> .....	54
Figure 11: UV-Vis of uranyl dissolved in IL, showing the effects of water and [HTFSI] acid. Where a) is a sample with no added water or acid, b) is a sample with both added water and acid, c) is a sample with added water but no added acid, and d) is a sample with no added water but with added acid. ....	56
Figure 12: Cyclic voltammetry of uranyl in IL (black) with IL background (gray). ....	59
Figure 13: Cyclic voltammetry of 1 M uranyl in IL. ....	61

Figure 14: CV of  $U_3O_8$  in IL where a. is a sample with no added water or acid, b. is a sample with added HTFSI acid, c. is a sample with added water but no acid, and d. is a sample with both water and HTFSI acid added. Gray represents a clean IL background. .... 62

Figure 15: a. uranium deposits at 35x magnification, b. uranium deposits at 1000x magnification, and c. EDX of uranium deposits at 1000x magnification with carbon tape background. .... 66

Figure 16: a. SEM image of  $U_3O_8$  synthesized standard at 1000x magnification, b. EDX spectrum of the standard at 1000x magnification and 300 second count time showing uranium (U), oxygen (O), and carbon (C) peaks..... 68

Figure 17: PXRD pattern of synthesized  $UO_2$  sample..... 74

Figure 18: PXRD pattern of synthesized  $UO_2$ , with the matching pattern of uraninite  $UO_2$ . .... 74

Figure 19: Dissolution over time of  $UO_2$  in IL, a) activity in counts per minute per gram of sample and b) % of sample dissolved. .... 76

Figure 20: The reaction rate of the  $UO_2$  dissolution over time..... 77

Figure 21: UV-Vis spectrum of dissolved  $UO_2$  sample showing  $UO_2$  dissolved in IL forming uranyl. .... 78

Figure 22: Cyclic voltammetry of uranyl from dissolved  $UO_2$  sample in IL. .... 80

Figure 23: Enhanced section of Figure 22, showing the oxidation and reduction peaks of the uranyl species in solution..... 81

Figure 24: Reduction of uranyl due to the expanded electrochemical potential window with a) ozone exposed IL sample background and b) uranyl in IL..... 83

Figure 25:  $UO_2$  standard material SEM image at 35x magnification. .... 85

Figure 26: The same standard  $UO_2$  material shown at 1000x magnification. .... 85

Figure 27: EDX of  $UO_2$  standard material at 16 kV beam energy and 1000x magnification. .... 86

Figure 28: SEM image of $\text{UO}_2$ deposit on gold mesh electrode at 15 kv beam energy and 250x magnification. ....	86
Figure 29: SEM image of $\text{UO}_2$ deposit on gold mesh electrode at 15 kv beam energy and 500x magnification. ....	87
Figure 30: EDX spectrum of $\text{UO}_2$ deposit on gold mesh electrode at 15 kv beam energy and 250x magnification. Sulfur and fluorine peaks indicate the presence of IL still on the electrode.....	87
Figure 31: PXRD pattern of synthesized $\text{UO}_3$ sample.....	92
Figure 32: PXRD pattern of synthesized $\text{UO}_3$ , with the matching pattern of $\text{UO}_3$ .....	93
Figure 33: Dissolution over time of $\text{UO}_3$ in IL, a) activity in counts per minute per gram of sample and b) % of sample dissolved. ....	95
Figure 34: The dissolution of $\text{UO}_3$ showing the rate of reaction. ....	96
Figure 35: UV-Vis spectrum of dissolved $\text{UO}_3$ sample showing a) $\text{UO}_3$ dissolved without ozone in IL forming uranyl ( $\text{UO}_2^{2+}$ ) showing peak suppression from added water and HTFSI, and b) $\text{UO}_3$ dissolved with ozone in neat IL forming uranyl ( $\text{UO}_2^{2+}$ ) with no peak suppression. Both spectra are background subtracted with the respective IL. ....	98
Figure 36: UV-Vis spectrum of $\text{UO}_3$ sample both prior to electrochemical analysis (a) and after electrochemical analysis (b).....	99
Figure 37: Cyclic voltammetry of uranyl from dissolved $\text{UO}_3$ sample in IL where a) is a sample dissolved with ozone and b) is a blank IL sample. ....	101
Figure 38: showing the oxidation and reduction peaks of the uranyl species in solution where a) shows the ozone dissolved sample and b) shows the non-ozone sample. ....	103
Figure 39: Reduction of uranyl due to the expanded electrochemical potential window with a) ozonated IL sample and b) the blank IL sample. ....	104

Figure 40: a) shows the complete reduction in solution of the uranyl species in the non-ozonated sample and b) shows the blank IL background in gray. .... 105

Figure 41:  $\text{UO}_3$  standard material SEM image at 35x magnification. .... 106

Figure 42: The same standard  $\text{UO}_3$  material shown at 500x magnification. .... 107

Figure 43: EDX of  $\text{UO}_3$  standard material at 16 kV beam energy and 500x magnification. .... 107

Figure 44: SEM image of  $\text{UO}_3$  deposit on gold mesh electrode at 15 kv beam energy and 250x magnification. .... 108

Figure 45: SEM image of  $\text{UO}_3$  deposit on gold mesh electrode at 15 kv beam energy and 500x magnification. .... 109

Figure 46: EDX spectrum of  $\text{UO}_3$  deposit on gold mesh electrode at 15 kv beam energy and 250x magnification. Fluorine peak indicates the presence of IL still on the electrode. .... 110

## Chapter 1

### 1.1 Motivation

This research explores a novel method of increasing the solubility of uranium oxides and other actinide oxides in room temperature ionic liquids (IL) using direct dissolution. The goal is to further expand our knowledge of actinide dissolution and possible nuclear fuel cycle material applications using ionic liquids. The novelty of the methods is focused on the use of oxidizing gas generated using air passed through an ozone generator. While examples of dissolution exist in IL using acidic functionalized ionic liquids, the solubility of all possible oxide species was not demonstrated even with the addition of water and heat to the system. The addition of aqueous acid to IL containing actinide oxides has been successfully demonstrated. However, the presence of large concentrations of water and secondary acid species complicates both the speciation and recovery of the actinides electrochemically using IL systems. Thus the direct dissolution of  $U_3O_8$ ,  $UO_2$ , and  $UO_3$  with air-generated oxidizing gas was evaluated separately in *n*-trimethyl-*n*-butylammonium bis(trifluoromethanesulfonyl)imide  $[Me_3NnBu][TFSI]$  both with and without addition of secondary species such as HTFSI. These soluble species for each compound were analyzed spectroscopically and characterized electrochemically with the goal of recovering the actinide materials at the electrode surface. Methods including cyclic voltammetry, bulk deposition, and pulse deposition electrochemical techniques were utilized to obtain uranium deposits at the electrode surface. These deposits were then analyzed by scanning electron microscopy and x-ray diffraction. These same processes and instrumental analyses were then applied to a mixture of uranium oxides. The goal of this dissertation work is to provide a robust pathway for the recovery of oxide material similar to spent fuel, and to provide comparison to modern techniques of nuclear material separation and recovery. This method will show that



uranium oxides, regardless of molecular form, can be dissolved and recovered using the same methods to create a consistent procedure that can contribute to technological advances or waste-reducing alternative processes in the nuclear fuel cycle. This dissertation hypothesizes a pathway to directly dissolve uranium oxides with minimal outside contaminants in a manner that allows for spectroscopic and electrochemical analysis, ultimately resulting in the recovery of uranium oxide.

## 1.2 Fuel Cycle

Uranium oxides are present in nearly every stage of the nuclear fuel cycle, or the process by which natural uranium is converted to a usable fuel. Uraninite, a major ore of uranium found naturally around the world, is composed of  $\text{UO}_2$  and a varying amount of  $\text{U}_3\text{O}_8$ . Uranium dioxide ( $\text{UO}_2$ ) is a black to brown solid material. It has a very high melting point (2847 °C) and is notably not soluble in water.<sup>1</sup> When dissolved in acid, it forms  $\text{UO}_2^{2+}$  and will complex with the solvent. Uranium trioxide ( $\text{UO}_3$ ) is similarly insoluble in water but can be soluble in acid, although it decomposes in air between 400 and 600°C.<sup>2,3</sup> Triuranium octoxide ( $\text{U}_3\text{O}_8$ ) is the thermodynamically preferred oxide state, and is also insoluble in water but soluble in acid. Most uranium compounds will decompose to  $\text{U}_3\text{O}_8$  above 650°, and  $\text{U}_3\text{O}_8$  itself decomposes at 800°C.<sup>3</sup> It is central to this dissertation to study all three oxides, since in addition to natural uranium ore  $\text{UO}_2$  is the oxide form of fuel,  $\text{UO}_3$  is a precursor to  $\text{UO}_2$ , and  $\text{U}_3\text{O}_8$  is the eventual final form once material decomposes. Notable amongst the other components of natural uranium ore are radium and thorium.<sup>4</sup> Isotopically, uranium ore is composed of the following uranium percentages:

Table 1.1: Isotopic percentages of natural uranium.<sup>5</sup>

Isotope	Natural Abundance	Half-life
U-238	99.2742%	4.468*10 <sup>9</sup> years
U-235	0.7204%	7.04*10 <sup>8</sup> years
U-234	0.0054%	2.46*10 <sup>5</sup> years

In order to produce power in a reactor, nuclear fuel must be able to sustain a chain reaction of fission based on the isotopic makeup of the fuel. U-235 is fissile and can be used as a fuel source until the material has been depleted (meaning there is not enough U-235 present for continued reactions). U-238 itself is not fissile, and the probability of a fission reaction occurring is not enough to support a continued and controlled system. U-238 is fertile, meaning that it can absorb neutrons in a nuclear reactor and undergo internal reactions to become a fissile isotope, specifically Pu-239.<sup>5</sup> Because of its primary use in nuclear weapons, the growth of Pu-239 inside a nuclear reactor is considered a proliferation risk by the United States, which does not use any U-238 based fuel in order to prevent prohibited states or entities from obtaining weaponized nuclear material. Therefore the reuse of fuel is limited and reactors must utilize newly mined natural uranium ore after conversion and enrichment as fuel for each cycle.

Spent fuel can be reprocessed and in some cases re-enriched using a “closed” fuel cycle where little to no new uranium is added to the system. However, as stated before this reprocessing method is not used in the United States, which makes use of an “open” or “once through” fuel cycle.<sup>6</sup> An open cycle requires new fuel for each run of the reactor, regardless of the amount of fuel consumed during a run. The primary benefit is nonproliferation of material suitable for a nuclear weapon, which is present in uranium fuels that have been “burned up,”

meaning used in a reactor. The drawback of an open cycle is the cost and material needed to create new fuel rods from fresh uranium ore. While fuel is mined, chemically converted, and enriched, and used in reactors in the “open” and “closed” procedures, the difference between the two processes lies entirely in what is done after the fuel is safe to handle. This is shown in the following figure 1.<sup>6</sup>

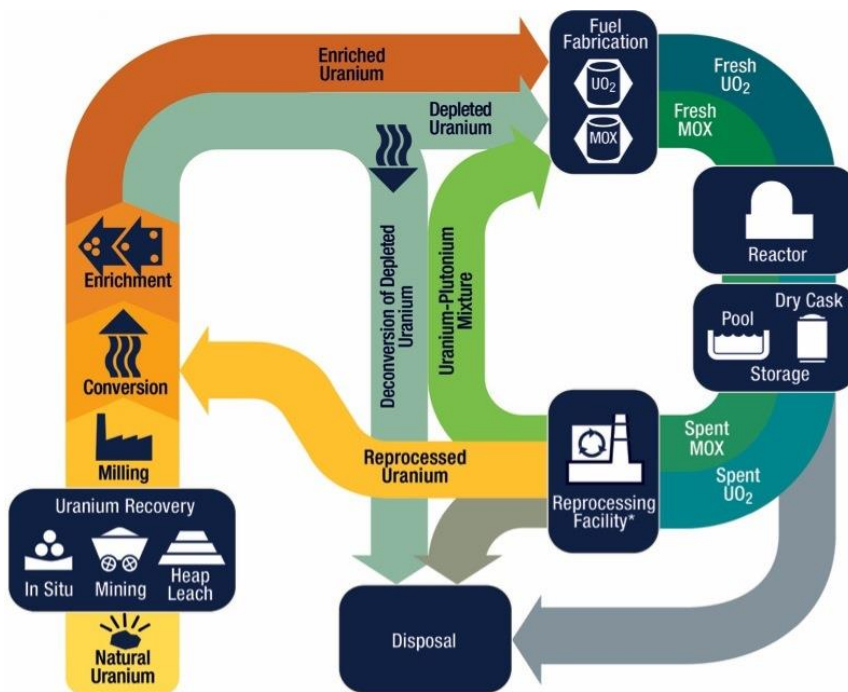


Figure 1: An infographic of the nuclear fuel cycle from mining natural uranium to fuel production, and then reprocessing for either disposal or reuse.

As shown, the open process takes fresh ore (labeled “Natural Uranium”) through enrichment to fabrication (which is the production of fuel pellets in a form suitable for use in a reactor), followed by power reactor use and finally storage (labeled “Disposal” for the final storage after the spent fuel has been cooled). The closed process reuses spent fuel (labeled

“Reprocessing Facility”) for additional reactor runs as mixed oxide or MOX fuel. The processing of MOX fuels are less intensive than creating new fuel directly from ore, but it does require separating out fission products and measuring the uranium consumption. By comparison for fuel used in the open cycle or the original fuel for a closed cycle, the natural ore must be milled into a concentrated yellowcake form,  $U_3O_8$ . Once in a consistent chemical form, the yellowcake is converted to gaseous  $UF_6$  for use in enrichment. The gaseous material can be diffused or centrifuged – where the lighter U-235 will move faster than the heavier U-238, thus allowing separation of the two isotopes. The material must be enriched to 3-5% U-235, significantly more than is found in natural uranium.<sup>6</sup> Uranium trioxide ( $UO_3$ ) is a common intermediate step during conversion steps.<sup>7</sup> The enriched uranium is then converted to  $UO_2$  to be formed into ceramic fuel pellets. The depleted uranium remaining after enrichment can either be formed into fuel pellets or reconverted back to  $U_3O_8$ .<sup>7</sup> This process of mining, enriching, and burning up new fuel in order to minimize proliferation risk has tradeoffs. The choice to not use natural uranium or reprocess depleted uranium fuel produces significant used fuel waste with each reactor cycle that must be stored.

### 1.3 Nuclear Waste and Storage

The US Department of Energy states that the United States has produced approximately 83,000 metric tons of spent nuclear fuel to date with 2,000 tons added each year, stored in 76 locations across the country.<sup>8</sup> Due to the high density of the materials, the total volume is relatively small compared to other energy sources, and can be stored safely on site at the reactor location. However this material is unavailable for further use. Meanwhile the total uranium mined in 2018 was 53,498 tons, which was converted to 63,087 tons of  $U_3O_8$ . This only represented 83% of the world demand.<sup>9</sup> While this deficit can be made up for with stockpiled

materials (such as decommissioned and milled nuclear weapons), or from reprocessed and re-enriched fuels in countries with a closed fuel cycle, the IAEA anticipates that after 2020 these sources will be depleted and production will have to increase to support global needs.<sup>10</sup> Currently 20% of all US energy is produced from commercial nuclear reactors.<sup>11</sup> Operating at 92% capacity at all times, most nuclear reactors have a lifespan of 40-80 years.<sup>12</sup> Regardless of the future of commercial nuclear power, these reactors will either produce spent fuel or decommissioned radioactive material. Low level waste includes items that came in contact with radioactivity but are not inherently radioactive or activated from that contact, must be stored until no longer radioactive or disposed of by certified waste disposal organizations. High level waste including spent fuel, reactor cladding that has been activated by the neutron flux necessary for the reactor, and solvents used in initial extraction and preparation must be stored in the absence of reprocessing.

In the United States, uranium and plutonium were first mined, milled, and enriched as part of the Manhattan Project during World War II. This material would eventually form atomic weapons, with several locations in the United States participating under government and military supervision. While the uranium was mined around the world, it was processed in a few main sites: Oak Ridge, Tennessee; Chicago, Illinois; Los Alamos, New Mexico; and Hanford, Washington.<sup>13</sup> In addition to these locations, spent nuclear fuel and other nuclear waste is currently stored in thirty-nine states, typically wherever it was produced, with the cost of management and storage at more than \$2 million dollars per day.<sup>14,15</sup>

Nuclear fuel rods pulled from a reactor must be stored under water to cool for several years before they can be prepared for external storage. The water pools provide both cooling for the spent fuel and occupational protection against radiation for workers. Once sufficiently

cooled, fuel rods are stored as solid waste with an inert gas filling the space in cement or metal casks suitable for short term storage or transportation.<sup>7</sup> Until the Yucca Mountain Repository is licensed and approved to store high level waste, the hazard of extending temporary storage into permanent storage at the site of production will continue. This burden also mandates the need to separate spent fuel into different waste streams, or types, prior to permanent storage.

#### 1.4 Standard PUREX Separations

The standard practice for separating uranium and plutonium from the other components of spent fuel is the PUREX process. Standing for Plутonium URanium EXtraction, this is a solvent extraction that relies on the different affinities of plutonium and uranium oxidation states for either the organic or aqueous phase. Once these two are separated from the bulk solution and then additionally from each other, other steps can be performed to recover transuranic actinides and fission products. This allows for the waste to be declassified as high level waste and becomes low level waste instead, which requires less controls to be eliminated.

To begin, uranium and plutonium must be extracted from the rest of the dissolved products. An organic solution of 30% tributylphosphate (TBP) in other hydrocarbons (such as dodecane) is contacted with the 3 M nitric acid aqueous phase.<sup>16</sup> If the nitric acid is more than 3 M, then neptunium will also extract with the uranium and plutonium.<sup>17</sup> The rate of neptunium extraction is increased as the molarity rises above 4.5 M.<sup>16</sup> At this point, the uranium is U(VI) and the plutonium is Pu(IV) – idea states for existing in the organic phase. In order to back-extract plutonium, it must be reduced to Pu(III), which has a much higher affinity for nitric acid. This was originally done by adding ferrous sulfamate, but now uses N,N-diethyl-hydroxylamine or electrochemical reduction with hydrazine present, to the combined U/Pu solution.<sup>17</sup> Pu(III) is then in a separate aqueous nitric acid stream, with the first nitric acid extraction removed and the

uranium continuing in the separate organic phase stream.<sup>16</sup> Each stream can be treated separately with any number of ion extraction methods to purify each element, including technetium. This process is shown in Figure 2.<sup>18</sup>

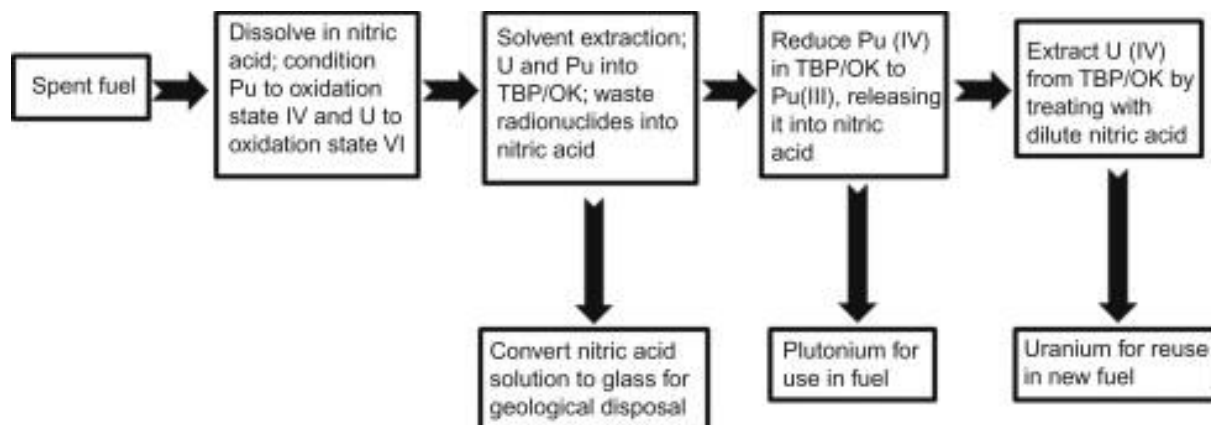


Figure 2: Pathway of a PUREX stream showing different extraction lines.

While this is the undoubted standard for nuclear fuel extraction, separation, and purification for more than fifty years, there are some drawbacks. Each solvent or additive that comes in contact with the material must be treated as radioactive waste. With several additional extractions to be sure that minimal material is unrecovered, this can amount to large volumes for even small masses of spent fuel solids. The solvents are susceptible to radiolysis damage, and as such are unsuitable for any time in storage – the nitric acid can be neutralized, but that will also greatly increase the volume. In addition, TBP is flammable and  $\text{HNO}_3$  is a strong acid. Both solvents are thus hazardous, and present worker risk. Here, ionic liquids are proposed as an alternative to these systems.

## 1.5 Ionic Solvent Systems

Part of the goal of this dissertation research is to show the capabilities of ionic liquids in regards to the dissolution and recovery of uranium oxides as discussed. The de facto standard method of treating spent nuclear fuel is in aqueous systems, which are often acidic, volatile, and toxic. Solid fuel pellets are formed from enriched and purified ore, and spent fuel pellets are separated the same way – through PUREX solvent extraction. This generates waste on both ends, as solvents can't often be reused, and the material needs to be transported as either acidic solutions or packed solids. An alternative to aqueous systems are ionic systems. There are two distinct but related options where nuclear material is concerned: molten salts and room temperature ionic liquids. While molten salts have a history of application to the nuclear fuel cycle, ionic liquids are by comparison under-utilized. Comparing these two ionic systems will show potential uses for ionic liquids within the nuclear fuel cycle, and reiterate the motivation of this dissertation research.

Molten salts are simple metal salts, usually consisting of a group 1 or 2 element such as lithium or beryllium and halides such as fluoride or chloride, which have a high melting point and low vapor pressure. Other characteristics of a molten salt required for use with nuclear fuel material is established solubility of fuel material, resistance to radiolysis, and thermal conductivity. Some systems will make use of two separate molten salts combined together, where one will contain the dissolved fuel material and the other will be viable for neutron absorption and act as the moderator to control the chain reaction. At the moment, existing large scale molten salts available for purchase are prone to impurities, which increases the rate of corrosion. To avoid impurities, molten salts must be produced to exact specifications and



analyzed through crystallography or other means. This can be expensive, especially compared to the availability, cost, and purity standards of most laboratory solvents.<sup>19</sup>

While the need for purity is important to the manufacturing of molten salts, once made the dissolved fuel can be recycled or recovered. Molten salts are frequently used in processing and reprocessing nuclear materials.<sup>20</sup> One study showed the possibilities of direct oxide dissolution and electrochemical recovery within a molten salt. By making use of pyroprocessing (necessary by default for molten salts) a reducing agent can be added to the system and drive the metal chloride or metal oxide compound to the metallic state. Calcium was found to work as a reducer in molten salts, and was able to reduce several transition metals as an analog for actinide species.<sup>21</sup>

Molten salts are already used in other energy industries – particularly in solar panels – for heat transfer.<sup>22</sup> A molten salt can also be applied to converting coal directly to carbon monoxide and hydrogen gasses, or to other solid organic wastes. Molten salts can also be used to directly process metals, specifically anything not iron or iron-like. The high temperatures necessary for sustaining a molten salt also allow for metal purification without evaporation or degradation of the solvent while impurities can be separated or decomposed. But there are significant advantages to molten salts in the field of nuclear reactors. Foremost is that an already liquid fuel can't meltdown, preventing a major hazard and safety issue. Less waste is generated, as the same solutions can be used for purification, separation, and burnup of fuel. What waste is generated is less toxic and corrosive than standard spent nuclear waste, and safer to transport. Compared to the spill possibilities of gaseous or potentially air-borne solids, liquid waste is easier to store and transport. Additionally, when molten salts solidify, they contract where water expands when it freezes.<sup>23</sup>

While many reactors make use of separate solid nuclear fuel and cooling mechanisms, molten salt reactors (MSR) make use of high temperatures to maintain a liquid core environment that provides power from direct heat transfer. These reactors were slowly disbanded after seeing peak usage in the 1960s and 1970s, but the concept has remained under investigation. One group has proposed a molten salt reactor design that offers better efficiency of operation and fuel use, more options for fuel materials and storage, and onsite reprocessing or ease of transportation.<sup>24</sup> Compared to standard reactors, which operate at around 315 °C and 150 atmospheres pressure, most MSRs can function at higher temperatures (up to about 1400 °C, though some are as low as 500 °C) and standard pressure. Even at higher temperatures, with already liquid fuel and nothing under pressure, the reactor is safe from meltdown. Graphite rods or molten salts containing boron can both be used as moderators to control the ongoing fission reactions.<sup>25</sup> Ideally, because molten salts can be miscible with room temperature ionic liquids, fuel preparation can be moved directly into or out of a reactor without having to change solvents. Even with a standard reactor instead of a MSR, ionic liquids can provide a safer and greener option for nuclear material work.

## 1.6 Properties of ionic liquids

It is clear from historical application and modern study that ionic liquids are a viable choice for working with nuclear materials and can do many of the things (separation, reprocessing, and in-situ fuel) that are being done currently in other media. A survey of the basic properties of ionic liquids, the benefits of using ILs over other solvents, and the potential drawbacks from such use follows below.

Where molten salts are made of simple metal salts, room temperature ionic liquids are made up of bulky organic compounds paired as cations and anions. They are nonvolatile, nonflammable, noncorrosive and nontoxic in many cation/anion combinations. While susceptible

to some degradation from nitric acid and acetone, ILs on the whole are robust solvents. When tested, less than 1% of ILs were damaged by radiolysis – a necessary property for work with high activity spent nuclear fuel. The superior electrochemical window for ILs is an inherent property – because the solution is equimolar cations and anions, electron transport is less disrupted.<sup>34</sup> In addition, the ionic character means that no salt bridge is needed for electron transport, which would normally add another chemical species to the solution and may act as a contaminant.

Just as aqueous solutions can have variable pH based on the concentration of acid added, ionic liquids can be similarly adjusted by adding the protonated anion to solution. This acts as a Bronsted-Lowry acid without having to mix an aqueous solution into the IL. Room temperature ionic liquids are often thermally stable up to 100 °C, but that can also be adjusted based on the IL chosen. Another component to many dissolutions is water, and ILs are both hygroscopic and hydrophobic – ambient water from the air can be absorbed by the IL (and intentional contact with an excess of water can saturate the sample) but after the saturation point is reached the two are not miscible.<sup>26</sup> The ionic liquid, which typically consists of either metallic or bulky organic ions, is usually denser and more viscous than water and will support a phase separation. While some have found water present in the IL to assist in dissolution, it will have a noticeable effect on the electrochemistry.<sup>27</sup>

With an ionic liquid as a solvent, not only can many properties be tuned by ion selection (electrochemical window, temperature stability, viscosity, density, etc.) but the solvent can be manipulated by chemistry while in use. Water has limited solubility, as do acids before they are concentrated enough to damage the IL, but polar organic solvents can be very miscible. Material solubility can be increased by increasing the temperature or adding the protonated anion as an acid (which will also decrease the pH). Catalysts can be added to assist dissolution when

necessary, or a material may be dissolved in one solvent and then dissolved or extracted into the IL. Electrochemistry can manipulate the oxidation state of a species in solution, allowing for deposition or precipitation.

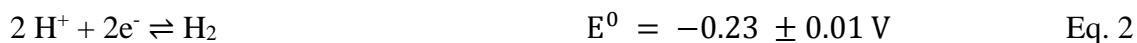
One study showed a [TFSI] anion-based ionic liquid extracted  $\text{UO}_2^{2+}$  better than dodecane and comparable to nitric acid, the compounds used for PUREX separations. However, mixing the IL with nitric acid led to degradation of the ionic liquid, likely from nitration reactions and acetone present on glassware surfaces. The authors also found that regarding reprocessing fuel, some ILs have a lower chance of criticality (because the IL acted as a neutron moderator) which would allow for more material to be processed at once.<sup>28</sup> Another study showed [TFSI] anion ILs were able to successfully extract  $\text{Th}^{4+}$ ,  $\text{UO}_2^{2+}$ ,  $\text{Pu}^{4+}$ ,  $\text{Np}^{4+}$ , and  $\text{Am}^{3+}$  from organic and acidic media. In acids this was done by adjusting the pH of the aqueous layer, and was very successful.<sup>29,30</sup>

Not only do ionic liquids work as solvent extractions, but they are also viable for direct or assisted dissolution. Many metallic cations or inorganic salts have been found to be soluble in [TFSI] anion ILs including transition metals<sup>31</sup> (where [TFSI] anion ILs were found to have superior solvation even over other ILs<sup>32</sup>) and actinides, especially uranium oxides which are insoluble in water alone.<sup>33,34,35</sup>

With proven solubility of actinides and metal ions, the next step is to determine the suitability of ionic liquids for recovery of those species. One method of recovery is electrochemistry, where electricity supplied and controlled by a potentiostat is directed into a solution and two electrodes measure the electron transport through the system. Specifically, electrochemistry can be used to reduce cations to ground state species which can be removed

from the solution they were dissolved in. This is enabled by the fact that [TFSI] anions are weak ligands, and the bond is easily broken in favor of electrochemical reduction.

While some electrochemistry can be done in aqueous solutions, it is limited by hydrolysis of water. At ~1.0 V vs Ag/AgCl reference, oxygen evolves out of water, while hydrogen gas forms at an electrode surface at ~-0.2 V vs Ag/AgCl reference. This means that the total window in which electrochemistry can occur in any water-based solution is limited to that 1.23 V range. The following equations show the necessary reduction potentials for selected actinide species relative to an Ag/AgCl reference electrode such as used in this research.<sup>36</sup>



From Figure 3<sup>37</sup>, the electrochemical window in aqueous species is insufficient to reduce most actinide species. However, ionic liquids have a much wider window and the added benefit of no side reactions. The electrochemical limit for ionic liquids is defined by the reduction potential of the cation and the oxidation potential of the anion – and thus, can be manipulated by selecting the most suitable ion pair.

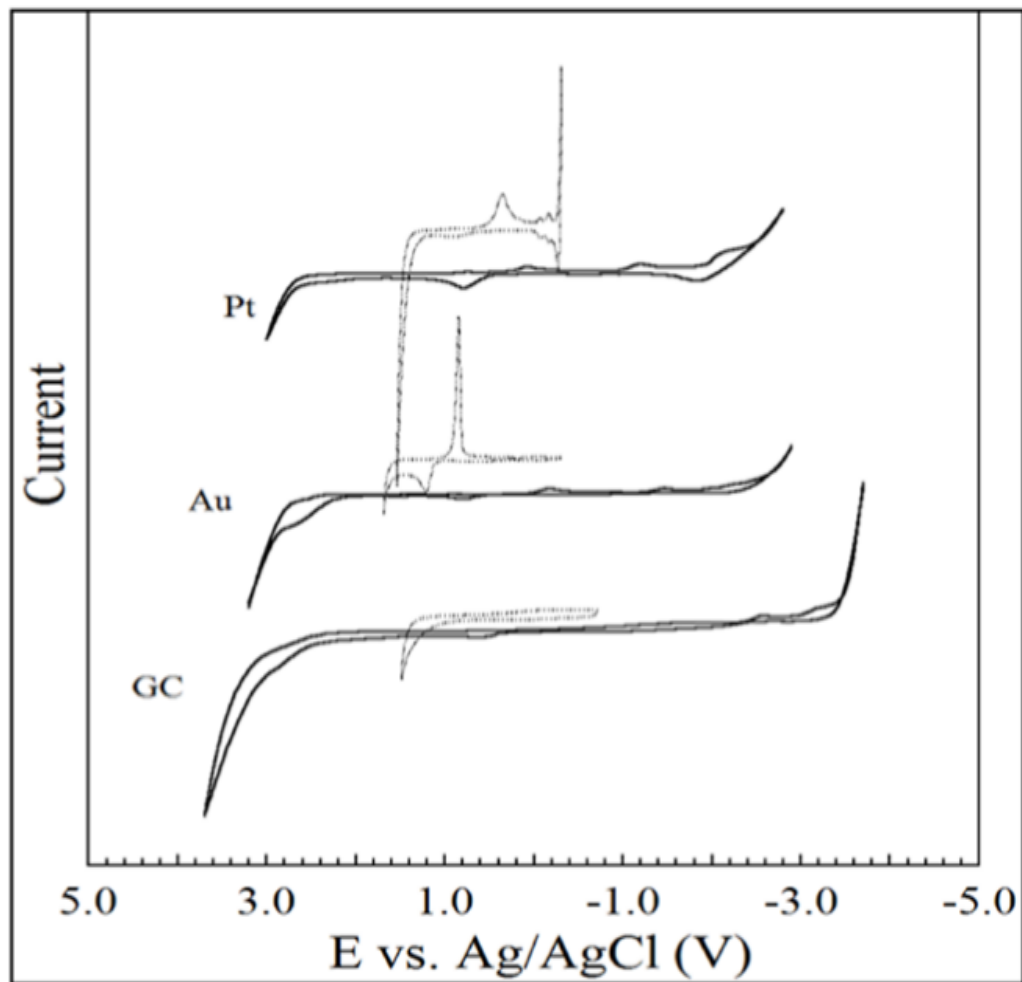


Figure 3: Electrochemical windows of aqueous (0.1 M H<sub>2</sub>O<sub>4</sub>) and ionic liquid ([Me<sub>3</sub>NnBu][TFSI]) solutions with various electrodes.

It has been demonstrated with cyclic voltammetry that Th<sup>+4</sup> can be reduced in a single step to the ground state in a [TFSI] ionic liquid. It was also observed at the time that other solvents (including aqueous and nonaqueous solvents and molten salts) were more difficult to work with than the room temperature ionic liquid.<sup>34</sup> Another study declared that species of neptunium are uncharacteristically stable in [TFSI] ionic liquids, resulting in ease of study as well as information on oxidation states that can't be measured in other solutions.<sup>38</sup>

## 1.7 Conclusion

With a demonstrated need for exploration of uranium oxide study in the field of nuclear waste and storage, this dissertation proposes a novel path of study. It has been shown that ionic solvents are well suited for actinide ion extraction and dissolution; liquid fuel use, transportation, and storage; and electrochemical study and recovery. The ionic liquid n-trimethyl-n-butylammonium bis(trifluoromethanesulfonyl)imide  $[\text{Me}_3\text{NnBu}][\text{TFSI}]$  is suitable for the direct dissolution and electrochemical recovery of uranium oxides with oxidizing gas generated from compressed air. In exploring this chemical pathway of a full range of uranium oxide compounds, comparisons to modern nuclear fuel cycle processes can be made and evaluated, thus adding knowledge to the field. The work of this dissertation will show the viability of a standard procedure for in-situ dissolution and recovery of any uranium oxide used in the nuclear fuel cycle.

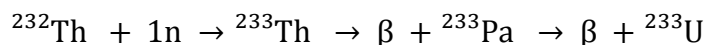
## Chapter 2

### Abstract

The following chapter discusses the synthesis of uranium oxides and the characterization methodologies used to dissolve, analyze, and recover the compounds. First, the uranium oxides were synthesized with a tracing spike of  $^{233}\text{U}$  to increase the activity of the samples and characterized with powder X-ray diffraction. The uranium oxides were then dissolved directly into the ionic liquid solvent with ozone generated from compressed air. Each sample was then analyzed with UV-vis spectroscopy, liquid scintillation counting, and cyclic voltammetry. Then electrochemical deposition was performed, and deposits were analyzed by scanning electron microscopy and energy dispersive X-ray spectroscopy.

### 2.1 Synthesis of Uranium Oxides with Trace $^{233}\text{U}$

The enrichment of natural uranium is required before it can be used as fuel in a nuclear reactor. The spent fuel still contains  $^{238}\text{U}$  as the majority isotope and is designated as depleted uranium. One such method is liquid scintillation counting, which measures the activity of a liquid sample. The time needed to have statistically significant results is dependent on the activity of the sample, where a higher activity would require less time to collect data than a lower activity sample. The half-life of  $^{238}\text{U}$  is  $4.468 \times 10^9$  years, whereas  $^{233}\text{U}$  has a half-life of  $1.592 \times 10^5$  years, four orders of magnitude less. Since activity is inversely proportional to half-life, the  $^{233}\text{U}$  has a much higher activity. However, there is no  $^{233}\text{U}$  present in natural or depleted uranium as it is produced from the neutron bombardment of  $^{232}\text{Th}$  in the process shown in Equation 2.1.



(Eq. 2.1)



The addition of  $^{233}\text{U}$  to the bulk material was required in the synthesis in order to have a solid uranium oxide sample that can be utilized for the experimental conditions required in this research and to allow LSC analysis. The “spiking” of the  $\text{U}_3\text{O}_8$  sample was accomplished early in the synthesis process. A standard of  $^{233}\text{U}$  with known activity was made prior to this research by dissolving the  $^{233}\text{U}$  in nitric acid and then diluting in water which can then be added to a uranium sample in aqueous solution.

The synthesis of uranium oxides consists of two stages: a “wet” process and a “dry” process. The wet process is the same for each of the three oxides produced. First, a standard of depleted uranium in the form of uranyl nitrate hexahydrate ( $\text{UO}_2(\text{NO}_3)_2 \cdot 6\text{H}_2\text{O}$ ) is dissolved in deionized water. Then, the  $^{233}\text{U}$  spike is added via micropipette for a specific known volume. The sample is mixed to ensure even distribution of the  $^{233}\text{U}$ , and then ammonium hydroxide ( $\text{NH}_4\text{OH}$ ) is added in excess to precipitate the uranium. The sample is then centrifuged until the bright yellow precipitate ammonium diuranate ( $(\text{NH}_4)_2\text{U}_2\text{O}_7$ ) or ADU is separated from the clear liquid supernatant. The solid material is dried in a furnace at a temperature exceeding  $50\text{ }^\circ\text{C}$  but less than or equal to  $200\text{ }^\circ\text{C}$  for several hours. This dried ADU is a yellow to orange solid ready for the “dry” synthesis process.

While the starting material is the same for each of the three uranium oxide final products ( $\text{UO}_2$ ,  $\text{UO}_3$ , and  $\text{U}_3\text{O}_8$ ) the heat treatment step to synthesize these oxides is different. The simplest of the three is  $\text{UO}_3$ , is heated in atmosphere at  $500\text{ }^\circ\text{C}$  for one hour. The literature suggests that this rapid heating process produces the  $\beta$  phase  $\text{UO}_3$ , where a longer heating process (such as heating at  $500\text{ }^\circ\text{C}$  for a week as compared to one hour) would produce the  $\alpha$  phase.<sup>39</sup> However, this phase distinction is not a significant factor in the dissolution process. The synthesis of  $\text{U}_3\text{O}_8$  is achieved by heating ADU slowly to  $800\text{ }^\circ\text{C}$  for six hours in atmosphere. In

fact, heating any uranium oxide in atmosphere above approximately 750 °C produces  $U_3O_8$ , which is the kinetically favorable state.<sup>40,41</sup> However, to synthesize  $UO_2$  the ADU must be heated slowly to 600 °C in a reducing atmosphere, in this case flowing  $H_2$  gas (5% hydrogen in 95% argon).<sup>42</sup> The structure of each product was confirmed by powder X-ray diffraction (PXRD) after each sample was pulverization to a fine powder. The final products were distinguishable with  $UO_3$  an orange powder,  $U_3O_8$  a dark green to brown powder, and  $UO_2$  a black powder. These materials were utilized in the dissolution process. Final % yield values were calculated for each synthesis reaction.

The  $U_3O_8$  was synthesized directly from uranyl nitrate hexahydrate ( $UO_2(NO_3)_2 \cdot 6H_2O$ ). Uranyl nitrate (0.9483 g) was dissolved in ~8 mL ultrapure deionized water. At this stage a spike aliquot (0.783 mL) of U-233, an isotope of uranium with a higher activity than the depleted U-238 used to make the uranyl nitrate, can be added to the solution. The U-233 used was dissolved in nitric acid, a complementary matrix to the dissolved nitrate. Adding an excess, ~1mL, of ammonium hydroxide ( $NH_4OH$ ) causes precipitation of the uranium in the form of ammonium diuranate, ( $(NH_4)_2U_2O_7$ ) or ADU. The ADU, a bright yellow solid, can be separated from the supernatant via centrifuge. This solid was dried in a box furnace at 50° C for 24 hours to remove any remaining water. The dried solid, now an orange color, is gently pulverized to remove any large clumps before being placed in a furnace at 800° C for 6 hours in atmosphere to synthesize  $U_3O_8$ . The material is then pulverized to form a fine homogeneous powder that can be used in dissolution. The fine powder was analyzed using powder X-ray diffraction (PXRD) to confirm the identity of the compound. The final mass recorded was 0.3959 g of  $U_3O_8$  which is a 74.69% recovery.

The  $\text{UO}_2$  was synthesized directly from uranyl nitrate hexahydrate ( $\text{UO}_2(\text{NO}_3)_2 \cdot 6\text{H}_2\text{O}$ ). Uranyl nitrate (1.8074 g) was dissolved in ~16 mL ultrapure deionized water. At this stage a spike aliquot (2.595 mL) of U-233 was added to the solution. The U-233 used was dissolved in nitric acid, a complementary matrix to the dissolved nitrate. Adding an excess, ~2mL, of ammonium hydroxide ( $\text{NH}_4\text{OH}$ ) caused precipitation of the uranium in the form of ammonium diuranate, ( $(\text{NH}_4)_2\text{U}_2\text{O}_7$ ) or ADU. The ADU, a bright yellow solid, was separated from the supernatant via centrifuge. This solid was then be dried in a box furnace at  $50^\circ\text{C}$  for 24 hours to remove any remaining water. The dried solid, now an orange color, was gently pulverized to remove any large clumps before being placed in a sealed furnace under 95% argon/5% hydrogen ( $\text{H}_5$ ) atmosphere with a slow temperature increase to  $600^\circ\text{C}$ , holding at that temperature for 90 minutes, and then slowly decreasing the temperature back to room temperature to synthesize  $\text{UO}_2$ . The material was then pulverized to form a fine homogeneous powder that can be used in dissolution. The fine powder was analyzed using powder X-ray diffraction (PXRD) to confirm the identity of the compound. The final mass recorded was 0.7604g  $\text{UO}_2$  which was a 78.24% recovery.

The  $\text{UO}_3$  was synthesized directly from uranyl nitrate hexahydrate ( $\text{UO}_2(\text{NO}_3)_2 \cdot 6\text{H}_2\text{O}$ ). Uranyl nitrate (0.7024 g) was dissolved in ~9 mL ultrapure deionized water. At this stage a spike aliquot (1.008 mL) of U-233 was added to the solution. Adding an excess (~1mL) of ammonium hydroxide ( $\text{NH}_4\text{OH}$ ) caused precipitation of the uranium in the form of ammonium diuranate, ( $(\text{NH}_4)_2\text{U}_2\text{O}_7$ ) or ADU. The ADU was separated from the supernatant via centrifuge. This solid was dried in a box furnace at  $50^\circ\text{C}$  for 24 hours to remove any remaining water. The dried solid was gently pulverized to remove any large clumps before being placed in a sealed furnace under atmosphere with a rapid temperature increase to  $600^\circ\text{C}$  for one hour, followed by decreasing the

temperature back to room temperature to synthesize  $\text{UO}_3$ . The material was then pulverized to form a fine homogeneous powder that can be used in dissolution. The fine powder was analyzed using powder X-ray diffraction (PXRD) to confirm the identity of the compound. The final mass recorded was 0.3431g  $\text{UO}_3$  which was a 85.76% recovery.

## 2.2 Dissolution of Uranium Oxide Powders in n-trimethyl-n-butylammonium bis(trifluoromethanesulfonyl)imide ( $[\text{Me}_3\text{N}^n\text{Bu}][\text{TFSI}]$ )

The dissolution of uranium oxide powders in n-trimethyl-n-butylammonium bis(trifluoromethanesulfonyl)imide ( $[\text{Me}_3\text{N}^n\text{Bu}][\text{TFSI}]$ ) ionic liquid (Solvionic, 99% purity) was conducted using a compressed air feed (Airgas Breathing Grade Air set to flow at ~1-2 L/min (19.5%-23.5% oxygen, 76.5%-80.5% nitrogen with trace amounts of  $\text{CO}_2$  and  $\text{H}_2\text{O}$  likely present); and an ozone generator, (model Ozone Solutions OZV-8 set to maximum ozone output for this generator) producing approximately 2.2 g of ozone per hour. The influence of acid (HTFSI) on the dissolution time was examined. However residual acid and water can hinder the eventual deposition of uranium due to hydrogen evolution. In addition, the presence of water in the solution increases the dissolution time. For comparison, pure oxygen feed gas does not result in dissolution with extended exposure times.

The compressed air is fed directly into the ozone generator described in more detail below. The ozone/air mixture is then bubbled into a sealed reaction vessel with an output to release the off-gas. The reaction vessel is monitored visually, and aliquots can be removed for liquid scintillation counting (LSC). Inside the reaction vessel are the uranium compound and the ionic liquid, with a stir bar to ensure that the uranium oxide is being constantly mixed into the solution until it is fully dissolved. For example, the exact masses of each oxide and the IL needed to make a 25 mM solution is shown in Table 2.1.

Table 2.1: Mass and volume specifications for 25 mM final uranyl concentration

Compound	Mass (g)	Mass IL (g)	Volume IL (mL)	Concentration (M)
U <sub>3</sub> O <sub>8</sub>	0.1403	28.20	20.00	0.025
UO <sub>2</sub>	0.1350	28.20	20.00	0.025
UO <sub>3</sub>	0.1430	28.20	20.00	0.025

### 2.2.1 Ozone Generator Use for Dissolution

The generation of ozone from air occurs through the process of coronal discharge. A heated plasma corona ionizes gas molecules into component parts, turning O<sub>2</sub> molecules into oxygen radicals. When supplied with breathing air as the feed gas, the ozone generator also ionizes the nitrogen and water present in the compressed air feed. While some oxygen radicals combine with O<sub>2</sub> molecules to form ozone, other molecules such as OH<sup>-</sup> and nitrogen oxides will also form. These components have a stabilizing effect on the ozone.<sup>43</sup> This could be why only compressed air feed gas can be used for dissolution, as pure oxygen gas does not contain these stabilizing species. The instrument used in this research is an OZV-8 from Ozone Solutions. The rate of ozone production and density for this model is shown in Figure 4.<sup>44</sup>

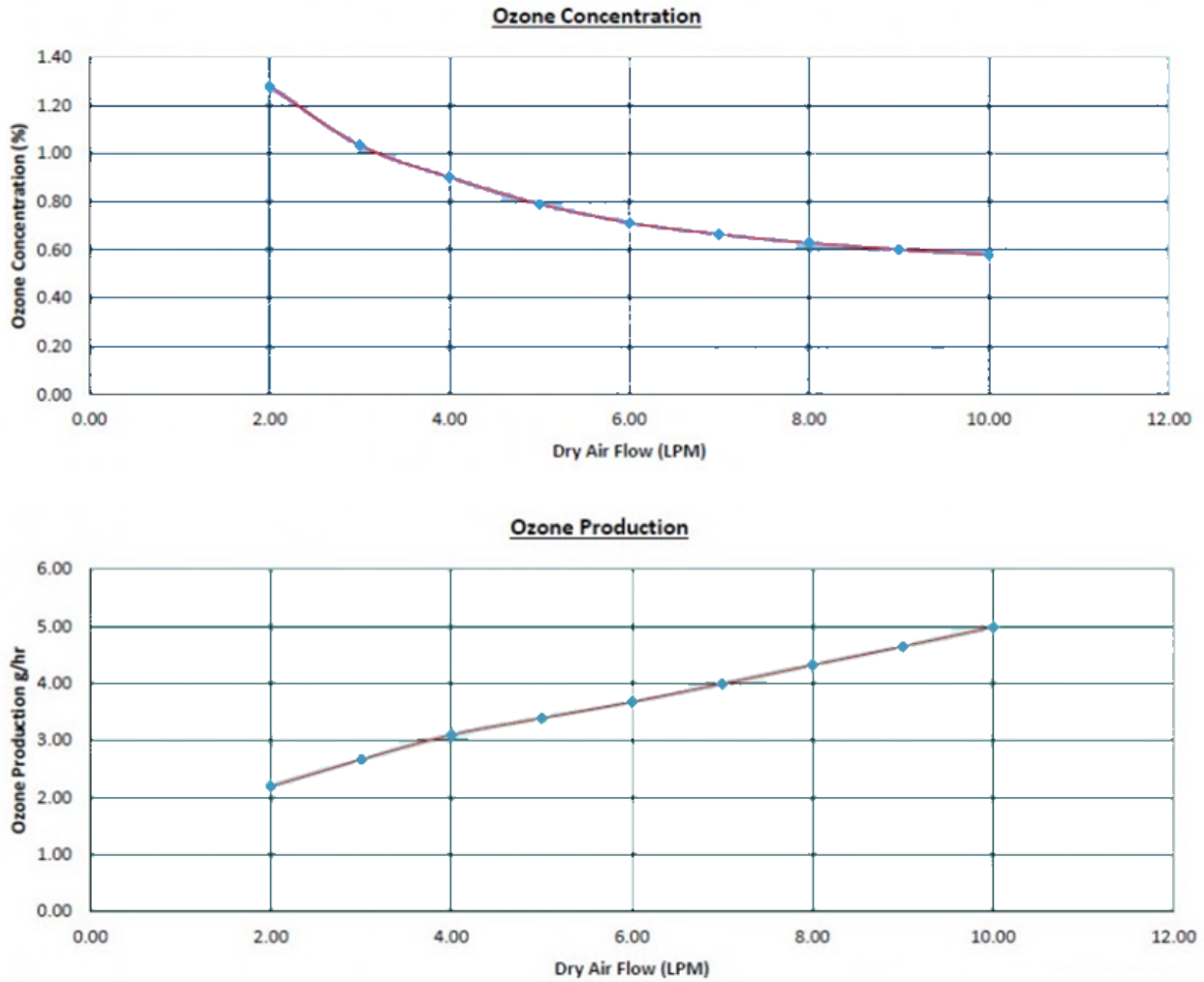
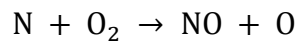


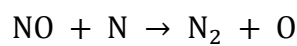
Figure 4: Ozone Concentration (top) and Ozone Production (bottom) in dry air flow

The ozone then reacts with the uranium oxide particles by indirect and direct methods.

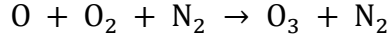
Stabilizing side reactions include the following:



Eq. 2.2

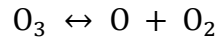


Eq. 2.3



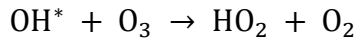
Eq. 2.4

The data suggests that the presence of nitrogen in compressed air feed gas promotes the dissociation of oxygen, and creates additional pathways for ozone formation. This increase in the overall efficiency of ozone generators when a portion of the feed gas is nitrogen has been reported.<sup>45</sup> The reactions taking place in an ozone generator are complex and compounding. The overall reaction is:

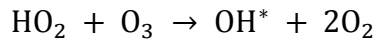


Eq. 2.5

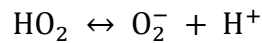
It is possible that the ozone also interacts with other species in solution from the ozone generator. The indirect reactions are the following:<sup>46,47</sup>



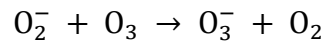
Eq. 2.5a



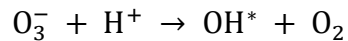
Eq. 2.5b



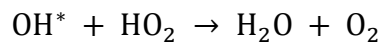
Eq. 2.5c



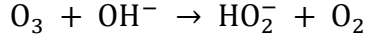
Eq. 2.5d



Eq. 2.5e



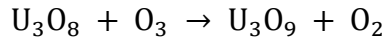
Eq. 2.5f



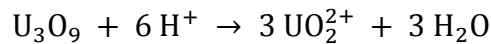
Eq. 2.5g

All of these species exist in solution with the uranium oxide compounds. The full dissolution equations for each compound are shown below, with the final product in each case is uranyl ( $\text{UO}_2^{2+}$ ) as shown below. The uranyl cations dissolved in solution can then be analyzed spectroscopically.

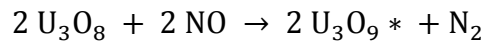
With  $\text{U}_3\text{O}_8$  specifically, there are two direct dissolution reactions where the products of ozone generation oxidize the whole compound to an unstable intermediate compound  $\text{U}_3\text{O}_9$  which then quickly decomposes in the presence of  $\text{H}^+$  to form uranyl and water and off-gasses oxygen or nitrogen. These are shown in equations 2.6a, 2.6b, 2.7a, and 2.7b. The indirect reaction, where ozone breaks apart the  $\text{U}_3\text{O}_8$  compound first and then ozone and other species continue reacting until the compound is fully dissolved as uranyl, is shown in equation 2.8.



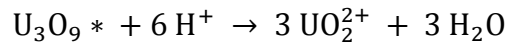
Eq. 2.6a



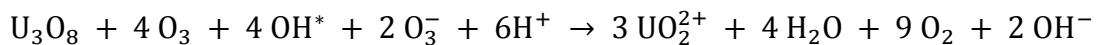
Eq. 2.6b



Eq. 2.7a



Eq. 2.7b



Eq. 2.8



The dissolution of  $U_3O_8$  in IL was performed at room temperature using bubbled ozone produced from compressed air gas. The dissolution was also performed with excess HTFSI, the acid form of the IL anion, and in water saturated IL. The ozone is made from the dry air via the use of a corona discharge ozone generator (Ozone Solutions OZV-8 generator) at  $\sim 2L/min$  at the ozone level 10 (maximum for this generator) producing approximately 2.2 g of ozone per hour. The feed gas is dry Airgas Breathing Grade Air (19.5%-23.5% oxygen, 76.5%-80.5% nitrogen with trace amounts of  $CO_2$  and  $H_2O$  likely present) which was injected into the sample with nonreactive teflon tubing.

To prepare a sample, the  $U_3O_8$  was added directly to the IL as a fine powder. Then the vessel was enclosed to control the inlet of ozone and direct the neutralized air to an external bubbler of water. The dry IL was used directly from an unopened container. The acid HTFSI, a water sensitive solid, was added directly to make the two acidic samples prior to the addition of  $U_3O_8$ . The water saturated samples were created by taking the neat, dry IL and contacting it with an equal volume of deionized ultrapure water. This resulted in an emulsified sample which slowly separated into two layers. The IL was removed by pipette and used to make the two water saturated samples. Four separate IL samples were created for dissolution. Sample A contained only the neat, dry IL. Sample B contained both the acid HTFSI at 0.5 M and was water saturated. Sample C did not contain acid, but was water saturated. Sample D was prepared to be 0.5 M HTFSI in the neat, dry IL. The masses of  $U_3O_8$ , IL, and HTFSI used in each sample are listed in Table 1. Each sample was monitored for 72 hours, though visible dissolution occurred between 24-48 hours.

Table 1: U<sub>3</sub>O<sub>8</sub> sample make-up

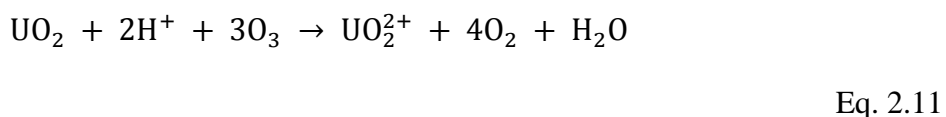
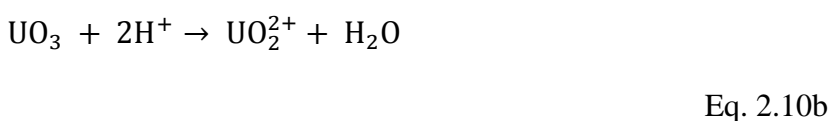
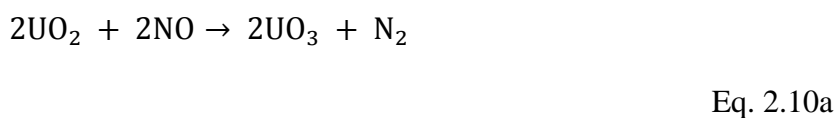
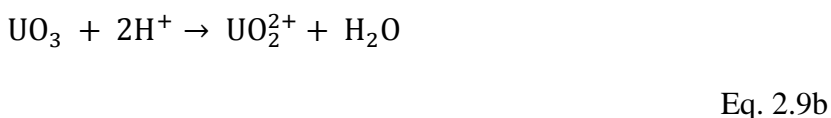
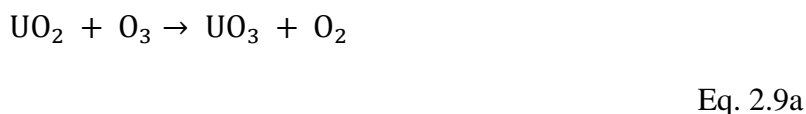
Sample	U <sub>3</sub> O <sub>8</sub> mass (g)	IL mass (g)	UO <sub>2</sub> <sup>2+</sup> Conc. (M)	HTFSI mass (g)/Conc. (M)	Water?
A	0.13532	25.4646	0.02670	No acid	No
B	0.14098	28.9	0.02451	2.92 / 0.5067	Yes
C	0.14275	29.46	0.02434	No acid	Yes
D	0.15157	29.14	0.02613	2.95 / 0.5077	No

Additionally, another sample was prepared to test the solubility limit of U<sub>3</sub>O<sub>8</sub> in the IL, with a goal of creating a 1 M concentration sample. For this sample, 2.8312 g of U<sub>3</sub>O<sub>8</sub> was placed in 15.08 g (10.70 mL) of the clean, dry IL and was dissolved using the same method over a period of five days. A small amount of material was not dissolved after that time. The final concentration was determined to be 0.94 M.

A sample was also generated from the synthesized U<sub>3</sub>O<sub>8</sub> product with the U-233 addition in order to monitor the speed of dissolution. This sample contained 0.1524 g U<sub>3</sub>O<sub>8</sub> into 28.20 g IL, for a concentration of 0.027 M uranyl in the final solution. To determine the dissolution over time, aliquots of ~100 μL were removed from the sample at the following time intervals from the start of dissolution (meaning the time from the start of ozone flow into the sample): 30 minutes, 1 hour, 2 hours, 4 hours, 6 hours, 9 hours, 12 hours, 24 hours, 30 hours, 36 hours, and 48 hours. Each aliquot was prepared as described below for liquid scintillation counting.

By comparison, UO<sub>2</sub> doesn't need to have any molecular bonds broken, so the direct reaction only serves to oxidize the uranium from U(IV) to U(VI). This is shown in equations 2.9a

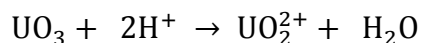
and 2.9b with ozone and 2.10a and 2.10b with nitric oxide. The indirect ozone reaction (in a simplified form, where the side reactions that produce the same species used as reactants) is shown in equation 2.10. This shows the need for side reactions and other compounds to stabilize the reaction.



The dissolution of  $\text{UO}_2$  in IL has been performed at room temperature using bubbled ozone produced from compressed air gas. The dissolution has also been performed with excess HTFSI, the acid form of the IL anion, and in water saturated IL. The ozone is made from the dry air via the use of a corona discharge ozone generator (Ozone Solutions OZV-8 generator) at ~2L/min at the ozone level 10 (maximum for this generator) producing approximately 2.2 g of ozone per hour. The feed gas is dry Airgas Breathing Grade Air (19.5%-23.5% oxygen, 76.5%-80.5% nitrogen with trace amounts of  $\text{CO}_2$  and  $\text{H}_2\text{O}$  likely present) which was injected into the sample with nonreactive teflon tubing.

A sample was also generated from the synthesized  $\text{UO}_2$  product with the U-233 addition in order to monitor the speed of dissolution. This sample contained 0.1472 g  $\text{U}_3\text{O}_8$  into 28.55 g IL, for a concentration of 0.0269 M uranyl in the final solution. To determine the dissolution over time, aliquots of  $\sim 100 \mu\text{L}$  were removed from the sample at the following time intervals from the start of dissolution (meaning the time from the start of ozone flow into the sample): 30 minutes, 1 hour, 2 hours, 4 hours, 6 hours, 9 hours, 12 hours, 24 hours, 30 hours, 36 hours, and 48 hours. Each aliquot was prepared as described below for liquid scintillation counting.

$\text{UO}_3$  dissolution is unique compared to the others, because the uranium doesn't need to be oxidized, and NO gas will not add another oxygen to the compound in the presence of ozone. This means that there is no direct oxidation reaction occurring where the ozone or a generator by-product donates and oxygen to form an intermediary species. However, there is an indirect reaction where hydrogen can react with the  $\text{UO}_3$  to dissolve the compound. As shown in equation 2.11, this reaction proceeds without ozone, so long as the hydrogen ions are provided in solution.



Eq. 2.11

The final product for each reaction, regardless of direct/indirect or which specific ozone generator product gas is used results in  $\text{UO}_2^{2+}$  (uranyl) in solution, which can be analyzed spectroscopically.

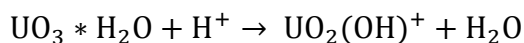
The dissolution of  $\text{UO}_3$  in IL was performed by two different methods. First, at room temperature using bubbled ozone produced from compressed air gas. The ozone was made from the dry air via the use of a corona discharge ozone generator (Ozone Solutions OZV-8 generator) at  $\sim 2\text{L}/\text{min}$  at the ozone level 10 (maximum for this generator) producing approximately 2.2 g of ozone per hour. The feed gas is dry Airgas Breathing Grade Air (19.5%-23.5% oxygen, 76.5%-

80.5% nitrogen with trace amounts of CO<sub>2</sub> and H<sub>2</sub>O likely present) which was injected into the sample with nonreactive teflon tubing. In this sample, ozone acted only as a physical agitator in solution as compared to a direct oxidizing agent, while the flowing gas also provided water continuously into the solution, plus side products of the ozone generator such as H<sup>+</sup>. A sample was also generated from the synthesized UO<sub>3</sub> product with the U-233 addition in order to monitor the speed of dissolution. This sample contained 0.1416 g UO<sub>3</sub> into 28.25 g IL, for a concentration of 0.0247 M uranyl in the final solution. To determine the dissolution over time, aliquots of ~100 μL were removed from the sample at the following time intervals from the start of dissolution (meaning the time from the start of ozone flow into the sample): 30 minutes, 1 hour, 2 hours, 4 hours, 6 hours, 9 hours, 12 hours, 24 hours, 30 hours, 36 hours, 48 hours, 54 hours, 60 hours, and 72 hours. Each aliquot was prepared as described below for liquid scintillation counting. As demonstrated with U<sub>3</sub>O<sub>8</sub>, UO<sub>3</sub> was observed to dissolve directly into the IL under ozone flow generated from compressed air. The sample dissolved over approximately 48-60 hours.

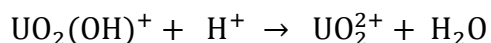
Second, the dissolution was also performed with ten times molar excess HTFSI (0.25 M in solution), the acid form of the IL anion, in water saturated IL with no ozone (UO<sub>3</sub> mass 0.1430 g in 28.20 gIL for a final 0.025 M sample.) Attempts to dissolve a UO<sub>3</sub> sample without ozone were successful, but required the presence of HTFSI acid and water and took 2-3 times longer to visually dissolve than an ozonated sample. Four identical UO<sub>3</sub> samples were created with different IL conditions. Only the sample that contained water saturated IL and HTFSI dissolved over the week of observation. The samples containing only acid, only water, and no acid or water did not dissolve. The sample containing water but no HTFSI acid did undergo a color change of the undissolved material, indicating a chemical reaction, but no dissolution was observed. This is

consistent with other studies, which found no solubility of  $\text{UO}_3$  in neat IL, but were able to dissolve the material in wet IL with nitric acid after complexing the  $\text{UO}_3$  with HTFSI.<sup>48</sup>

However, the HTFSI acid is not strong enough to drive this reaction without the complexation with water. This dissolution reaction takes advantage of the gaseous side reactions happening in solution to dissolve the  $\text{UO}_3$  by complexing with water. It has been shown that this complex can form in perchloric acid, resulting in an equilibrium with hydroxide.<sup>49</sup> With a water saturated solution and excess protons, this intermediary state quickly converts to uranyl with more water as a byproduct. Equation 2.12 shows the first step, where water complexed with the  $\text{UO}_3$  can dissociate to form a hydroxide complex, and equation 2.13 shows acid interacting with the polar molecule to form water and the dissolved uranyl.



Eq. 2.12



Eq. 2.13

## 2.3 Instrumental Analysis of Dissolved Uranyl Samples

### 2.3.1 UV-Vis Spectroscopy

Ultraviolet-Visible spectroscopy (UV-Vis) analyzes the interaction between a standard light source and the sample to determine the identity and concentration of that sample. The lamp (tungsten, mercury, or deuterium for various light ranges) provides a steady light source, which is directed using optical mirrors. These mirrors bounce the light to a monochromator, which filters out background noise by focusing the beam through a diffraction grating. The diffraction

grating directs unwanted light away from the beam path, narrowing the range of light allowed to hit the sample. This increases the precision of the instrument because the beam is more specific than full spectrum white light. The beam is then split into two separate channels, allowing for interaction with the unknown sample as well as a blank or calibration standard. This is known as double beam mode and is another method of noise reduction, as any electronic noise will be equally present for both measurements and can thus be removed. The sample may then absorb some or all of the beam, while the remaining light passes through. The light absorbed by the sample causes excitation of the electrons present in solution. The de-excitation of these electrons emits a characteristic spectrum of radiation. The ratio of the light that passes through the sample to the detector and the full possible intensity of the beam if there were no absorption represents the transmittance of the sample. Equation 2.14 shows the Beer-Lambert Law relating transmittance and absorption.<sup>50</sup>

$$A = -\log(T) = \epsilon bc$$

Eq. 2.14

In this equation, T represents the transmittance of the sample, the unitless ratio of the light intensity passing through the sample over the maximum beam intensity. A represents the absorbance, which is also unitless.  $\epsilon$  is the molar absorptivity constant, in units of L/(mol\*cm), and is an inherent property of the sample and matrix; b is the pathlength of the sample cell in cm (a 1 cm length sample cell is the standard for use); and c is the concentration of the sample in mol/L.

Figure 5 shows the internal schematic of the instrument used, a Cary6000 UV-Vis-Near IR spectrophotometer.<sup>51</sup> All UV-Vis spectroscopy was performed with sealed optical quartz

cuvettes, with a clean, dry IL blank sample for comparison. The range analyzed for the samples was 200-1600 nm, at a scan rate of 200 nm/minute.

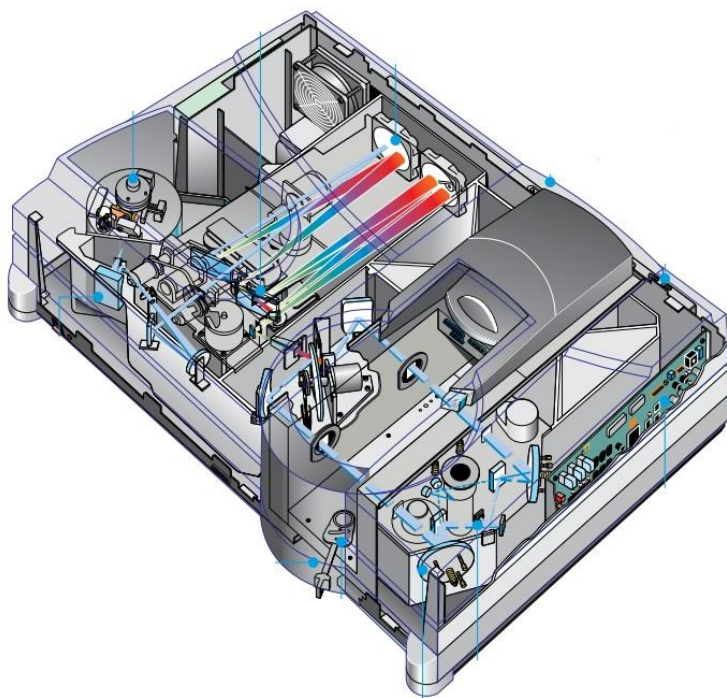


Figure 5: Internal Schematic of a Cary6000 UV-Vis Spectrophotometer<sup>51</sup>

### 2.3.2 Liquid Scintillation Counting

Unlike UV-Vis spectroscopy which can identify a liquid sample, liquid scintillation counting (LSC) can determine the alpha and beta radioactivity of a sample. LSC is a counting technique that uses an internal detector within the sample to determine the radiation present. A scintillator is an organic compound that emits light when it interacts with radiation. For LSC, the scintillator is an organic liquid cocktail that the liquid radioactive sample is mixed with inside a



proper LSC vial. This allows for full geometry of counting, as the radiation detector is fully surrounding the sample and radiation emitted in any direction will interact with the scintillator. The light emitted from this interaction is then directed to a photomultiplier tube which creates an electronic signal that can be counted by the computer. Some LSC detectors make use of two opposite facing PM tubes. A true signal from the scintillator would be seen by both tubes, whereas electronic noise in the tube itself would only show in one of the two tubes. This setup, called coincidence counting, reduces electronic or instrumental noise which is the largest source of error for LSC detection. Because the instrument is so sensitive to radiation and the sample geometry is fully spherical the efficiency of the detector is very high - approaching 100%. This makes LSC an excellent technique for low energy radiation or low activity samples. Lower activity requires longer count times to ensure that enough raw counts are detected to be statistically significant. Adding a small amount of a higher activity isotope, such as the process described previously, reduces the count time needed to ensure the sample has been counted properly. Ionic liquid samples are suited for LSC detection since the IL is an organic compound and doesn't require any additional mixing or added emulsifiers to be integrated into the LSC cocktail.

While the efficiency of the detector is very high, internal sample effects can reduce the accuracy of the instrument. This effect, called quenching, is a matrix effect where the sample itself can absorb the light emitted by the scintillator. This can be subtracted manually from the sample by creating a blank that includes the sample solvent and any other additives except the radiation emitter to approximate the quenching effect. It is also standard procedure to run known standard samples in the same run as any unknown samples, as part of a quality control measure.

The counts detected for these samples can be compared to known values to confirm the efficiency of the detector.<sup>52</sup>

Aliquots of in-progress and dissolved  $U_3O_8$ ,  $UO_2$ , and  $UO_3$  samples were taken for liquid scintillation counting to determine the activity (and thus the rate of dissolution over time). These samples were removed by micropipette at  $\sim 100 \mu\text{L}$  at each time point. Samples were centrifuged at 4000 rpm for 5-10 minutes, depending on the opacity of the solution. The liquid was then removed and added to a plastic scintillation vial while the undissolved solid was returned to the original sample. The scintillation vial was filled with 10 mL of Ultima Gold scintillation cocktail and massed prior to the addition of each solution aliquot. The vial was then massed a second time to determine the mass of the aliquot added. This mass was then used to normalize each sample in the set when determining the activity. When the dissolution was complete, the samples were analyzed using a Beckman LS 6500 liquid scintillation counter for 10 minutes in triplicate counting. This method calculated the average activity of each sample, which could then be normalized by mass and plotted to determine the rate of dissolution.

## 2.4 Electrochemical Analysis

The dissolution of uranium oxides into ionic liquids provides a system for direct electrochemical analysis. An ionic liquid solvent acts as an electrolyte for charge transport. The IL also allows for a wider voltage range (compared to an aqueous solution) that can be applied to the system without causing hydrolysis, which can interfere with deposition of uranium. This, plus the advantage of using ozone to dissolve with no added compounds aside from water, means that the uranyl solutions are free from impurities and can be analyzed via different electrochemical techniques. The techniques described here used a three electrode cell set up for all analyses.

Charge transfer through an ionic solution must include a working electrode, a counter electrode, and a reference electrode connected to a potentiostat that can apply a known voltage to the system. The current flows between the working and counter electrodes, with reduction occurring at the working electrode or cathode for deposition experiments and oxidation occurring at the counter electrode or anode for deposition experiments. The reference electrode is important for measuring the current, as it is non-inhibitive and creates no resistance that would alter the current as it is measured.<sup>53</sup>

A functional reference electrode must match the solution it is placed in. For ILs, this means making a non-aqueous electrode with the same IL as the base solution. This is done by using a base electrode kit with a silver wire, a permeable membrane tip, contained in a glass casing. This is then filled with a solution of dilute  $\text{Ag}^+$  ions, which is made by dissolving  $\text{AgCl}$  or  $\text{AgNO}_3$  in a minimum volume of acetonitrile, and then diluting the solution in the base IL to a final  $\text{Ag}^+$  concentration of 0.1 M. To be a viable reference electrode, it must then be tested against a ferrocene solution. The ferrocene cation has a known reduction potential compared to a standard hydrogen electrode (SHE), which is a universal standard measurement. The difference between the ferrocene cyclic voltammogram with an SHE reference and the measured voltammogram with the created reference electrode represents a potential shift that can then be applied to any sample in order to compare to known standard reduction potentials.<sup>54</sup>

The electrochemical analyses (cyclic voltammetry, amperometric deposition, and pulse deposition) were performed on a CH Instruments 760C potentiostat and software in a three electrode cell. The working electrode was gold foil or gold mesh from Alfa Aesar cut from sheets to approximately  $1 \text{ cm}^2$  size. The reference electrode was made using a glass tube with Vycor semi-permeable frit, and a silver wire in contact with 0.1 M  $\text{Ag}^+$  solution.<sup>55</sup> The counter

electrode was a platinum sheet with size in excess of the working electrode. Reference electrodes were calibrated using a solution of 55 mM ferrocene dissolved in IL and the resulting voltammograms were adjusted by +0.618 V for  $U_3O_8$ , +0.623 V for  $UO_2$ , and +0.536 V for  $UO_3$  relative to an Ag/AgCl reference voltage.

#### 2.4.1 Cyclic Voltammetry

Cyclic voltammetry is a technique to analyze the composition and concentration of ions in a solution. In this technique, a voltage scan is performed where a starting voltage is applied to the system and is then increased or decreased at a specified scan rate while the current is measured. The resulting diagram shows the current response on the y-axis and the applied voltage on the x-axis. An example of this is shown in Figure 6.

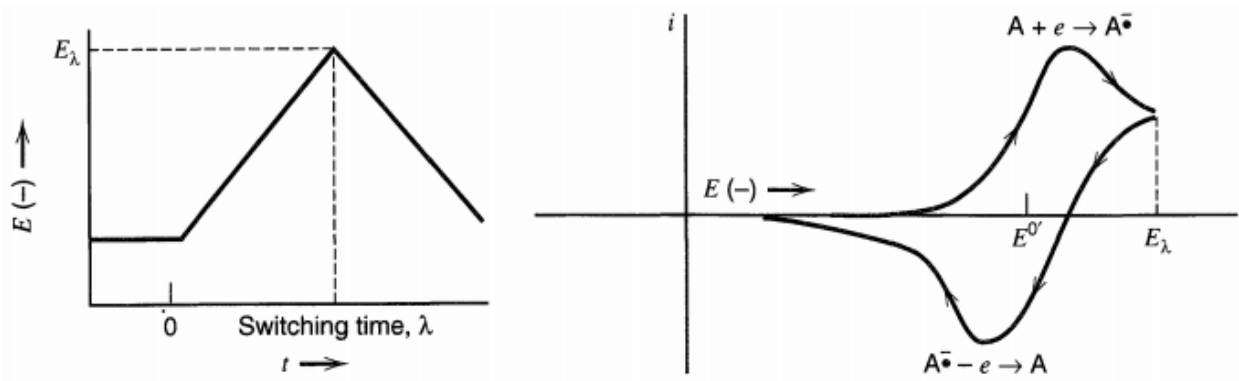


Figure 6: Voltage change over time, and the resulting voltammogram showing a typical current response<sup>13</sup>

The first diagram shows the voltage becoming increasingly negative until the switching time is reached. This switching time represents the maximum negative potential that will be

applied to the system. This appears on the voltammogram to the right as the top half of the sweep where species in solution are being reduced. The voltage is then increasingly positive until the starting potential is reached, seen on the voltammogram as the bottom half of the sweep where species in solution are being oxidized. A peak will appear on the voltammogram every time a species in solution undergoes a change in oxidation state.

An ideal, or Nernstian, solution is one where the kinetics of the electron transfer are fast enough to ensure equilibrium between the oxidized species and the reduced species. The cell potential of such a solution can be determined by Equation 2.7.

$$E = E_0 + \frac{RT}{nF * \ln\left(\frac{C_o}{C_r}\right)}$$

Eq. 2.7

Here, E is the cell potential in V,  $E^0$  is the standard reduction potential of the species being calculated in V, R is the gas constant of 8.314 J/mol\*K, n is the number of electrons being exchanged, T is the temperature in K, F is the Faraday constant of 96,500 J/(V\*mol),  $C_o$  is the concentration of the oxidized species and  $C_r$  is the concentration of the reduced species in any concentration unit. This determines the potential shift of the peaks.

The intensity of the peaks on a CV diagram is dependent on multiple properties of the solution. Assuming an ideal Nernstian solution, the peak current can be determined as shown in equation 2.8, with proportionality dependent on the temperature.

$$I_p \propto n^{3/2} * A * D_o^{1/2} * C_o * v^{1/2}$$

Eq. 2.8

Where  $I_p$  is the current in Amps, n is the number of electrons exchanged in the redox reaction being measured, A is the surface area of the working electrode in  $\text{cm}^2$ ,  $D_o$  is the

diffusion coefficient (an inherent property of the solution) in  $\text{cm}^2/\text{s}$ ,  $C_o$  is the concentration of the oxidized species in  $\text{mol}/\text{cm}^3$ , and  $v$  is the scan rate in  $\text{V}/\text{s}$ . Each peak will vary based on these factors and the reversibility of the system. A reversible reaction will show equal peaks for oxidation and reduction for a given electron exchange in equilibrium. An irreversible reaction will show only the one peak for the kinetically favorable electron transfer. A quasi-reversible reaction will show a diminishing peak over time as the reaction proceeds and one species is slowly consumed and the other slowly grows in concentration.<sup>13</sup> Once a solution has been analyzed by CV, it is ready for deposition.

#### 2.4.2 Deposition Techniques

There are two main deposition techniques used in this research - amperometric or bulk deposition and pulse voltammetry deposition. Amperometric deposition uses a single potential negative enough (approximately -3 V) to reduce the uranyl in solution to uranium oxide on the electrode surface. The half-cell reactions showing the standard reduction potentials of the species in solution are shown below.<sup>56</sup>



This is usually done over a period of 24 hours and can be done multiple times in succession without stirring using simple diffusion. The advantage of this technique is that the potential is set below the standard reduction potential for the cations in solution to be reduced and deposited on the electrode. The disadvantage of this technique is that extended time under negative potentials can cause damage to the IL solvent, eventually diminishing the ability of the solution to continue to deposit as the IL breaks down. When a negative potential is applied to the working electrode, positive ions in solution are drawn to that surface and given sufficient potential will deposit there. A “double layer” is formed extending out from the negatively charged electrode where the positive ions are attracted to the negative region, and negative ions (the anion base of the IL) are attracted to the concentrated positive ions. Outside of that layer, the bulk of the solution remains unaffected by the electrode. At -3 V the cations in the diffusion layer are quickly depleted, and it takes additional time to reach the bulk solution to draw more cations to the electrode for deposition. For a viscous sample such as an IL, the time for charge transfer to bring more cations to the electrode surface is even greater, meanwhile, hydrogen evolution could be occurring at the electrode surface. In order to continue deposition in a uniform manner, the double layer must be replenished with fresh cations.<sup>13</sup>

A suitable technique for this replenishment is pulse voltammetry, which takes advantage of the inherent diffusion layer present in the IL solution. With pulse voltammetry, a negative potential is applied to the system for a short time, followed by a longer pulse of a less negative (or even positive) potential. This allows the depletion zone to replenish with new cations, which are then deposited on the electrode. The advantage of this technique is that more of the solution is available for deposition. The disadvantage is that the technique makes use of several parameters: at least two different potentials, sometimes more if using the “staircase” method

where the potential is increased in steps; the time of each pulse; and the number of cycles of pulses. These parameters can be solution specific, and more exploration is needed to ensure optimum performance compared to only needing a single voltage and time for amperometric deposition. However, the deposits from pulse voltammetry are usually more homogeneous and even than those formed from bulk deposition. These deposits are suited for solids analysis techniques.<sup>57</sup>

## 2.5 Solids Analysis Techniques

### 2.5.1 Powder X-Ray Diffraction (PXRD)

For solids with a defined crystalline structure, powder X-ray diffraction (PXRD) can be used to identify the compound, phase, and lattice parameters. This technique was used to confirm the success of uranium oxide compound synthesis, however, solid deposits generated from electrodeposition were found to be too amorphous for PXRD analysis. PXRD makes use of an X-ray generator placed in a collimator and directed at a movable sample stage. The sample stage can rotate a sample through a wide angle rotation perpendicular to the collimator. The X-ray beam is aimed at the sample stage, and interacts with the sample by diffraction off the atoms in the crystal lattice. These X-rays are diffracted at an angle  $\theta$  in a pattern expressed by Bragg's Law in Equation 2.9.

$$n * \lambda = 2d * \sin(\theta)$$

Eq. 15

Here,  $n$  is an integer value,  $\lambda$  is the wavelength of the X-ray beam,  $d$  is the distance between each layer of the lattice structure, and  $\theta$  is the angle of diffraction. The detector combines the X-rays taken over the full angle spectrum to create a spectrum that can then be compared to a database of known compounds.<sup>10</sup> The PXRD instrument used for this dissertation



was a Bruker D8 Advance powder X-ray diffractometer. Synthesis product samples were analyzed for powder X-Ray Diffraction, from 10-120° 2 $\theta$ . Patterns were analyzed using Bruker TOPAS software. Deposition samples were analyzed using the same method, but no pattern was observed as deposits were too amorphous.

### 2.5.2 Scanning Electron Microscopy and Energy Dispersive X-Ray Spectroscopy

For solid samples with any structure, crystalline or amorphous, Scanning Electron Microscopy/Energy Dispersive X-Ray Spectroscopy (SEM/EDS) analysis can provide high magnification imagery and elemental analysis. The SEM works by focusing a high intensity (15 keV) electron beam onto a conductive sample. The electrons are then scattered or absorbed (which results in secondary electrons being produced from the sample) and the surrounding detector collects the signal. A black and white image is formed based on the scatter pattern, with the ability to magnify in excess of 1000x depending on the instrument and the quality of the sample. Uranium oxides are inherent semiconductors, which means no additional conductive coating needs to be applied to gather an image of the sample. Another component of SEM analysis is Energy Dispersive X-Ray Spectroscopy. EDS makes use of the electrons absorbed by the sample, which then generate X-rays from de-excitation. These X-rays are detected by a silicon or other semiconductor detector, and are characteristic of a given sample. The X-ray spectrum can then be used to semi-quantitatively identify the elemental makeup of the sample.<sup>10</sup> The images obtained by scanning electron microscopy (SEM) and the energy dispersive X-ray spectroscopy (EDX) were from a JEOL-5610 instrument with backscatter and secondary electron detection and a silicon detector for elemental analysis. The accelerating voltage used was 15-16 kV. The sample stage was an aluminum base, and samples were affixed using carbon tape. No conductive coating was necessary for analysis.

## Chapter 3

### Abstract

$U_3O_8$ , is a form of uranium oxide important to the nuclear fuel cycle with limited solubility. However, the oxide was dissolved direction into n-trimethyl-n-butylammonium bis(trifluoromethanesulfonyl)imide, or  $[Me_3NnBu][TFSI]$ , ionic liquid using ozone generated from compressed air. The synthesized  $U_3O_8$  was confirmed by PXRD analysis prior to dissolution using multiple conditions into IL. Dissolution was monitored over time with LSC analysis. Fully dissolved samples were analyzed by UV-Vis spectroscopy and cyclic voltammetry. Electrochemical deposition techniques were applied to recover uranium oxide from solution, which was confirmed by SEM/EDX. The final product is indicated to be amorphous uranium oxide, most likely  $UO_2$  from the two electron reduction of  $UO_2^{2+}$ .

### 3.1 Introduction

The continued need of uranium oxides for the nuclear fuel cycle combined with the lack of current reprocessing of spent nuclear fuels in the United States suggests that the current stockpile is not a strategic material. More over the stockpile is not being used in the recovery of strategically important materials including unspent nuclear fuel. In particular,  $U_3O_8$  is the thermodynamically favored state of uranium oxide material and a common compound in processing and storage of nuclear materials. However,  $U_3O_8$  has limited solubility in water or organic solvents, requiring high concentrations of acid to be fully soluble. There are multiple established methods of dissolution for f-block elements and oxides, including concentrated acid dissolution (as seen in PUREX processes<sup>58,59</sup>) and high temperature melting (such as in molten salt reactors<sup>60,61</sup>).

Yet neither of these methods is suitable for electrochemical study or recovery of the actinide species. The ideal solvent for actinide electrochemistry would be non-aqueous, as an aqueous solution undergoes hydrolysis under electric current before the necessary reduction potentials can be reached. The limits of an aqueous solution are approximately +1.00 V (vs. Ag/AgCl) when oxygen gas is formed from the destruction of water molecules, and -0.23 V (vs. Ag/AgCl) when hydrogen gas is evolved. Since uranium deposits at -1.61 to -1.89 V (vs. Ag/AgCl) which is far in excess of the limits of any solution containing water, deposition in an aqueous solution will be hindered or non-existent. Thus a new method of dissolution and recovery of f-element species is explored here.

When determining an ideal solvent for actinide oxides, electrochemical viability is only one characteristic. Other important properties for a solvent are that it be liquid at room temperature, non-volatile, non-toxic, and non-flammable. The sample must also be free of contaminants that would prohibit deposition or complexation species that would alter the properties of the dissolved actinide. These conditions are found in ionic liquids comprised of cation/anion pairs that can be selected for specific electrochemical windows suitable for actinide deposition. Ionic liquids, or ILs, are solutions that are typically comprised of bulky cation-anion pairs that can be varied to influence the physical properties.

ILs have been shown as viable solvents for actinide analysis through direct dissolution and the synthesis of complexed species containing common anion as ligands. However, complexation can alter the properties of the actinide, including the added difficulty in displacing the ligand during deposition (e.g. IL ligands attached to the actinide may have to be removed before the actinide can be fully reduced). For example, previous studies have shown that after complexation of uranium and lanthanide species, the coordination geometry, crystal structure,

and polymerization had changed for each base metal. In addition, these changes were unique to the IL ligand used.<sup>62</sup> In addition, studies that have utilized  $\text{Cl}_2$  as an oxidant to dissolve uranium oxide in an IL have resulted in chloride containing species in the electrochemically recovered deposits.<sup>63</sup> Complexation can also impact the electronic structure as observed through changes in the spectroscopic properties of dissolved uranyl species.<sup>64</sup> Although ILs are also miscible or semi-miscible with other organic compounds, such as acetonitrile, and can be used for liquid-liquid extraction with aqueous solvents<sup>65</sup>, the process introduces pathways for contaminants that can similarly interfere with the electrochemical analysis.<sup>66</sup>

Previous studies have shown that without acid and/or high temperatures, the direct dissolution of uranium oxides such as  $\text{UO}_2$ ,  $\text{UO}_3$ , and  $\text{U}_3\text{O}_8$  in neat ionic liquids is minimal. In contrast, the dissolution of  $\text{UO}_2$  and  $\text{UO}_3$  is possible with the addition of acid functional groups and with inclusion of water. In contrast, the addition of acid functionality and water in the dissolution of  $\text{U}_3\text{O}_8$  was shown to be ineffective for dissolution of the oxide species in IL. The development of dissolution methods applicable to all oxide species without the inclusion of secondary species which can contaminate and minimize the recovery of species is preferable. . The introduction of ozonated species in the IL that act as strong oxidizing agents to dissolve the  $\text{U}_3\text{O}_8$  without the inclusion of secondary reactive species is the solutions. The ozonated species are highly reactive and are neutralized as they are bubbled out of solution. While this process does generate a small amount of water in solution, the limited solubility of water in the IL combined with the thermal stability of the IL allow the solution to be dried using a rotavap.

The ionic liquid selected for this dissertation work is n-trimethyl-n-butylammonium bis(trifluoromethanesulfonyl)imide, abbreviated here as  $[\text{Me}_3\text{NnBu}][\text{TFSI}]$ . The useful properties of ionic liquids have been mentioned previously. In addition, the  $[\text{Me}_3\text{NnBu}]$  cation

has a wide electrochemical window capable of analysis and deposition of uranyl. The combined cation/anion pair is also relatively less viscous than some other ILs, has a low vapor pressure, and is thermally and radiologically stable. The [TFSI] anion also can be protonated to form [HTFSI], a compatible non-aqueous acid that can be added to a sample. Similarly the TFSI anion can form a stable radical when oxidized (ref). This chapter will show that the addition of a constant flow of ozone during the reaction will enable the full direct dissolution of  $U_3O_8$  at high concentrations with no chemical byproducts. The study of actinide oxides can be accomplished using a combination of solid and liquid analysis techniques. Solid analysis can confirm the identity, crystal structure, or elemental makeup of actinide species. Liquid analysis can inform research on solubility, speciation, and electrochemical properties.

To begin the analysis,  $U_3O_8$  was synthesized from uranyl nitrate hexahydrate ( $UO_2(NO_3)_2 \cdot 6H_2O$ ) with an added spike of U-233 to aid in later radiation counting. The chemical composition of the product was confirmed via powder X-ray diffraction (PXRD). The dissolution of the sample was achieved in  $[Me_3NnBu][TFSI]$ , with some samples containing added water and/or HTFSI acid. Aliquots were removed during the dissolution, centrifuged to remove any not yet dissolved solid material, and prepared for liquid scintillation counting. The final solution was analyzed by UV-Vis spectroscopy and electrochemical study by cyclic voltammetry. Deposition was achieved by both amperometric deposition and pulse deposition, with deposits analyzed by scanning electron microscopy (SEM) and elemental analysis by energy dispersive X-ray (EDX) spectroscopy. The dissolution produces  $UO_2^{2+}$  in solution and the final deposits from the electrochemical reduction of uranyl are amorphous uranium oxide, consistent with  $UO_2$ .

## 3.2 Materials

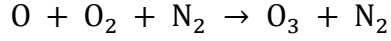
Ionic liquids were used with no alteration from the source and were trimethyl-n-butylammonium bis(trifluoromethanesulfonyl)imide, [Me<sub>3</sub>NnBu][TFSI] (Solvionic, >99.5% purity) and the protonated acid counterpart bis(trifluoromethanesulfonyl)imide [HTFSI] (Fluka, >95% purity). Ultrapure water was generated on site and obtained from laboratory stock. All other materials and instruments used are described in respective sections in chapter 2.

## Results and Discussion

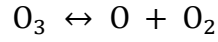
### 3.3 Synthesis and Dissolution

Direct dissolution of U<sub>3</sub>O<sub>8</sub> in aqueous solutions requires high concentrations of nitric acid and is not suitable for electrochemical deposition. However, dissolution in IL has not been shown to occur unless ozone produced from compressed air is present in the solution. With ozone present at maximum output a U<sub>3</sub>O<sub>8</sub> sample will dissolve in 24-48 hours depending on the presence of water or HTFSI acid, which were shown to slightly inhibit dissolution. Unsuccessful attempts at dissolution using the exact setup and ozone generator discussed here but using pure O<sub>2</sub> gas instead of compressed breathing air shows that some other component of air is necessary for dissolution. The major reactions occurring in the ozone generator with compressed air feed gas are as follows:<sup>67</sup>





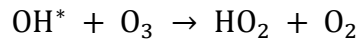
Eq. [3]



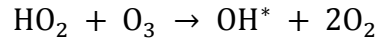
Eq. [4]

Not only does the presence of nitrogen produce gasses that add potential sources of oxygen radicals, but the gasses themselves can be oxidizing and may assist in the dissolution of  $\text{U}_3\text{O}_8$ . The nitrogen itself is a stabilizing factor for ozone.<sup>68</sup>

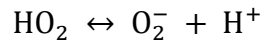
It is possible that the ozone also interacts with other species in solution produced from the ozone generator.<sup>69,70</sup> The following indirect reactions are also possible that include:



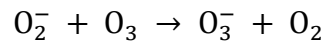
Eq. [5]



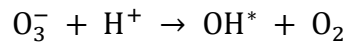
Eq. [6]



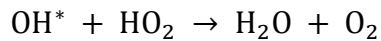
Eq. [7]



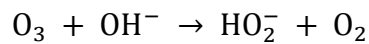
Eq. [8]



Eq. [9]

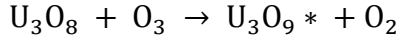


Eq. [10]

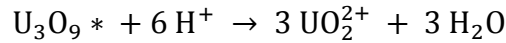


Eq. [11]

These reactions show a multiplicity of species in solution that can react with the  $U_3O_8$ , resulting in three likely mechanisms for dissolution. The first is shown in Eq. 12a and 12b. These equations show the dissolution through a radicalization mechanism exclusively using ozone. Here, the ozone directly creates an unstable  $U_3O_9^*$  radical intermediate species that quickly reacts with hydrogen cations to form uranyl and water.

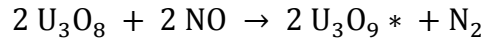


Eq. [12a]

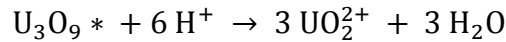


Eq. [12b]

A second possible dissolution mechanism, which has been previously suggested,<sup>71</sup> is shown in Eq. 13a and 13b. These equations show the dissolution occurring exclusively with nitric oxide gas, which then also disassociates to uranyl and water.

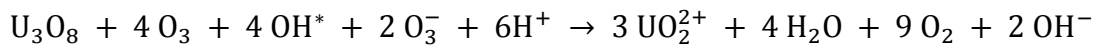


Eq. [13a]



Eq. [13b]

A third possible mechanism is shown in Eq. 14, which demonstrates the indirect dissolution of  $U_3O_8$  with ozone and other ozone generator products. In this mechanism, the  $U_3O_8$  is not radicalized but instead reacts chemically with the species in solution (as opposed to the direct charge transfer shown in previous equations).



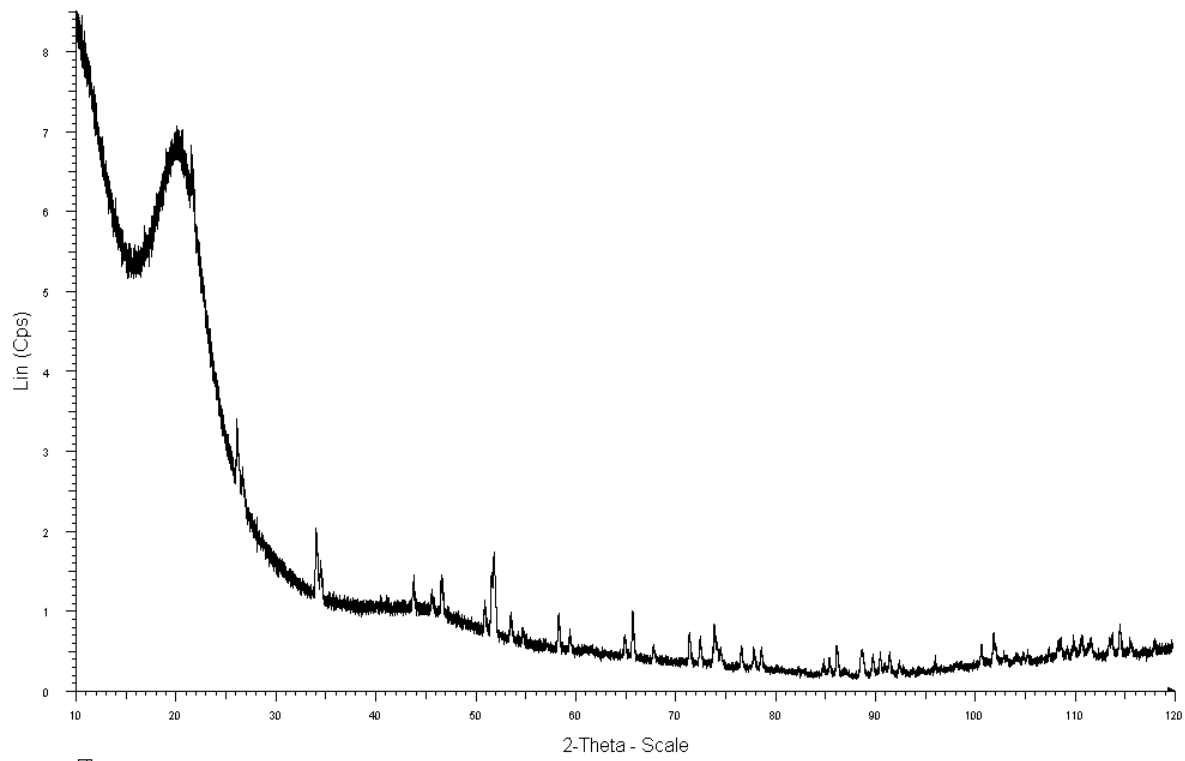
Eq. [14]



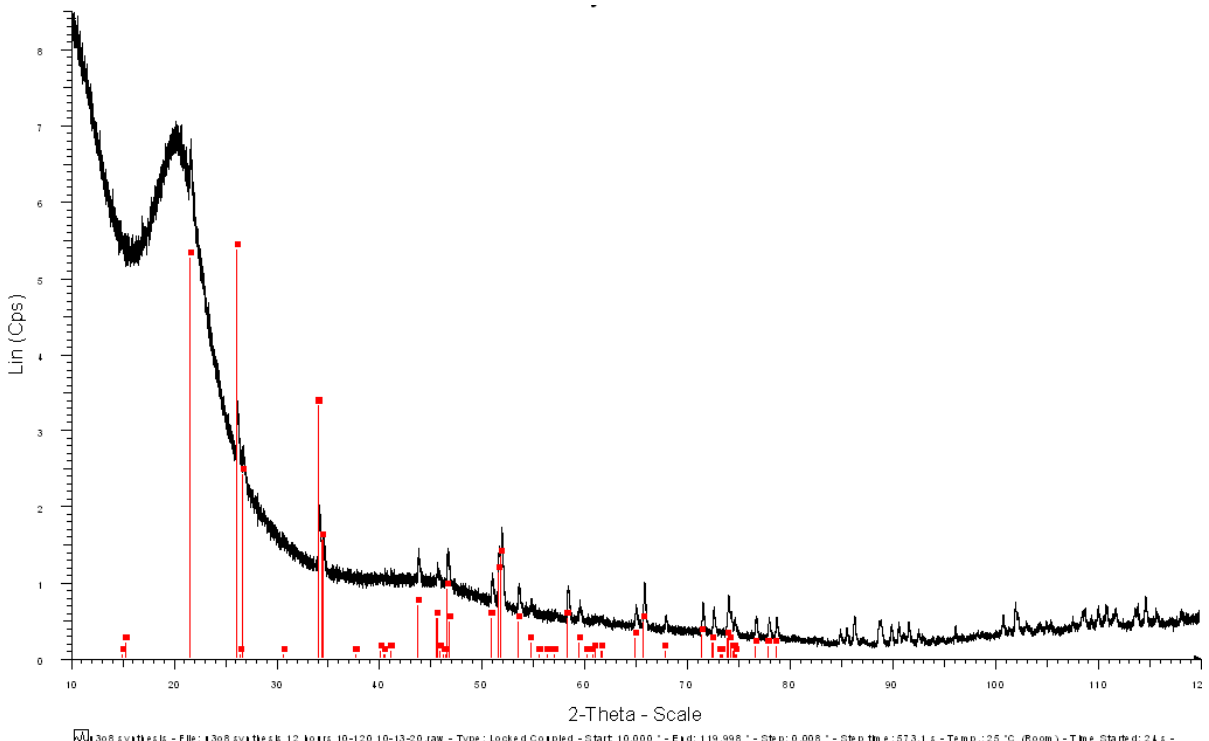
It is possible (and likely) that all three potential dissolution reactions are occurring simultaneously, along with the various side reactions from the ozone generator products. Since the side reactions are all either gaseous products that would bubble out of solution or unstable radicals that are consumed in another reaction, with the exception of water which remains in solution. The only end product is uranyl ( $\text{UO}_2^{2+}$ ) which is then analyzed by various techniques. All samples were prepared as discussed in chapter 2.

### 3.4 Powder X-Ray Diffraction

The synthesized  $\text{U}_3\text{O}_8$  was analyzed by PXRD to confirm the identity of the compound. The pattern, shown in Fig. 7, shows that the  $\text{U}_3\text{O}_8$  has an orthorhombic unit structure, consistent with the alpha phase.<sup>72</sup> Electrolytic deposits were also analyzed via PXRD to attempt to identify the compound, but no distinguishable pattern was found. This indicates that the electrolytic deposits are amorphous, meaning that no one single crystalline structure is formed during deposition. The broad peak at 20 2-theta value is an effect of the domed sample stage and is present in all PXRD sample collection presented here.



7a.



7b.

Figure 7: a) PXRD pattern of  $U_3O_8$  and b) the same pattern with software matched identity.

### 3.5 Liquid Scintillation Analysis

A sample of  $U_3O_8$  at 0.027 M final uranyl concentration was prepared for dissolution as previously described. The sample appeared to be fully dissolved visually after 24 hours (sample was clear and yellow, with no undissolved solid material). The results of LSC analysis are shown in Figure 8 below, which shows the activity of each aliquot in counts per minute per gram of IL solution taken at each time interval. The data show that the sample appears to reach saturation at 24 hours, which confirms the visual observation. The error bars on the graph were calculated as the square root of the mean number of counts after triplicate analysis.

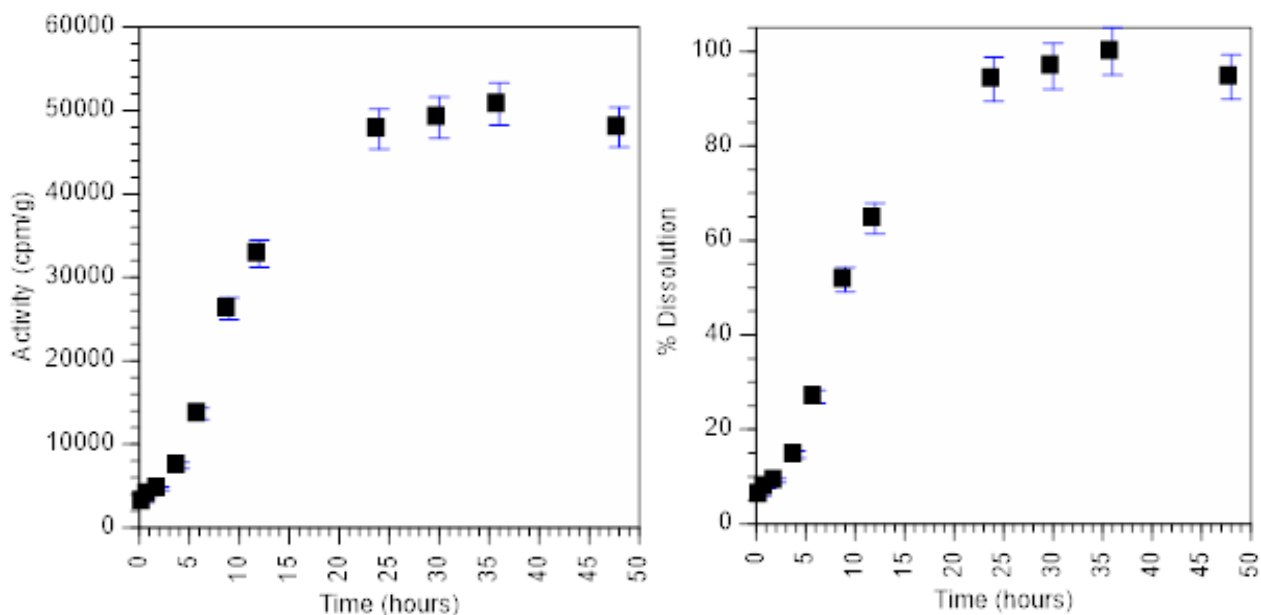


Figure 8: LSC showing dissolution over time of  $U_3O_8$  in activity (cpm/g), left, and percent dissolution of each sample, right.

The same data from figure 8 showing the activity over time is also represented in figure 9, which shows the best fit trendline matched to the data, a second order polynomial. Taking the

derivative of the equation of the trendline provides a rate of dissolution, and the slope of that line provides a rate constant. For  $U_3O_8$  the equation  $y = -40.462x^2 + 2911.3x + 206.38$  provides a rate constant of -80.9. This is the fastest of the three reactions, even though the initial time points show a slower rate. The initial slower rate is limited by the ozone saturating the three uranium centers and breaking apart the molecule mostly to uranyl ions. At that point, any remaining U(IV) ions are quickly oxidized to U(VI) resulting in an overall fast reaction rate. Though this reaction rate is only an estimate, and is limited by the two step nature of the reaction, it also indicates that most of the dissolution is happening in the first 12 hours, with full dissolution occurring by approximately 24 hours.

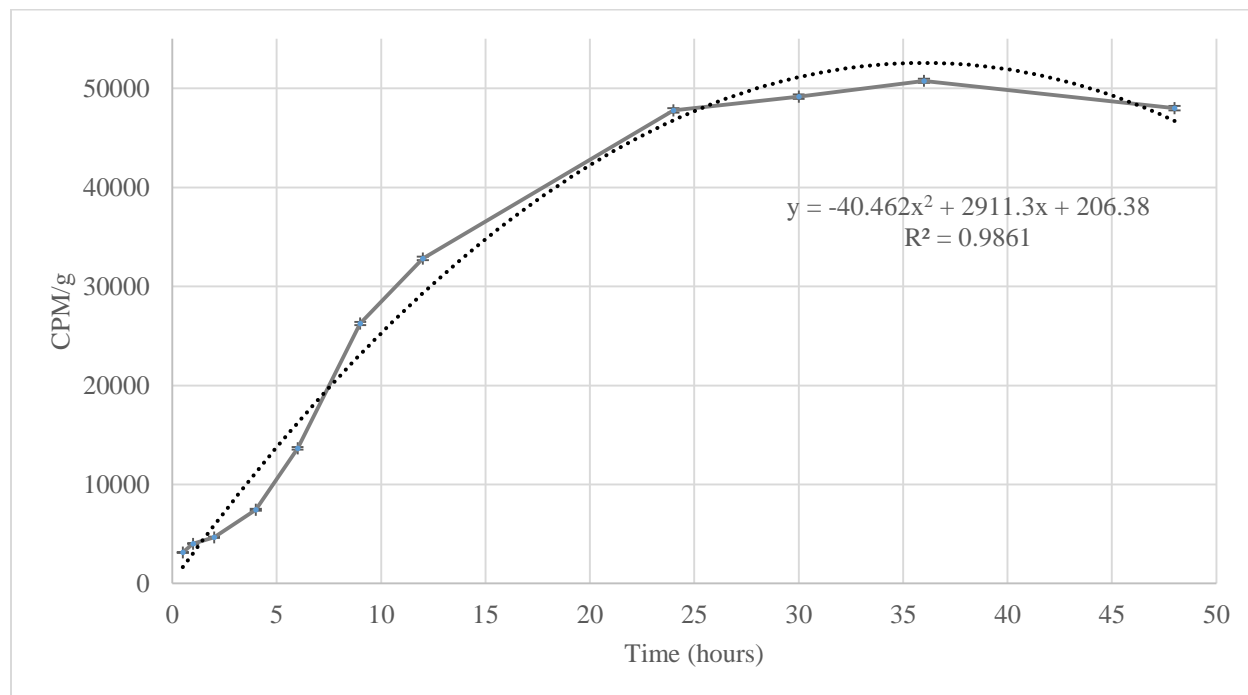


Figure 9: The reaction rate of the  $U_3O_8$  dissolution over time.

### 3.6 UV-Vis

As UV-Visible spectroscopy can be used both qualitatively and quantitatively, it is ideally suited for the determination of dissolution in the studied samples. Uranyl ( $\text{UO}_2^{2+}$ ) has a unique five banded signature peak in ionic liquids. These absorbance bands (seen at 470 nm, 454 nm, 437 nm, 425 nm, and 413 nm in Fig.5) are a clear indication of the presence of uranyl. The exact identity of the molecular orbital transitions that produce these peaks is disputed by many sources,<sup>73,74</sup> but a suggested list of the major transitions is as follows, based in part on the diagram shown in Figure 10.<sup>75</sup>

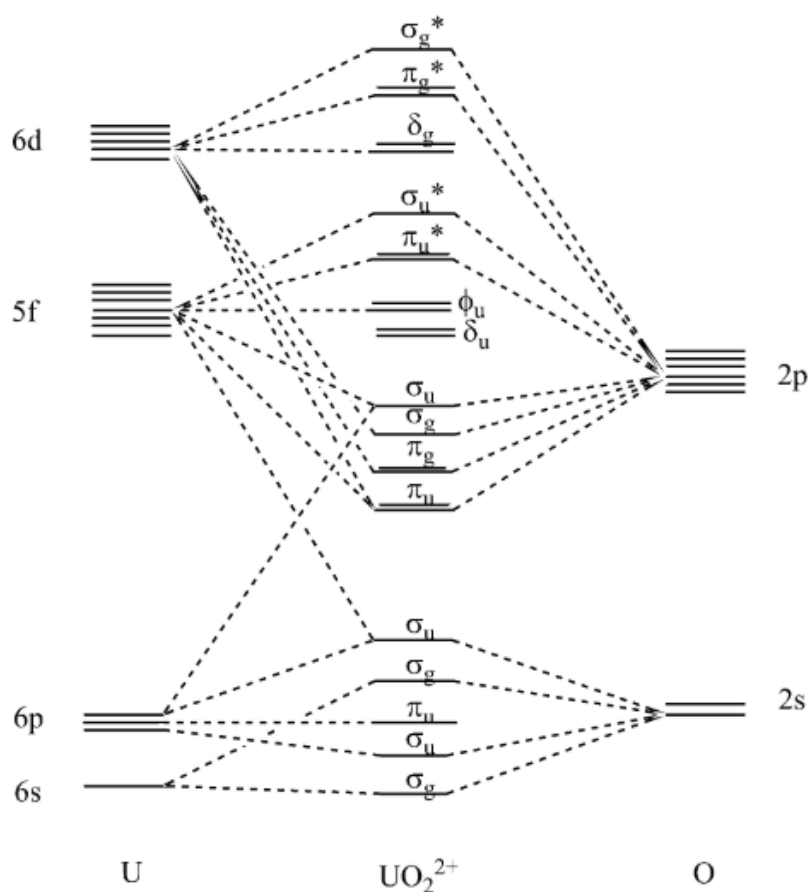


Figure 10: Qualitative molecular orbital diagram for the bonding in the free uranyl ion.<sup>75</sup>

The lower wavelength peaks are represented by higher energy transitions, since the two are inversely proportional. So the first major peak at ~424 nm matches the highest energy 6p to 5f  $\sigma_u$  to  $\sigma_u^*$  molecular orbital transition. The peak at ~438 nm matches to a lower energy 6p to 5f  $\sigma_u$  to  $\sigma_u^*$  transition. The peak at ~454 nm matches a higher energy 6p to 5f  $\sigma_u$  to  $\sigma_u$  transition. The last major peak is at ~468 nm, which could represent either the lowest energy 6p to 5f  $\sigma_u$  to  $\sigma_u$  transition or the low energy 6p to 5f  $\sigma_u$  to  $\pi_u$  transition. The intensity of absorbance bands is a factor of concentration in solution, however matrix effects can influence the intensity of the signal and some small shift in observed energy as well. This effect is clearly seen in the difference in signals for the samples containing water or [HTFSI].

The dissolution of  $U_3O_8$  in the absence of water and acid is provided in Figure 11a) providing the characteristic bands associated with  $UO_2^{2+}$  in the spectral region between 350 and 500 nm. Absorbance associated with the anion species  $TFSI^-$  and oxidation of the IL is observed between 300 and 350 nm, which is off scale exceeding absorbance values of one. The absorbance increases and extends to ~375 nm when HTFSI is added and the anion concentration increases. Many of the bands observed for the dry sample without acid are obscured with the increased absorbance associated with  $TFSI^-$  anion, seen in Figure 11d). In addition, the characteristic bands associated with the uranyl ion are diminished between 400 – 500 nm. The addition of water to the dissolution of a  $U_3O_8$  sample with 0.5 M HTFSI shows both the decreased band intensity seen in the acid only sample, as well as an increase in the baseline relative to the dry sample, seen in Figure 11b). Adding water to the dissolution without adding acid results in the increased baseline seen in 11b (the sample with water and acid) but without the diminished peak intensity shown in 11b and 11d (the dry sample with added acid), as shown in Figure 11c).

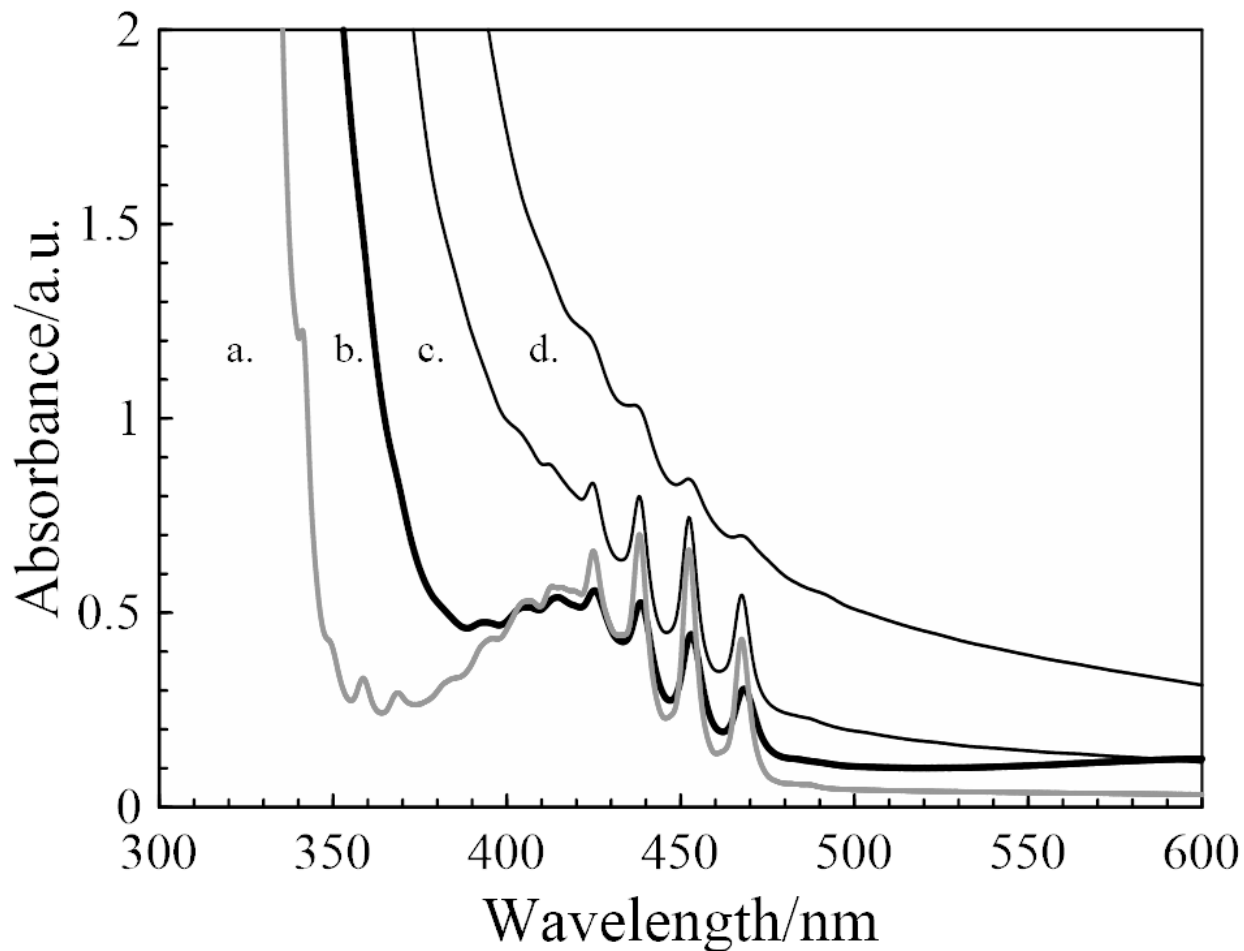


Figure 11: UV-Vis of uranyl dissolved in IL, showing the effects of water and [HTFSI] acid. Where a) is a sample with no added water or acid, b) is a sample with both added water and acid, c) is a sample with added water but no added acid, and d) is a sample with no added water but with added acid.

Relative to the comparable samples without water, the two samples containing water (samples b and c) have increased baseline absorbance. This could be due to an interaction between the IL and water (which would result in a stronger IL background signal) or from the scattering of the light beam on water molecule inclusions in the sample (which would cause noise in the signal unrelated to the uranyl sample). However, the likely cause of these changes is the aqueous micro-environment within the sample, where water molecules will form occlusions

within the IL (since the IL is hydrophobic). Since water will absorb uranyl from the IL as it would in a solvent extraction, the aqueous uranyl peaks will overlap with the IL uranyl peaks and reduce the peak resolution. Additionally, the samples containing [HTFSI] (samples b and d) relative to the respective samples without acid have diminished peak intensity. This diminished peak intensity could be a factor of the [HTFSI] having increased hydrogen bonding with the IL as well as a matrix effect of the more acidic pH change. The sample containing both water and acid (b) suffers from both of these effects, such that even with the increased baseline, the uranyl absorbance bands appear to be severely reduced. The sample containing only [HTFSI] (d) has an absorbance band that is barely distinguishable above the baseline. The sample containing only excess water (c) appears much as the neat IL sample does, except with an increased baseline. The neat IL sample (a) not only shows a clear signal, but also a “resonance” band of the repeated uranyl signal.

The molar absorptivity coefficient was calculated for each of these samples. In order to show the impact of matrix effects, the calculation was performed by normalizing each baseline to zero and the most resolved peak (located at 454 nm) was used for the maximum absorbance. Using equation 2.14, this value can be used to quantify the absorbance changes due to water and acid present in solution. For sample a) with no acid or water,  $\epsilon$  is equal to 14.56. For sample b) with both water and acid added,  $\epsilon$  is equal to 5.88. For sample c) with only added water,  $\epsilon$  is equal to 11.08. For sample d) with only added acid,  $\epsilon$  is equal to 0.12. A lower molar absorptivity coefficient when comparing equimolar solutions represents a lower absorbance, meaning that the measured electron transition is occurring with less frequency or is being hindered by matrix effects. In this case, the measured transition between uranium and oxygen atoms in uranyl is occurring less frequently in the solutions with acid or water possibly because of competing side



reactions outside of the measured UV-Vis range, with acid being the more significant of the two additives.

### 3.7 Electrochemical Analysis

#### Cyclic Voltammetry

As shown from the UV-Vis spectroscopy, the species once dissolved in solution is uranyl ( $\text{UO}_2^{2+}$ ). An exploration of this solution using cyclic voltammetry shows the redox reactions occurring in the sample, as shown in Fig 12. The sample was analyzed using a three electrode cell, with a platinum sheet counter electrode, a gold mesh working electrode, and a silver wire/silver chloride ( $\text{Ag}/\text{AgCl}$ ) reference electrode. The reference electrode was calibrated using 5 mM ferrocene, and then adjusted to the aqueous  $\text{Ag}/\text{AgCl}$  reference, a total shift of +0.618 V. The scan rate of 10 mV/s was selected to ensure the data collection was sensitive to the signal. The initial scan direction was positive, and multiple consecutive scans were performed until stasis was achieved.

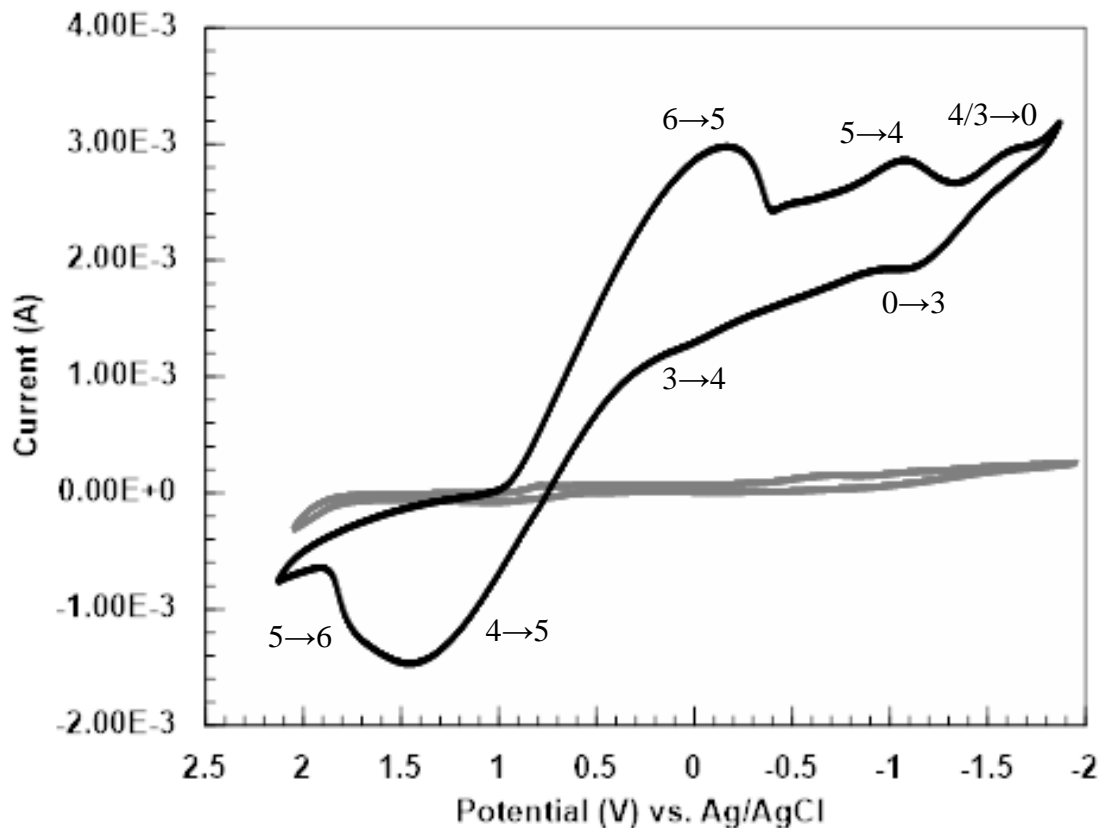


Figure 12: Cyclic voltammetry of uranyl in IL (black) with IL background (gray).

Fig. 12 shows the quasi-reversible reduction of  $\text{UO}_2^{2+}$  to  $\text{UO}_2$  at the surface of the gold mesh electrode. This reduction is a multi-step process, requiring first the reduction of  $\text{UO}_2^{2+}$  to  $\text{UO}_2^+$ . This peak is seen at  $-0.18$  V vs Ag/AgCl. A second reduction step occurs at  $-1.10$  V vs Ag/AgCl, where the  $\text{UO}_2^+$  is reduced to  $\text{UO}_2$  (s). This reduction of U(VI) to U(V), an unstable transition state, and then to U solid deposit, is the expected two-electron transfer reaction. The oxidation of the multiple species in solution is observed at  $+1.43$  V vs Ag/AgCl, and may reflect both the release of  $\text{UO}_2$  (s) off the electrode surface and the oxidation of  $\text{UO}_2^+$  back to  $\text{UO}_2^{2+}$ . The much smaller peaks relating to the U(IV) and U(III) reduction and then re-oxidation around

-1.6 V can be seen at this mid-range voltage sweep but is less obvious compared to dominant species at more negative voltages.

Similar analysis of the samples containing acid (HTFSI), water, or both was done. The water and acid acted as contaminants interfering with the voltammetry with no peaks resolving. Likewise, the  $\sim 1 \text{ M UO}_2^{2+}$  solution was analyzed, showing two reduction peaks and a quasi-reversible oxidation peak, seen in Fig. 7. However, the density of the final solution had a much higher viscosity than the lower concentration solutions. Since viscosity can inhibit electron transfer, the potential of the redox peaks has shifted. As such, the peaks previously observed at -0.18 V and -1.10 V are now seen at +0.50 V and -0.15 V vs. Ag/AgCl. Within these peaks is the U(V) to U(IV) transition, which occurs rapidly in solution but isn't seen due to the reduced peak resolution caused by the high concentration and viscosity. Another factor of the limited electron transfer is the reduced current in the sample. The IL background was too large to be seen on the graph with this sample. Another change in the high concentration sample is the diminished oxidation peak at +1.00 V. The negative potential sweep would reduce any available cations at the electrode surface, and the limited electron transport would inhibit any remaining partially reduced species from moving to the anode. Since the current response on the CV is proportional to the charge produced (where more electrons correspond to more REDOX reactions occurring in solution) the smaller total peak area indicates that fewer uranyl cations are being either reduced or oxidized throughout the voltammetry program.

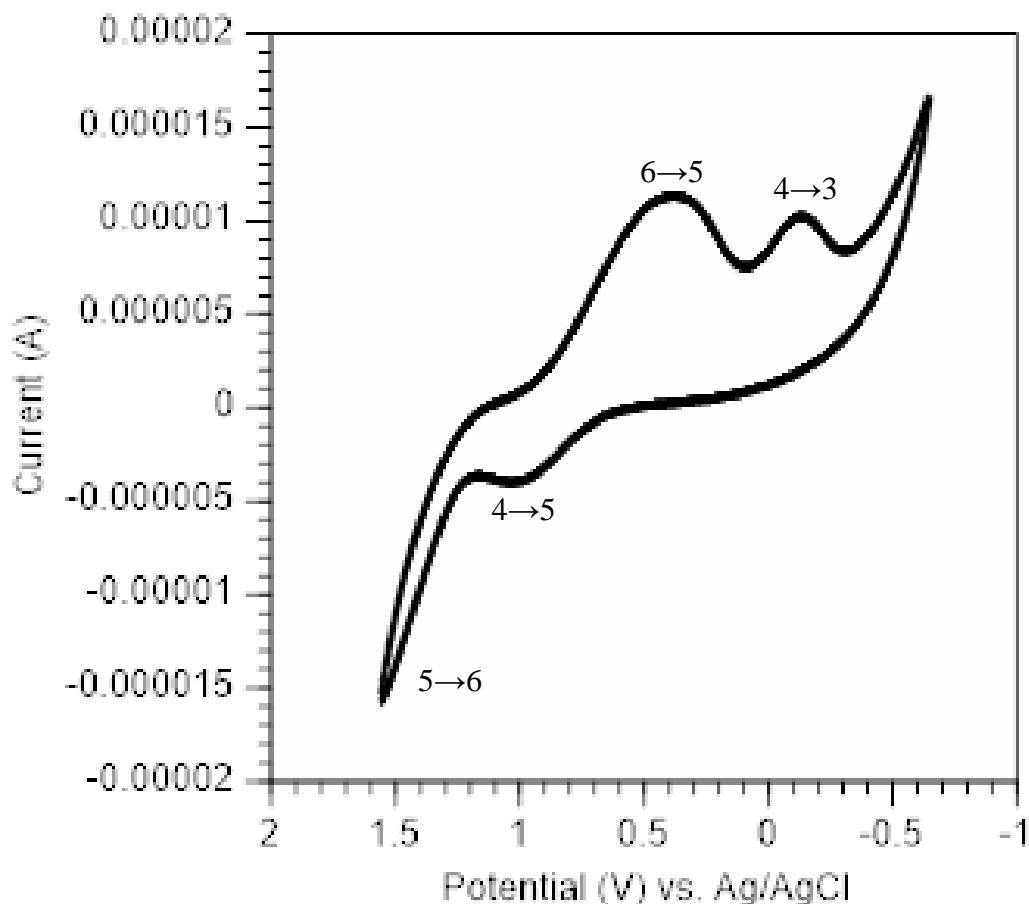


Figure 13: Cyclic voltammetry of 1 M uranyl in IL.

The electrochemical response for the dissolution of  $U_3O_8$  in solutions containing water and acid was also measured shown in Figure 13. The concentration of acid when included in the sample was 50 mM and the water concentration was based on contacting the IL with water for 24 hours to achieve saturation on the order of 1.36% using Karl Fischer titration, as detailed in the experimental section. The time require for the dissolution was not dramatically influenced by the addition of water and acid. However, the voltammetry is strongly influenced by the addition of these two secondary species.

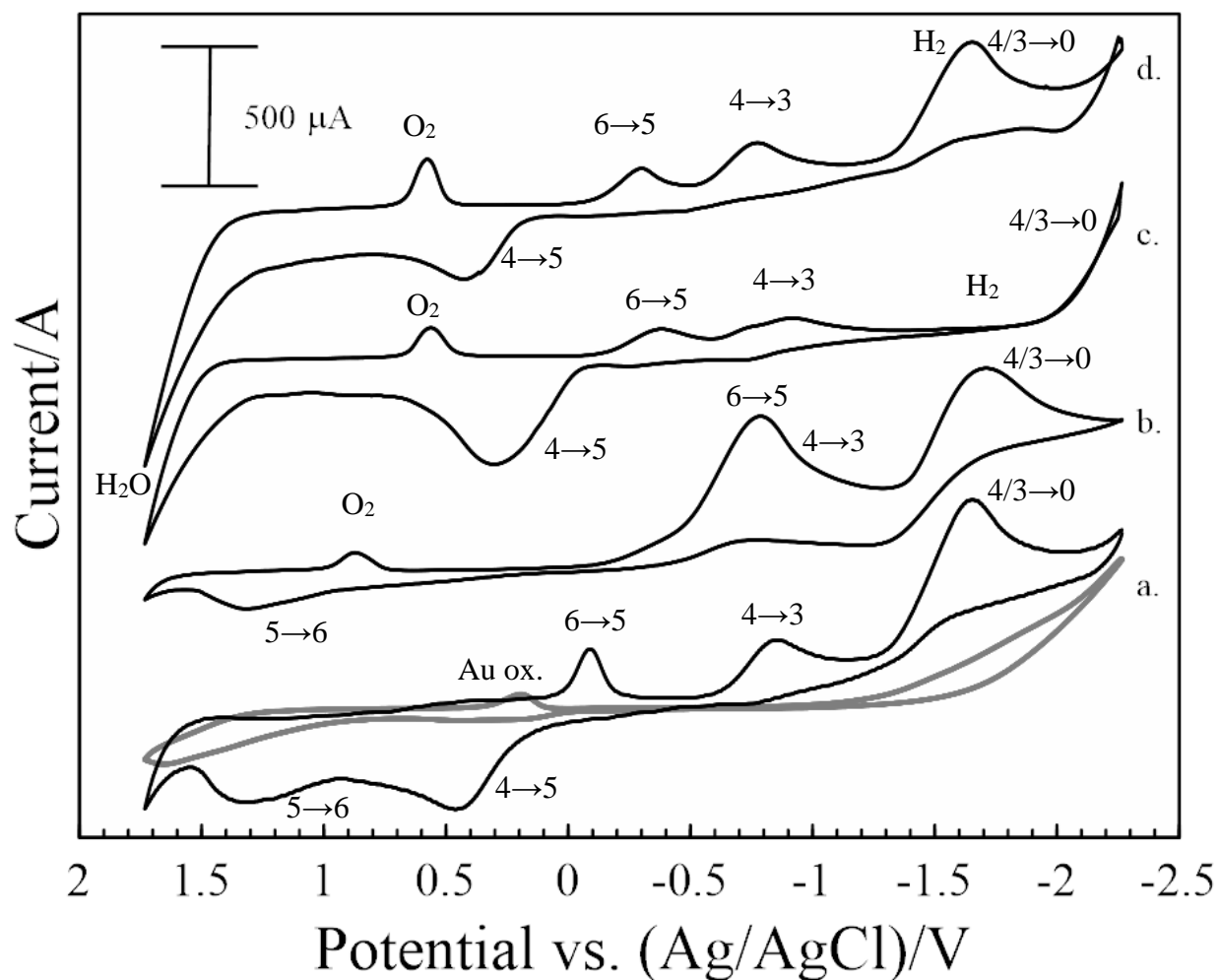


Figure 14: CV of  $\text{U}_3\text{O}_8$  in IL where a. is a sample with no added water or acid, b. is a sample with added HTFSI acid, c. is a sample with added water but no acid, and d. is a sample with both water and HTFSI acid added. Gray represents a clean IL background.

The CV for the second voltammetric cycle is provided in Figure 14a for the dissolution of  $\text{U}_3\text{O}_8$  in the absence of water and HTFSI. The second cycle is utilized for the reduction/deposition of  $\text{UO}_2^{2+}$  to minimize the voltammetric waves at potentials more negative of 0 V vs. Ag/AgCl under the different solution conditions utilized for dissolution. The data provided in Figure 14a are consistent with the two step reduction of  $\text{UO}_2^{2+}$  and deposition of

UO<sub>2</sub>. More importantly, the reverse scan shows the corresponding oxidation of the UO<sub>2</sub> at potentials greater than 0.1 V when water and acid are minimized.

For comparison, the inclusion of 50 mM HTFSI shows a much different response, seen in Figure 14b. The first reduction step at -0.1 V in Figure 14a is not resolved and the current associated with the reduction at ~ -0.9 V is larger suggesting that the two step reduction has merged. The bulk reduction process at ~-1.5 V to -2.5 V remains consistent for the two samples. In contrast, the oxidative processes observed for the sample without water or acid are absent and are replaced by the oxidation/reduction of the gold electrode observed previously in IL containing HTFSI.<sup>76</sup>

Furthermore the addition, of water without acid results in the clear evolution of hydrogen gas at the electrode surface in Figure 14c at potentials more negative of -1.5 V. The reduction of the soluble UO<sub>2</sub><sup>2+</sup> is observed between -0.1 V to -1.4 V after the gold oxide is reduced at reduced current when compared to the samples containing only water and with no water or acid. The oxidation shows only one voltammetric wave consistent with the oxidation of UO<sub>2</sub> from the surface at 0.3 V. The oxidative current beginning at ~+1.3 is likely due to the oxidation of the anion in the presence of water and formation of gold oxide.

Finally the voltammetric response for a sample containing both water and acid are presented in Figure 14d and is comparable to both Figure 14b and 14c with similar reduction processes for gold oxide, the reduction of UO<sub>2</sub><sup>2+</sup> between -0.1 V to -2.3 V, and subsequent hydrogen evolution from -2.3 to -2.5 V. The reverse scan shows a diminished voltammetric wave for the oxidation of UO<sub>2</sub> and the current associated with the oxidation of the gold surface and TFSI anion.

In samples containing acid (b and d), reduction peaks are less resolved, and even conflated in the acid-only sample b. In samples containing water (c and d) the effects of hydrogen evolution interfere with bulk deposition at the gold electrode surface. Over time, as the electrode is slowly coated in the uranium oxide reduction product, this effect lessens. Adding water increased the reverse oxidation for the U(IV) to U(V) couple but inhibited the U(V) to U(VI) oxidation, meanwhile hydrogen evolution interfered with the final reduction of the U(III) and U(IV) species. Adding either HTFSI or water to the IL sample inhibited the reverse oxidation processes – though this may be preferred in situations where deposition is the end goal, this could be a problem for the IL quality and does slow the analysis down. In each case the deposition of  $\text{UO}_2$  was observed albeit diminished with the presence of water and acid but with differing overall effects.

### 3.8 Scanning Electron Microscopy and Energy Dispersive X-Ray Spectroscopy (SEM/EDX)

The deposit analyzed using scanning electron microscopy (SEM) and energy dispersive X-ray spectroscopy (EDX) was prepared from a 25 mM uranyl in IL solution. The technique used was bulk deposition, with a constant voltage of -2.4 V held for a period of 24 hours. The working electrode used was gold foil, and black dendritic deposits formed on the surface. These deposits were removed using a razor edge and then soaked in acetone for an additional 24 hours to remove any lingering IL. The acetone was allowed to evaporate, and then the deposits were adhered to carbon tape, which was then affixed to the SEM sample stage for analysis. The resulting images and X-ray spectroscopy are shown in Figure 15 below. Figure 15a shows the electron image of the dried deposits at 35x magnification. Figure 15b shows the same deposits at 1000x magnification. The craggy nature of this image indicates that deposition is not occurring in a single layer, but that inclusions of the IL are forming as deposition progresses. This matches

the amorphous characterization found in PXRD results, since a crystalline deposit may have a more uniform appearance.

Figure 15c shows the EDX spectra of the deposits at 1000x (black spectra) with an overlay of the carbon tape background (gray spectra). The major peaks found belong to uranium (U), fluorine (F), oxygen (O), and carbon (C). The small fluorine peak is a remnant of the IL, which contains fluorine. The carbon peak is reduced in the uranium deposit sample as expected, since the sample covers the carbon tape. The uranium and oxygen peaks show a clear signal, indicating that the sample is uranium oxide recovered successfully from the ionic liquid.



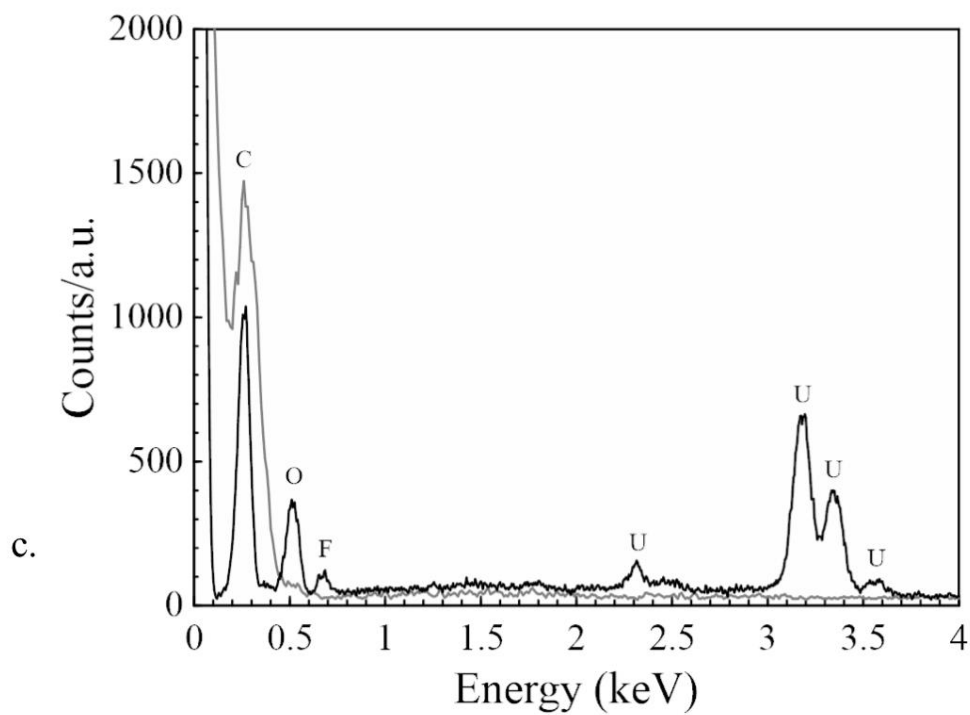
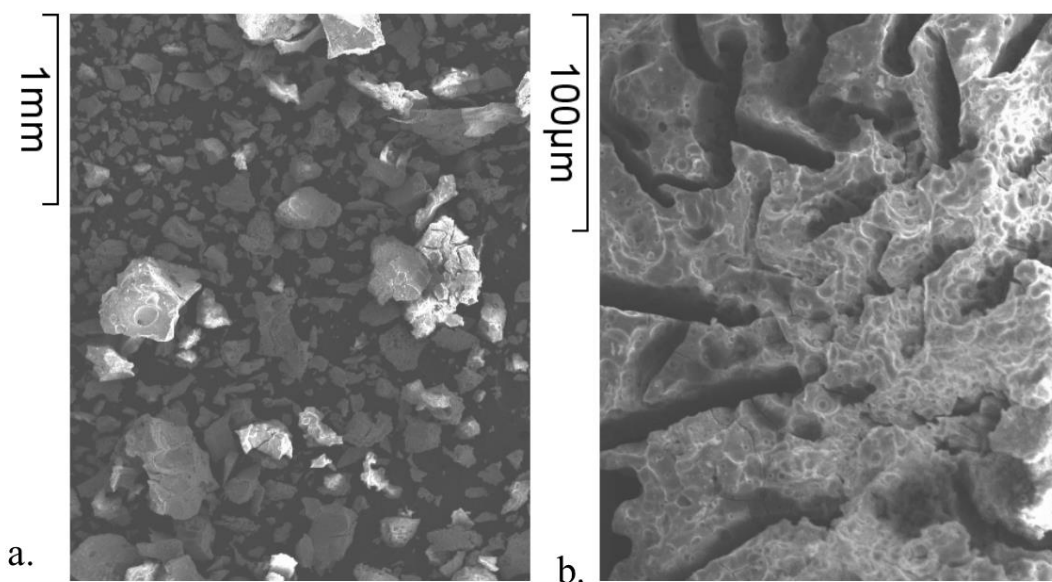
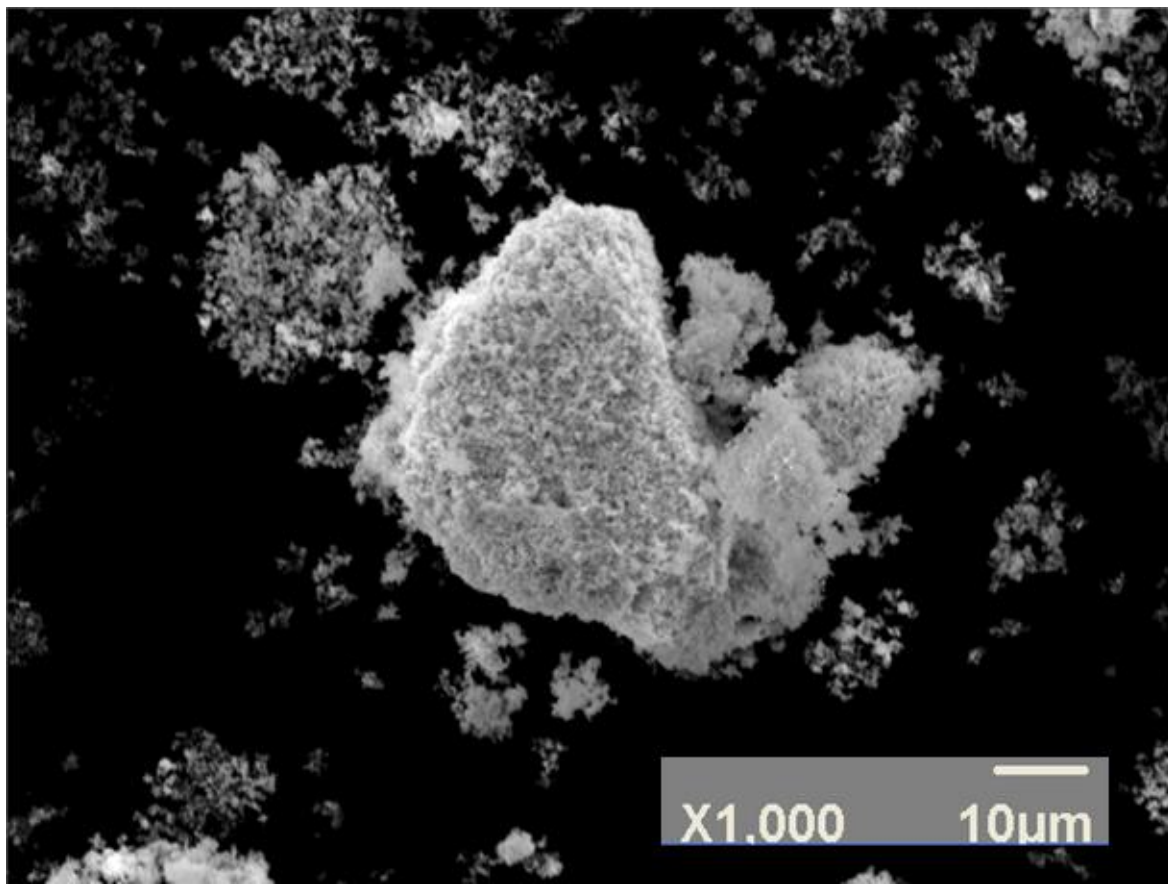
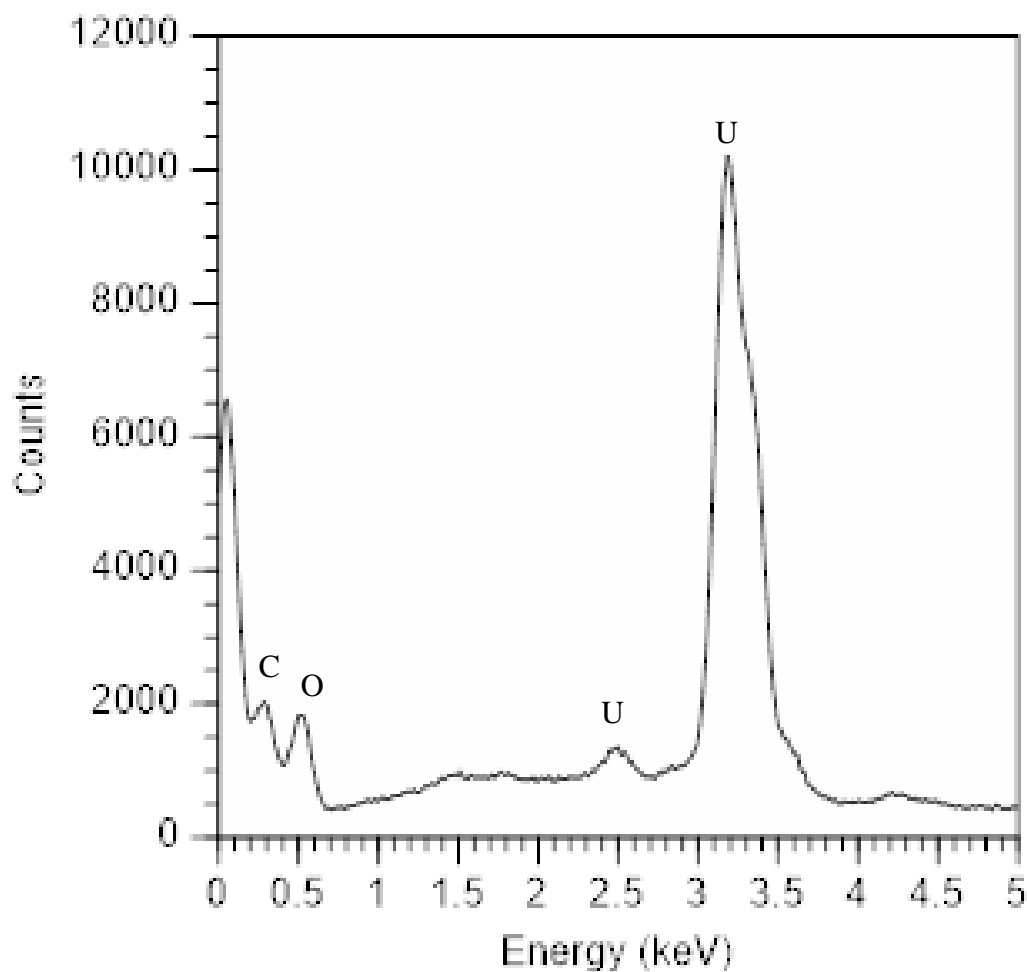


Figure 15: a. uranium deposits at 35x magnification, b. uranium deposits at 1000x magnification, and c. EDX of uranium deposits at 1000x magnification with carbon tape background.

This can be compared to a similar EDX spectrum of the synthesized  $U_3O_8$  standard shown in figure 16. This shows the peaks representing carbon (C), oxygen (O), and uranium (U). The carbon signal is due to the carbon tape used to affix the sample to the instrument stage, while the oxygen and uranium show clearly that the sample is uranium oxide. While this method is only semi-quantitative, it is qualitative for the present elements.



16a.



16b.

Figure 16: a. SEM image of  $U_3O_8$  synthesized standard at 1000x magnification, b. EDX spectrum of the standard at 1000x magnification and 300 second count time showing uranium (U), oxygen (O), and carbon (C) peaks.

## Conclusion

The dissolution and recovery of synthesized  $U_3O_8$  in was explored in n-trimethyl-n-butylammonium bis(trifluoromethanesulfonyl)imide ionic liquid. The synthesis was successful, with the final mass recorded as 0.3959 g of  $U_3O_8$ , a 74.69% recovery. PXRD confirmed the material was alpha phase  $U_3O_8$ . Dissolution was successful at both 27 mM and 0.94 M concentrations, and in the presence of water and acid [HTFSI]. Dissolution was monitored by

liquid scintillation counting with a rate constant of -80.9, and fully dissolved samples were analyzed by UV-Visible spectroscopy (with a molar absorptivity coefficient of 14.56) and cyclic voltammetry. Cyclic voltammetry indicates that even in the presence of water and/or HTFSI the uranyl species in solution would undergo electron transitions to the reduced solid state, though reversibility depended on the matrix conditions. Both spectroscopic and electrochemical techniques suggest the species in solution is uranyl,  $\text{UO}_2^{2+}$ . Deposition was performed and black dendritic deposits were collected. SEM/EDX analysis shows amorphous uranium oxide deposits, results that match PXRD analysis. The most likely identity of these deposits is  $\text{UO}_2$  based on the species in solution.

## Chapter 4

### Abstract

UO<sub>2</sub> is a form of uranium oxide used primarily as a fuel with limited solubility, similar to U<sub>3</sub>O<sub>8</sub>. However, the oxide was dissolved direction into n-trimethyl-n-butylammonium bis(trifluoromethanesulfonyl)imide, or [Me<sub>3</sub>NnBu][TFSI], ionic liquid using ozone generated from compressed air. The process relies on oxidation of UO<sub>2</sub> using oxidative species produced using an ozone generator and air. The synthesized UO<sub>2</sub> was confirmed using PXRD analysis prior to dissolution into IL. Dissolution was monitored over time with LSC analysis. Fully dissolved samples were then analyzed by UV-Vis spectroscopy and cyclic voltammetry. Electrochemical deposition techniques, primarily pulse deposition, were applied to recover uranium oxide UO<sub>2</sub>(s) from solution to close the cycle, which was confirmed by SEM/EDX. The final product is indicated to be amorphous uranium oxide, from the two electron reduction of UO<sub>2</sub><sup>2+</sup>.

### 4.1 Introduction

Uranium dioxide (UO<sub>2</sub>) is the primary form of nuclear fuel throughout the world. Purified and refined from uraninite ore as described previously, UO<sub>2</sub> is abundant in the nuclear fuel cycle. Even though U<sub>3</sub>O<sub>8</sub> is the more thermodynamically stable uranium oxide compound, UO<sub>2</sub> has advantages over U<sub>3</sub>O<sub>8</sub> when used as fuel in a nuclear reactor. The higher ratio of uranium to oxygen in UO<sub>2</sub> compared to other uranium oxides provides a denser structure, which provides improved fuel interactions. UO<sub>2</sub> also has a higher thermal conductivity allowing for more efficient heat distribution. In addition to the chemical properties, UO<sub>2</sub> can also better retain gaseous fission products, resulting in a more stable fuel. The oxidation of UO<sub>2</sub> to U<sub>3</sub>O<sub>8</sub> can be

reduced by increasing the density of the fuel pellet through sintering and providing a controlled non-oxygenated atmosphere.<sup>77</sup>

Like  $U_3O_8$ ,  $UO_2$  has limited solubility outside of concentrated acid (like PUREX acid extractions)<sup>78,79</sup> or high temperatures.<sup>80,81</sup> In fact,  $UO_2$  has been shown to have significant solubility in nitric acid - at high temperatures and over time.<sup>82</sup> This limits reprocessing and isotopic analysis (such as may be used in materials verification processes and inspections) and adds worker hazards from acid and high temperatures. While this is an ideal property for fuel in a nuclear reactor, reprocessing that fuel for recycling or safe storage purposes is limited. Some work dissolving  $UO_2$  has been shown using ionic liquids, however this was done with acid functionalized cationic species with sufficient water present to facilitate dissociation of the proton. In addition, the synthesis of precursor materials where the uranium oxide is complexed with the ionic liquid has led to success.

As previously discussed, ionic liquids provide a suitable solvent for dissolution, analysis, and electrochemical study of the uranyl dissolution product. This chapter shows that the previously described ozone flow dissolution process also works for  $UO_2$  samples. To demonstrate this, the  $UO_2$  was first synthesized from uranyl nitrate hexahydrate ( $UO_2(NO_3)_2 \cdot 6H_2O$ ) with an added spike of U-233 to aid in later radiation counting. The chemical composition of the product was confirmed via powder X-ray diffraction (PXRD). The dissolution of the sample was achieved in  $[Me_3NnBu][TFSI]$ . Aliquots were removed during the dissolution, centrifuged to remove any not yet dissolved solid material, and prepared for liquid scintillation counting. The final solution was analyzed by UV-Vis spectroscopy and electrochemical study by cyclic voltammetry. Deposition was achieved by both amperometric deposition and pulse deposition, with deposits analyzed by scanning electron microscopy (SEM)

and elemental analysis by energy dispersive X-ray (EDX) spectroscopy. The dissolution produces  $\text{UO}_2^{2+}$  in solution and the final deposits from the electrochemical reduction of uranyl are amorphous uranium oxide, consistent with  $\text{UO}_2$ .

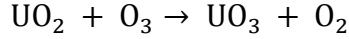
## 4.2 Materials

Ionic liquids were used with no alteration from the source and were trimethyl-n-butylammonium bis(trifluoromethanesulfonyl)imide,  $[\text{Me}_3\text{NnBu}][\text{TFSI}]$  (Solvionic, >99.5% purity) and the protonated acid counterpart bis(trifluoromethanesulfonyl)imide  $[\text{HTFSI}]$  (Fluka, >95% purity). Ultrapure water was generated on site and obtained from laboratory stock. All other materials and instruments used are described in respective sections in chapter 2.

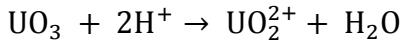
## Results and Discussion

### 4.3 Synthesis and Dissolution

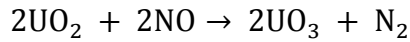
As demonstrated with  $\text{U}_3\text{O}_8$ ,  $\text{UO}_2$  can be dissolved directly into the IL under ozone flow generated from compressed air. The sample dissolved over approximately 24 hours. Attempts to dissolve a  $\text{UO}_2$  sample without ozone were unsuccessful, even in the presence of acid and water, as were attempts to dissolve the sample with ozone generated from  $\text{O}_2$  gas. Unlike  $\text{U}_3\text{O}_8$ ,  $\text{UO}_2$  doesn't need to have any U-U bonds broken, so the direct reaction only serves to oxidize the uranium from U(IV) to U(VI). This is shown in equations 1a and 1b with ozone and 2a and 2b with nitric oxide, using the reactions discussed previously. The indirect ozone reaction (in a simplified form, where the side reactions that produce the same species used as reactants) is shown in equation 3. This shows the need for side reactions and other compounds to stabilize the reaction.



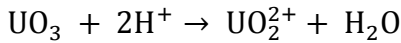
Eq. 1a



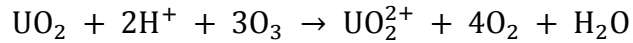
Eq. 1b



Eq. 2a



Eq. 2b



Eq. 3

This dissolution reaction takes advantage of the gaseous side reactions happening in solution to oxidize the uranium oxide solid to the soluble uranyl species, generating water in solution while off-gassing oxygen.

#### 4.4 PXRD

The synthesized  $\text{UO}_2$  was analyzed by PXRD to confirm the identity of the compound. The pattern, shown in Figures 17 and 18, shows that the  $\text{UO}_2$  is face-centered cubic uraninite ( $\text{UO}_2$ ), the only phase of this compound which is separate from  $\text{UO}_{2x}$ .<sup>72</sup> Electrolytic deposits were also analyzed via PXRD to attempt to identify the compound, but no distinguishable pattern was found. This indicates that the electrolytic deposits are amorphous, meaning that no one single crystalline structure is formed during deposition.



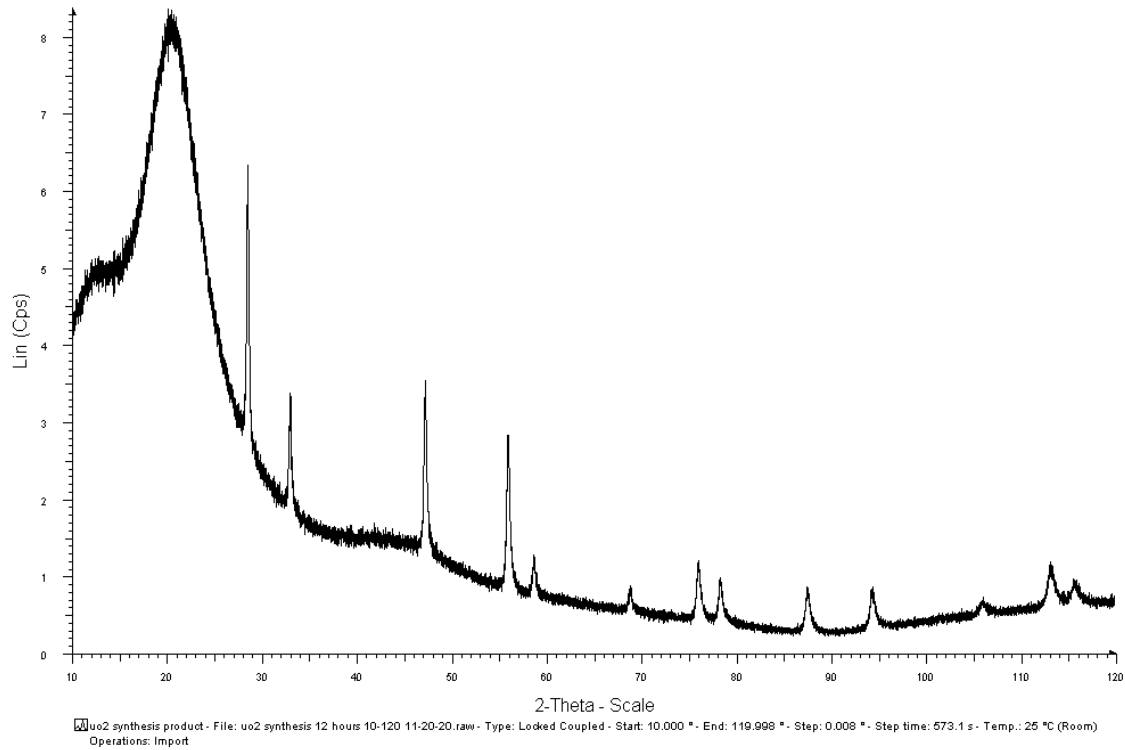


Figure 17: PXRD pattern of synthesized  $\text{UO}_2$  sample.

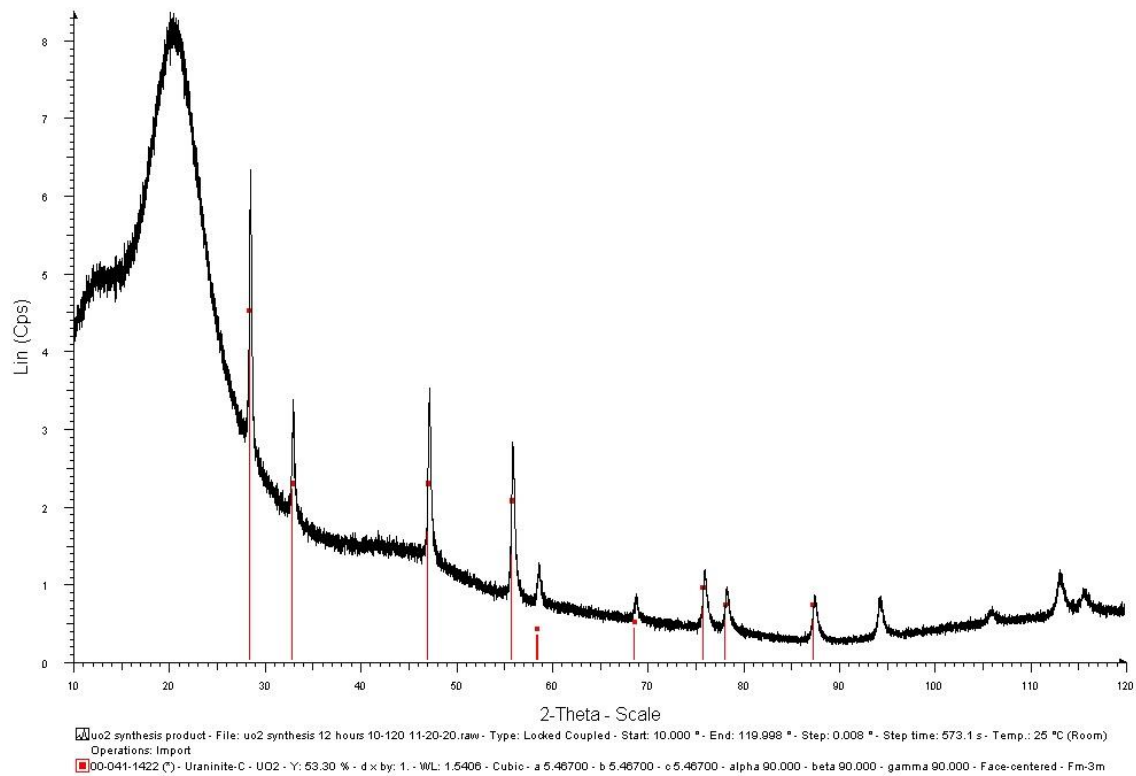


Figure 18: PXRD pattern of synthesized  $\text{UO}_2$ , with the matching pattern of uraninite  $\text{UO}_2$ .

#### 4.5 LSC

A sample of  $\text{UO}_2$  synthesized as described above for a 0.0269 M final uranyl concentration was dissolved in the IL. The sample appeared fully dissolved at 24 hours (clear yellow solution, with no undissolved material remaining). Aliquots were removed as described and prepared for LSC analysis. The resulting figure (FIG. 19) below shows that the sample was fully dissolved between 24 and 30 hours from the start of the dissolution, consistent with visual observation. The graph shows the activity in counts per minute per gram of each sample over the elapsed time from the start of the dissolution. The data shows saturation at around 24 hours, which was consistent with visual analysis.

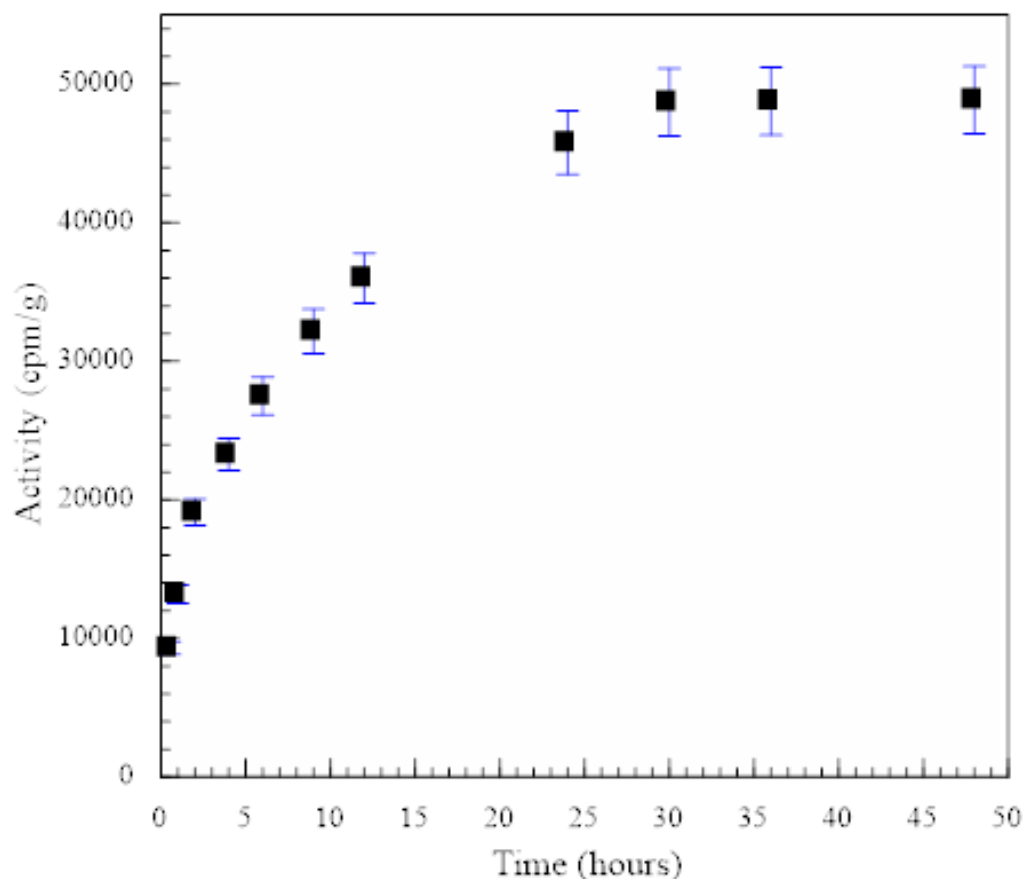


Figure 19a

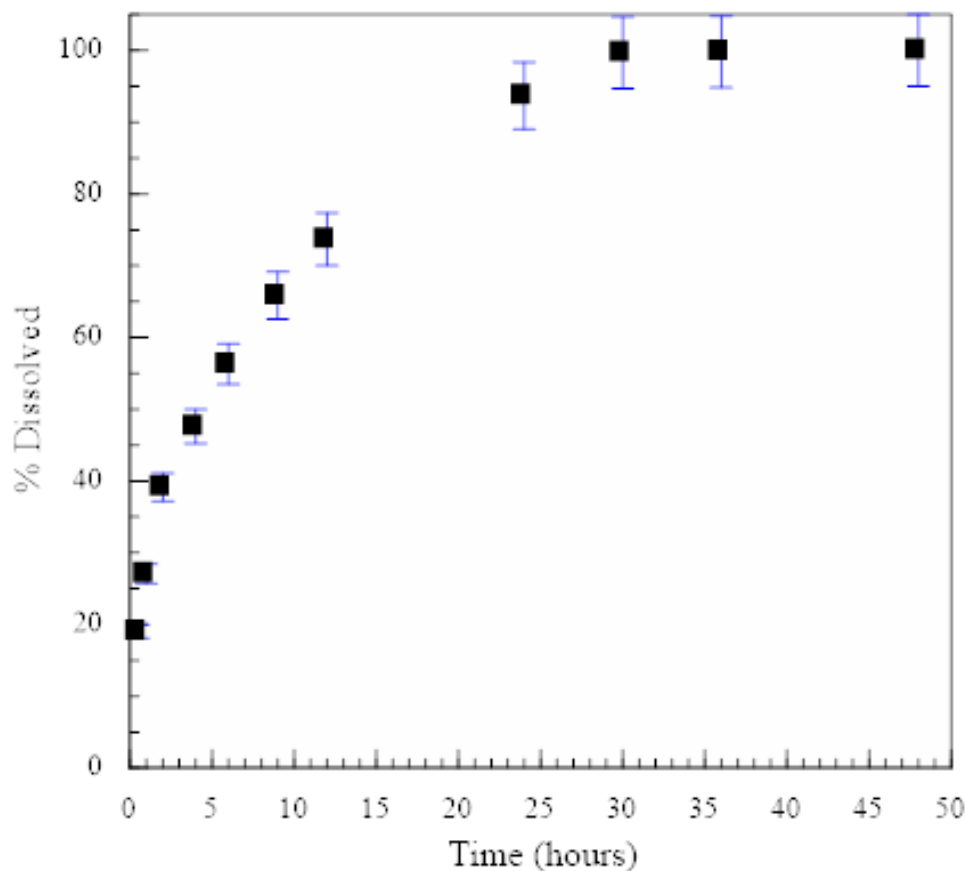


Figure 19b

Figure 19: Dissolution over time of  $\text{UO}_2$  in IL, a) activity in counts per minute per gram of sample and b) % of sample dissolved.

The same data from figure 19 showing the activity over time is also represented in figure 20, which shows the best fit trendline matched to the data, a second order polynomial. Taking the derivative of the equation of the trendline provides a rate of dissolution, and the slope of that line provides a rate constant. For  $\text{UO}_2$  the equation  $y = -29.227x^2 + 2102.8x + 13321$  provides a rate constant of  $-58.5$ . This is the middle of the three reactions, because  $\text{U(IV)}$  is quickly oxidized to  $\text{U(VI)}$  resulting in an overall fast reaction rate. This reaction is somewhat slower than that of  $\text{U}_3\text{O}_8$  because every molecule has to be directly oxidized by the ozone, with each uranium atom gaining another oxygen bond. Though this reaction rate is only an estimate it indicates that most

of the dissolution is happening in the first 12 hours, with full dissolution occurring by approximately 24-30 hours, not significantly slower than  $U_3O_8$ .

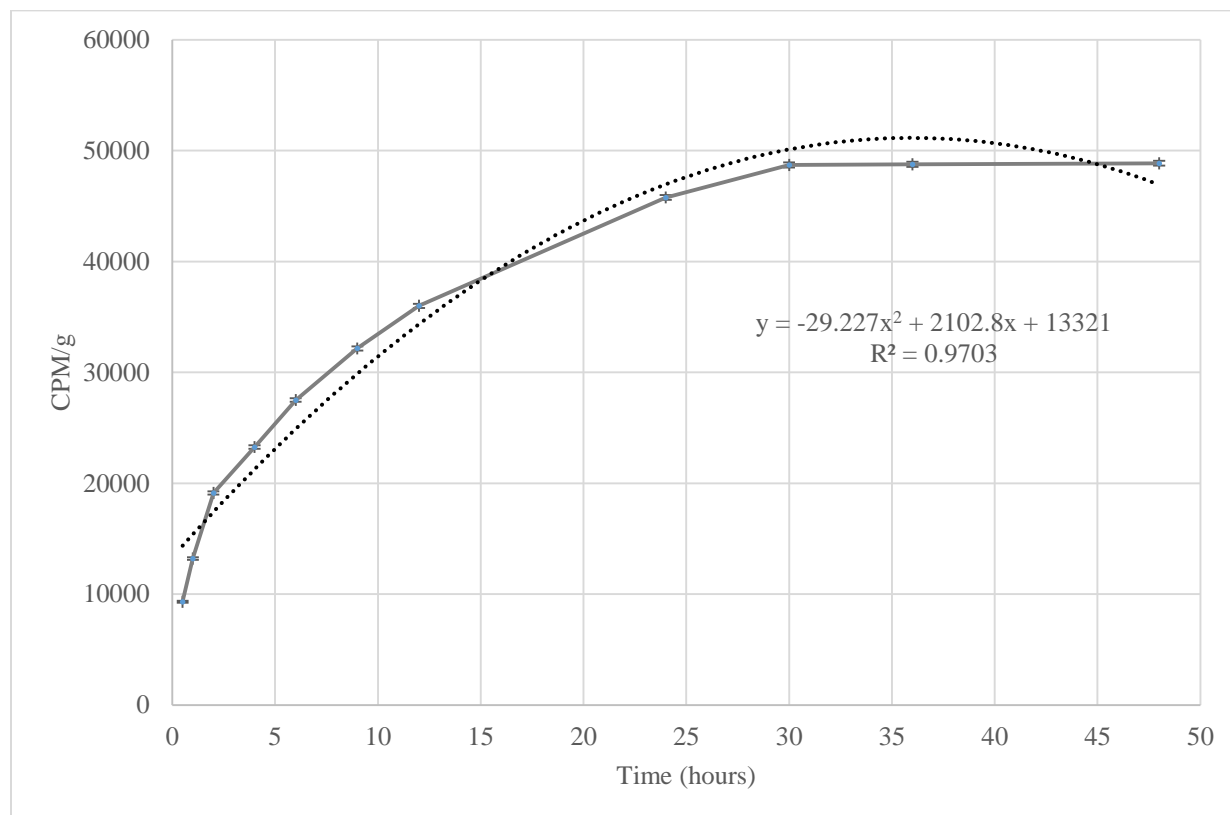


Figure 20: The reaction rate of the  $UO_2$  dissolution over time.

#### 4.6 UV-Visible spectroscopy

The final species in solution of a dissolved sample is uranyl,  $UO_2^{2+}$ . This species has a characteristic UV-Vis spectrum with a five banded peak, seen in Figure 21 with peaks at 466 nm, 453 nm, 439 nm, 423 nm, and 414 nm. The electron transition representing each of these bands is the same as discussed previously in chapter 3. This provides a qualitative identification of

uranyl in the sample. As done previously, the molar absorptivity coefficient was calculated using equation 2.14 with the peak intensity at 453 nm. First, the spectrum was normalized to the baseline, then the peak height was used as the absorbance value A. The solution concentration was 0.0269 M and the cell pathlength was the standard 1 cm. This resulted in the molar absorptivity coefficient  $\epsilon$  of 13.11. This is a similar value to those calculated for the  $U_3O_8$  samples, with potential error coming from matrix effects such as the amount of water in solution.

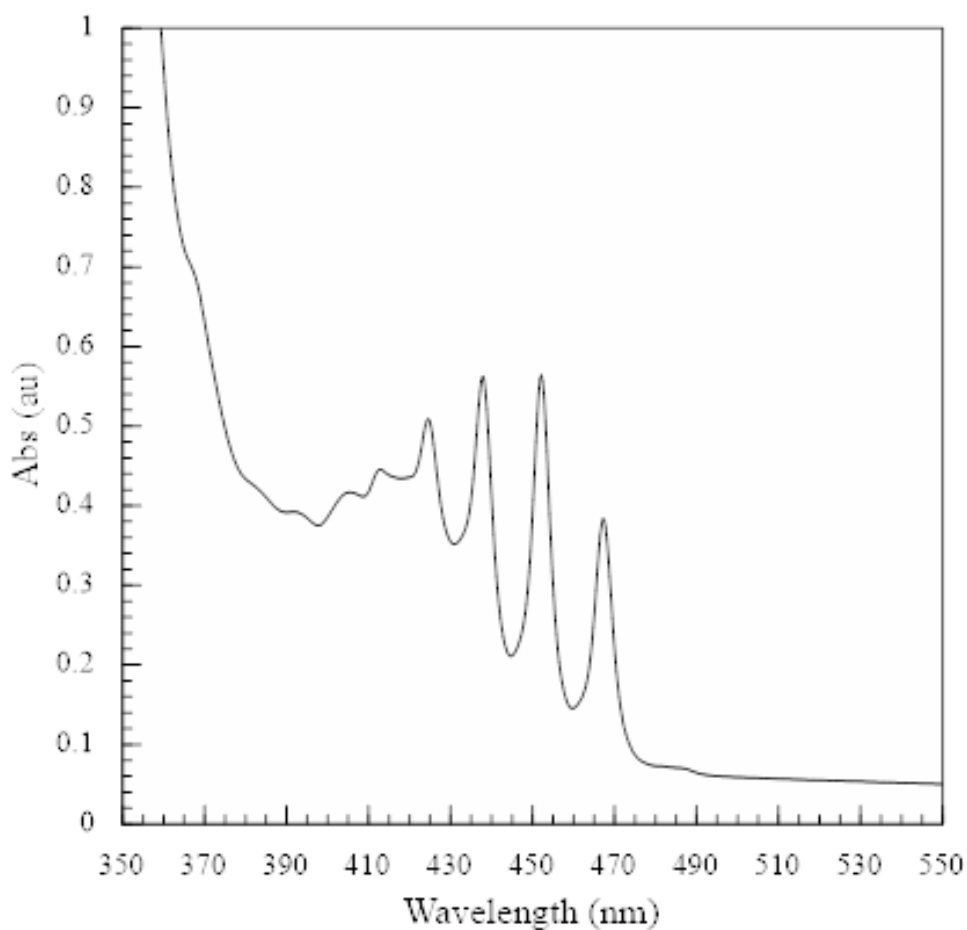


Figure 21: UV-Vis spectrum of dissolved  $UO_2$  sample showing  $UO_2$  dissolved in IL forming uranyl.

## 4.7 Electrochemical Analysis

### Cyclic Voltammetry

As shown from the UV-Vis spectroscopy, the species once dissolved in solution is uranyl ( $\text{UO}_2^{2+}$ ). An exploration of this solution using cyclic voltammetry shows the redox reactions occurring in the sample, as shown in Fig 22-24. The sample was analyzed using a three electrode cell, with a platinum sheet counter electrode, a gold mesh working electrode, and a silver wire/silver chloride (Ag/AgCl) reference electrode. The reference electrode was calibrated using 5 mM ferrocene, and then adjusted to the aqueous Ag/AgCl reference, a total shift of +0.623 V (a separate sample shown in Fig 24 used a separate reference electrode resulting in a total shift of +0.547 V). The scan rate of 10 mV/s was selected to ensure the data collection was sensitive to the signal. The initial scan direction was positive, and multiple consecutive scans were performed until stasis was achieved.

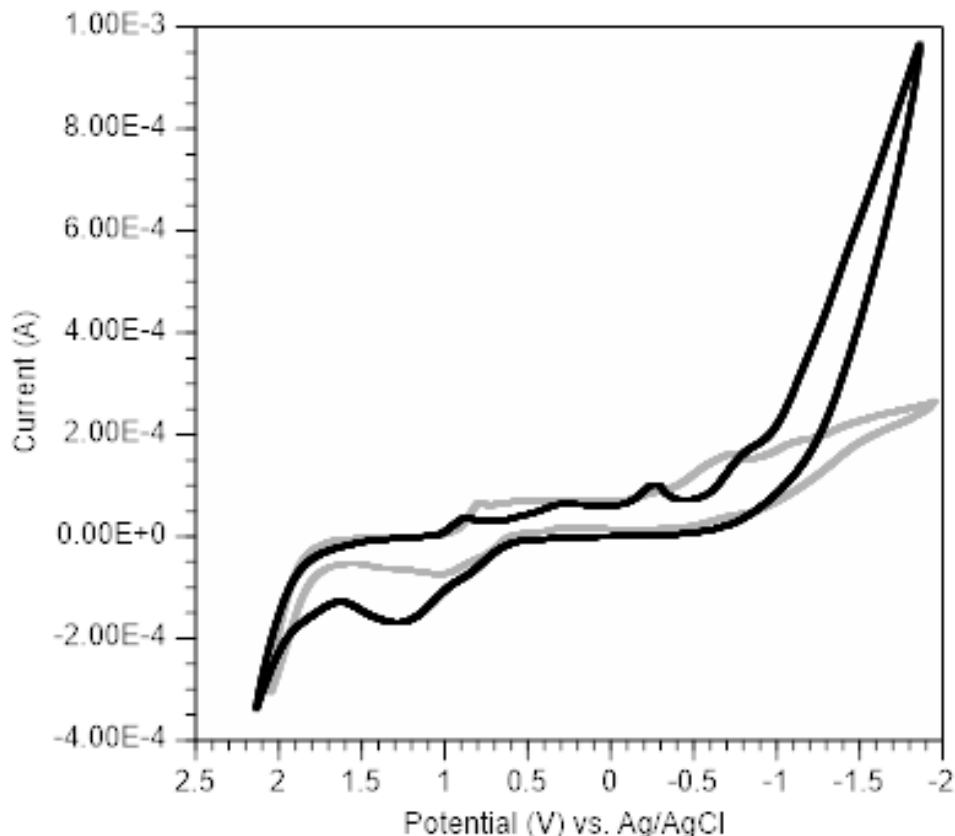


Figure 22: Cyclic voltammetry of uranyl from dissolved  $\text{UO}_2$  sample in IL.

Figure 22 shows the quasi-reversible reduction of  $\text{UO}_2^{2+}$  to  $\text{UO}_2$  at the surface of the gold mesh electrode. This reduction is a multi-step process, requiring first the reduction of  $\text{UO}_2^{2+}$  to  $\text{UO}_2^+$ . This peak is seen at  $-0.28$  V vs Ag/AgCl. A second reduction step occurs at  $-0.870$  V vs Ag/AgCl, where the  $\text{UO}_2^+$  is reduced to  $\text{UO}_2$  (s). This reduction of U(VI) to U(V), an unstable transition state that doesn't appear on this CV due to the speed of further reduction, and then to U(IV) is the expected two-electron transfer reaction.<sup>83</sup> The oxidation of the multiple species in solution is observed at  $+1.26$  V vs Ag/AgCl, and may reflect both the release of  $\text{UO}_2$  (s) off the electrode surface and the oxidation of  $\text{UO}_2^+$  back to  $\text{UO}_2^{2+}$ . Figure 23 shows an enhanced graph of these transitions with labels.

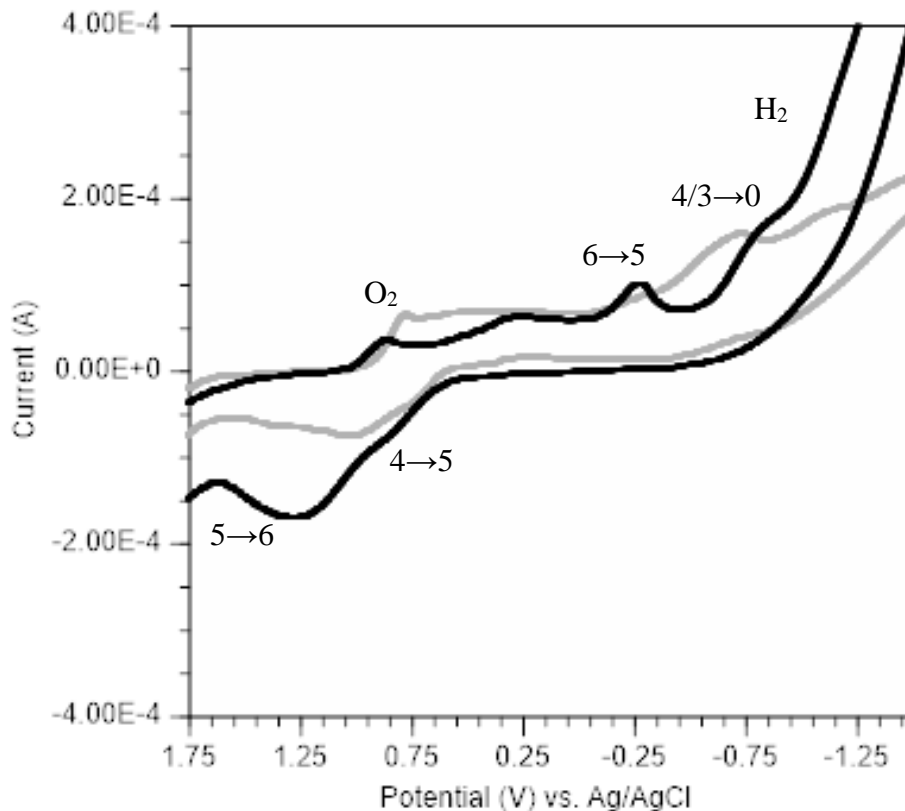


Figure 23: Enhanced section of Figure 22, showing the oxidation and reduction peaks of the uranyl species in solution.

The cyclic voltammetry shown in figures 22 and 23 represent a mid-range of the potential window available for exploration. When the potential window is expanded, the quasi-reversible electron transitions seen can become non-reversible reduction on the electrode. In Figure 24, the potential window was expanded to -2.5 V vs. Ag/AgCl. By driving the solution to more negative potentials, more of the solution reduced to  $\text{UO}_2$  (s) and deposited at the electrode surface as seen at -2.0 V. This deposition has some competition at the electrode surface with the observed hydrogen evolution, which reduced peak resolution of the U(IV) and U(III) species peaks. However, compared to the less negative CV, figure 24 shows a more equivalent peak area for the



U(VI) to U(V) transition (+0.2 V) and its reversed oxidation U(V) to U(VI) (+2.0 V). By sweeping to more negative potentials, more of the +6 oxidation state species was reduced, resulting in an increased peak area and a slight shift to more positive potential. This oxidation state is then regenerated in the positive voltage sweep. As before, the U(IV) to U(V) oxidation peak is likely also conflated with the release of the ground state U deposit off the electrode. Compared to the U<sub>3</sub>O<sub>8</sub> samples analyzed, this sample contained more water, likely from incomplete drying of the sample. This resulted in the observed hydrolysis peaks and the tailing end seen at positive 2.5-3.5 V.

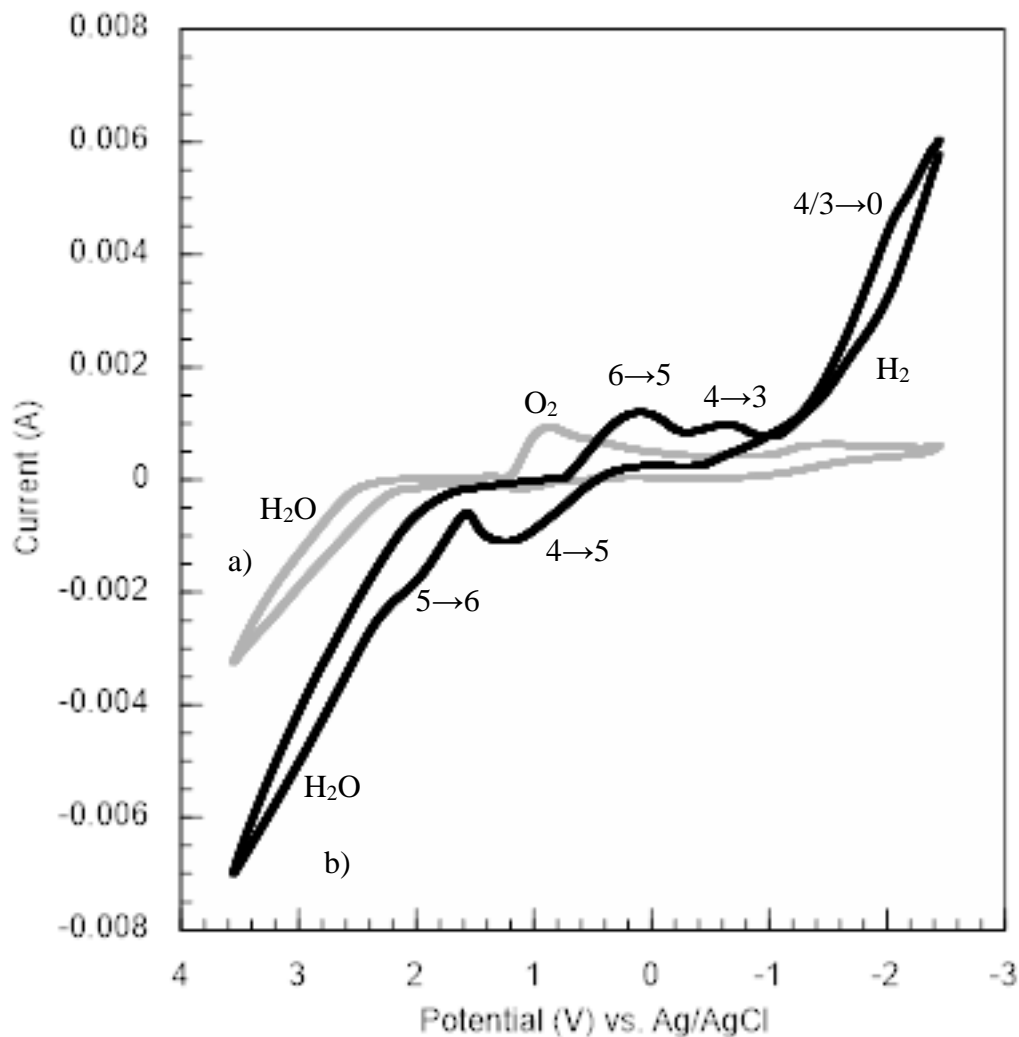


Figure 24: Reduction of uranyl due to the expanded electrochemical potential window with a) ozone exposed IL sample background and b) uranyl in IL.

#### 4.8 SEM/EDX

Scanning electron microscopy is an electron scatter imaging technique that can be used in conjunction with EDX to semi-quantitatively determine the elemental composition of a sample. SEM analysis was used to image multiple UO<sub>2</sub> samples, including standard and synthesized materials. The UO<sub>2</sub> standard is shown in figures 25-27, with the uranium oxide deposit shown in

figures 28-30. The deposit analyzed using scanning electron microscopy (SEM) and energy dispersive X-ray spectroscopy (EDX) was prepared from a 25 mM uranyl in IL solution. The technique used was pulse deposition, with varying pulses of negative and positive potentials applied to the gold mesh electrode. The major peaks found in the  $\text{UO}_2$  standard belong to uranium (U), oxygen (O), and carbon (C). Because oxygen is a smaller atom than uranium, both the signal energy and intensity for oxygen will appear small relative to the uranium peaks. This is consistent with other results.<sup>84</sup> The same peaks are found in the uranium oxide deposit, as well as a sulfur (S) and fluorine (F) peak which was a remnant of the IL. The carbon peak is reduced in the uranium standard sample relative to the deposit sample as expected, since the standard covers the carbon tape while the deposit on the gold mesh electrode leaves some of the carbon tape revealed. The uranium and oxygen peaks in the deposit show a clear signal, indicating that the sample is uranium oxide recovered successfully from the ionic liquid.

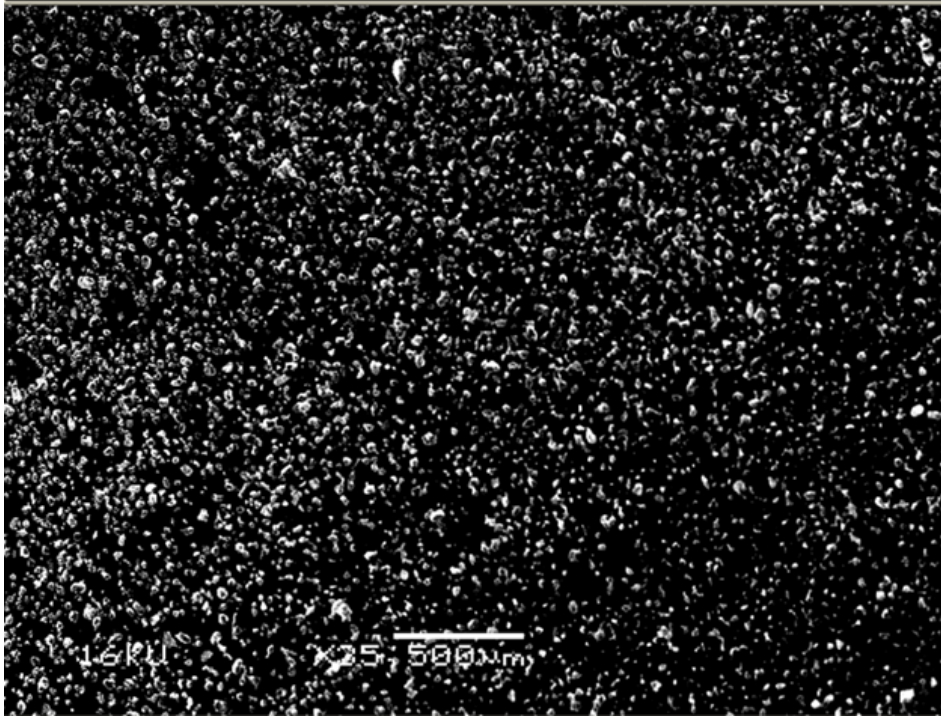


Figure 25:  $\text{UO}_2$  standard material SEM image at 35x magnification.

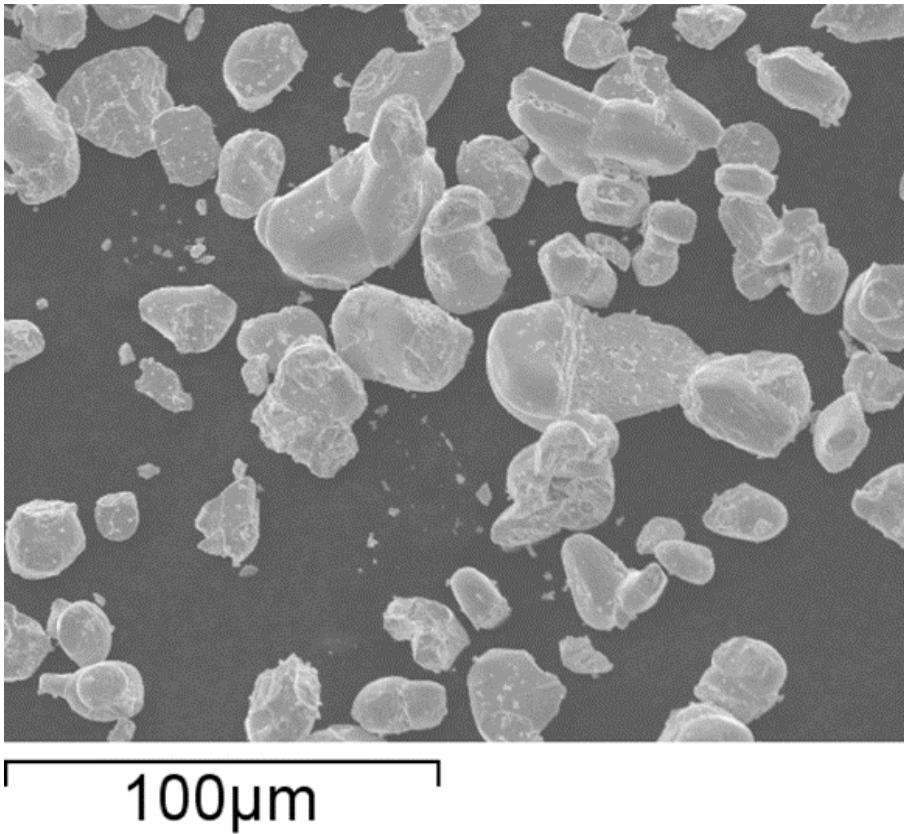


Figure 26: The same standard  $\text{UO}_2$  material shown at 1000x magnification.

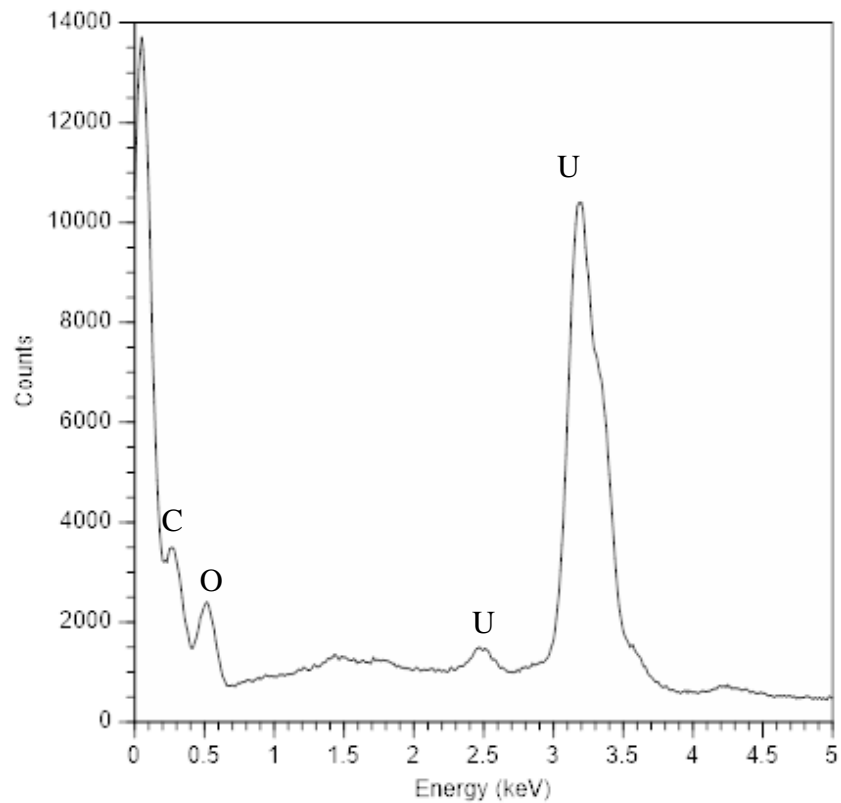


Figure 27: EDX of  $\text{UO}_2$  standard material at 16 kV beam energy and 1000x magnification.

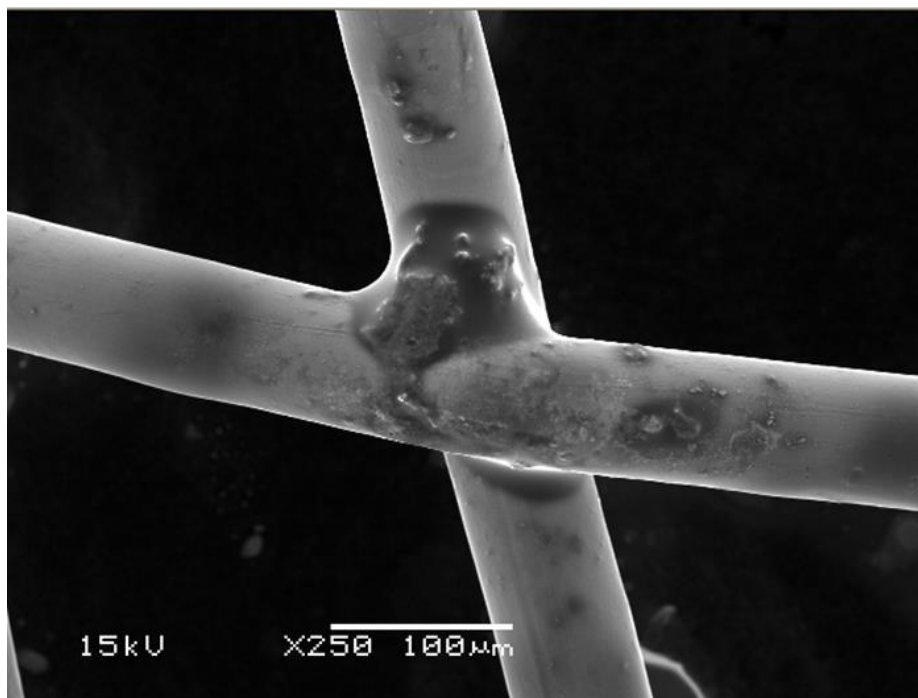


Figure 28: SEM image of  $\text{UO}_2$  deposit on gold mesh electrode at 15 kv beam energy and 250x magnification.

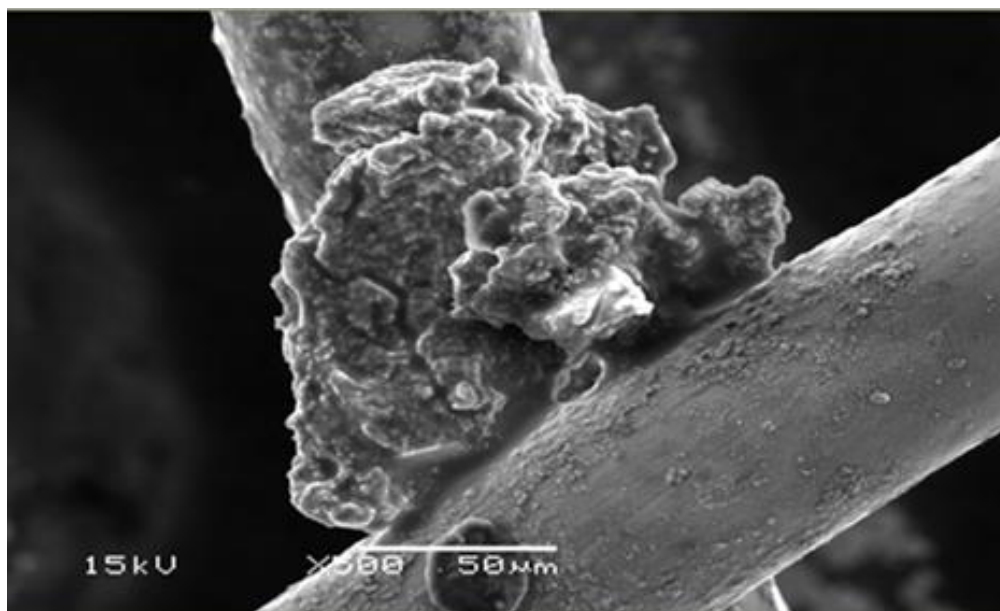


Figure 29: SEM image of UO<sub>2</sub> deposit on gold mesh electrode at 15 kv beam energy and 500x magnification.

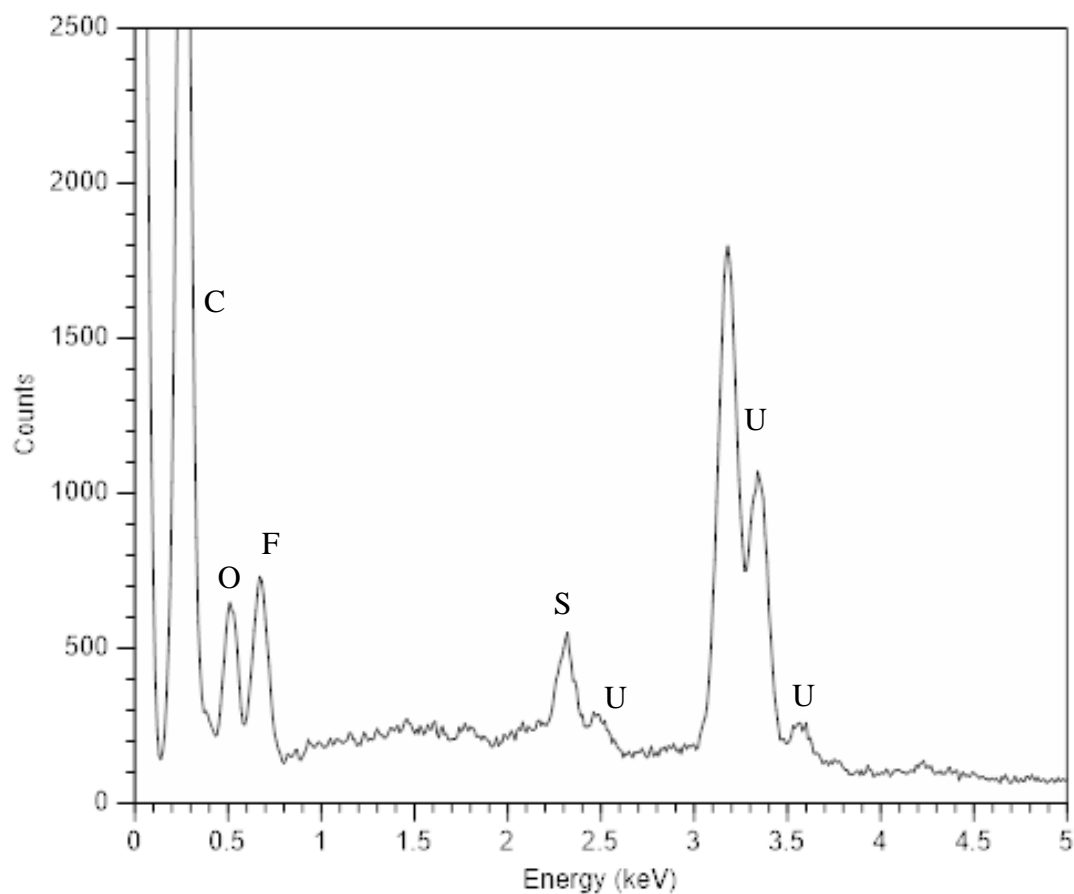


Figure 30: EDX spectrum of UO<sub>2</sub> deposit on gold mesh electrode at 15 kv beam energy and 250x magnification. Sulfur and fluorine peaks indicate the presence of IL still on the electrode.

## Conclusion

The dissolution and recovery of synthesized  $\text{UO}_2$  was explored in n-trimethyl-n-butylammonium bis(trifluoromethanesulfonyl)imide ionic liquid. The synthesis was successful, with the final mass recorded as 0.7604g  $\text{UO}_2$  which was a 78.24% yield. PXRD confirmed the material was face-centered cubic uraninite ( $\text{UO}_2$ ), the only phase of this compound. Dissolution was successful at 25 mM and was monitored by liquid scintillation counting with a rate constant of -58.5, and fully dissolved samples were analyzed by UV-Visible spectroscopy (with a molar absorptivity coefficient of 13.11) and cyclic voltammetry. Cyclic voltammetry indicates that the solution would undergo electron transitions to the reduced solid state, though reversibility depended on the matrix conditions and the electrochemical window studied. Both spectroscopic and electrochemical techniques suggest the species in solution is uranyl,  $\text{UO}_2^{2+}$ . Deposition was performed and black dendritic deposits were collected. SEM/EDX analysis shows amorphous uranium oxide deposits. The most likely identity of these deposits is  $\text{UO}_2$  based on the species in solution.

## Chapter 5

### Abstract

$\text{UO}_3$ , is a form of uranium oxide used primarily as an intermediary compound with some solubility in multiple solvents. The synthesized  $\text{UO}_3$  was confirmed using PXRD analysis prior to dissolution into IL. The oxide was dissolved directly into n-trimethyl-n-butylammonium bis(trifluoromethanesulfonyl)imide, or  $[\text{Me}_3\text{NnBu}][\text{TFSI}]$ , ionic liquid in two different methods. One using ozone generated from compressed air and the other without ozone in a solution containing water saturated IL and excess acid HTFSI. The fact that dissolution occurs in the absence of ozonated air indicates that the process is not dependent on the oxidation/reduction of species in the reaction matrix. Rather, the process relies on the chemical reaction of  $\text{UO}_3$  with protons to form  $\text{UO}_2^{2+}$  and water. To compare to samples of the other uranium oxides, an ozonated air dissolution was monitored over time with LSC analysis. Fully dissolved samples of both types were then analyzed by UV-Vis spectroscopy and cyclic voltammetry. Electrochemical deposition techniques, primarily pulse deposition, were applied to recover uranium oxide  $\text{UO}_2(\text{s})$  from solution to close the cycle, which was confirmed by SEM/EDX. The final product is indicated to be amorphous uranium oxide, from the two electron reduction of  $\text{UO}_2^{2+}$  and one electron reduction of  $\text{UO}_2^+$  complexed species.

### 5.1 Introduction

Uranium trioxide ( $\text{UO}_3$ ) is a common intermediary form of uranium oxide used in the nuclear fuel cycle. Although not as thermodynamically stable as  $\text{U}_3\text{O}_8$ ,  $\text{UO}_3$  is easily produced by heating  $\text{UO}_2$ , ammonium diuranate, or other compounds in air between  $\sim 500\text{-}750\text{ }^\circ\text{C}$  for even a short period of time. Of the three uranium oxides studied in this dissertation,  $\text{UO}_3$  has the lowest uranium to oxygen ratio resulting in the least dense crystal structure. The uranium is also



at its highest oxidation state with no mixed valency. The most common phase is the  $\gamma$  phase, which has an orthorhombic structure.<sup>85</sup> As a solid,  $\text{UO}_3$  is a bright orange powder. Though historically used to color ceramics, modern usage of the compound is as a reactive compound that is central to uranium synthesis processes.

Part of that synthesis, and the chemical importance of  $\text{UO}_3$ , involves the increased solubility of  $\text{UO}_3$  over other uranium oxides. While still not as soluble as other compounds,  $\text{UO}_3$  has some solubility in sodium hydroxide, perchloric acid, and water<sup>86</sup> in addition to the high temperature melting and concentrated acid dissolutions used in molten salts<sup>87,88</sup> and the PUREX<sup>89,90</sup> process as previously described. Some work has shown solubility of  $\text{UO}_3$  complexes<sup>91</sup> or with the addition of aqueous acids<sup>92</sup> in ionic liquid solvents.

As previously discussed, ionic liquids provide a suitable solvent for dissolution, analysis, and electrochemical study of the uranyl dissolution product. To demonstrate this, the  $\text{UO}_3$  was first synthesized from uranyl nitrate hexahydrate ( $\text{UO}_2(\text{NO}_3)_2 \cdot 6\text{H}_2\text{O}$ ) with an added spike of U-233 to aid in later radiation counting. The chemical composition of the product was confirmed via powder X-ray diffraction (PXRD). The dissolution of the sample was achieved in  $[\text{Me}_3\text{NnBu}][\text{TFSI}]$ .

Because  $\text{UO}_3$  does not have an oxidation dissolution pathway, and instead has a chemical dissolution reaction, two different experimental conditions were explored. First, to compare to previous experiments with  $\text{U}_3\text{O}_8$  and  $\text{UO}_2$ , the standard conditions used previously with an ozone generator and compressed air was performed. Aliquots were removed during the dissolution, centrifuged to remove any not yet dissolved solid material, and prepared for liquid scintillation counting.

Second, a set of four samples of  $\text{UO}_3$  were placed in sealed containers under four different acid/water states with stir bars. The sample containing no HTFSI or water and the sample containing only HTFSI with no water showed no change or dissolution over a week. The sample containing no HTFSI but with a water saturated IL showed a color change, but no dissolution. Only the sample containing both HTFSI and water saturated IL showed dissolution, occurring spontaneously with no other assistance outside of stirring.

The final solutions from both methods were analyzed by UV-Vis spectroscopy and electrochemical study by cyclic voltammetry. Deposition was achieved by both amperometric deposition and pulse deposition, with deposits analyzed by scanning electron microscopy (SEM) and elemental analysis by energy dispersive X-ray (EDX) spectroscopy. The dissolution produced  $\text{UO}_2^{2+}$  in solution and the final deposits from the electrochemical reduction of uranyl were amorphous uranium oxide, consistent with  $\text{UO}_2$ .

## 5.2 Materials

Ionic liquids were used with no alteration from the source and were trimethyl-n-butylammonium bis(trifluoromethanesulfonyl)imide,  $[\text{Me}_3\text{NnBu}][\text{TFSI}]$  (Solvionic, >99.5% purity) and the protonated acid counterpart bis(trifluoromethanesulfonyl)imide  $[\text{HTFSI}]$  (Fluka, >95% purity). Ultrapure water was generated on site and obtained from laboratory stock. All other materials and instruments used are described in respective sections in chapter 2.

## Results and Discussion

### 5.3 PXRD

The synthesized  $\text{UO}_3$  was analyzed by PXRD to confirm the identity of the compound. The pattern, shown in Figures 31 and 32, shows that the  $\text{UO}_3$  is monoclinic  $\text{UO}_3$  which is the beta phase.<sup>72</sup> Electrolytic deposits were also analyzed via PXRD to attempt to identify the compound, but no distinguishable pattern was found. This indicates that the electrolytic deposits are amorphous, meaning that no one single crystalline structure is formed during deposition.

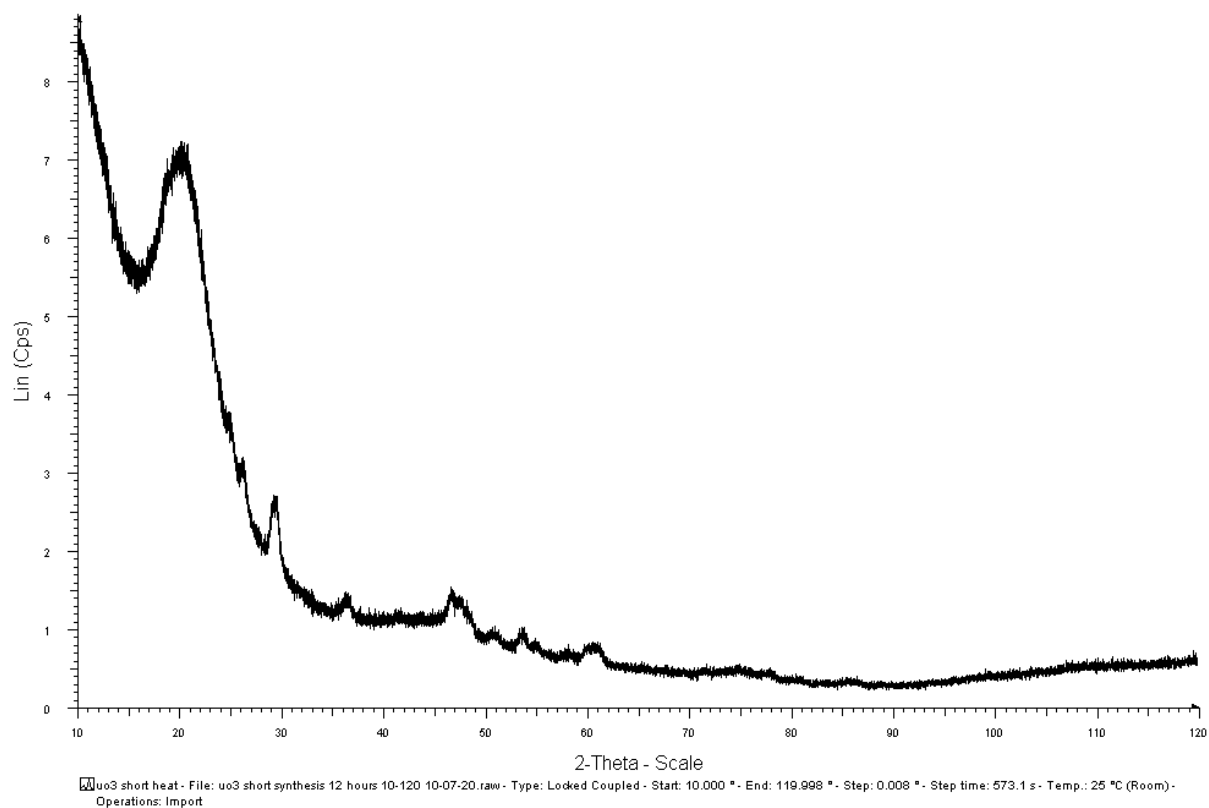


Figure 31: PXRD pattern of synthesized  $\text{UO}_3$  sample.

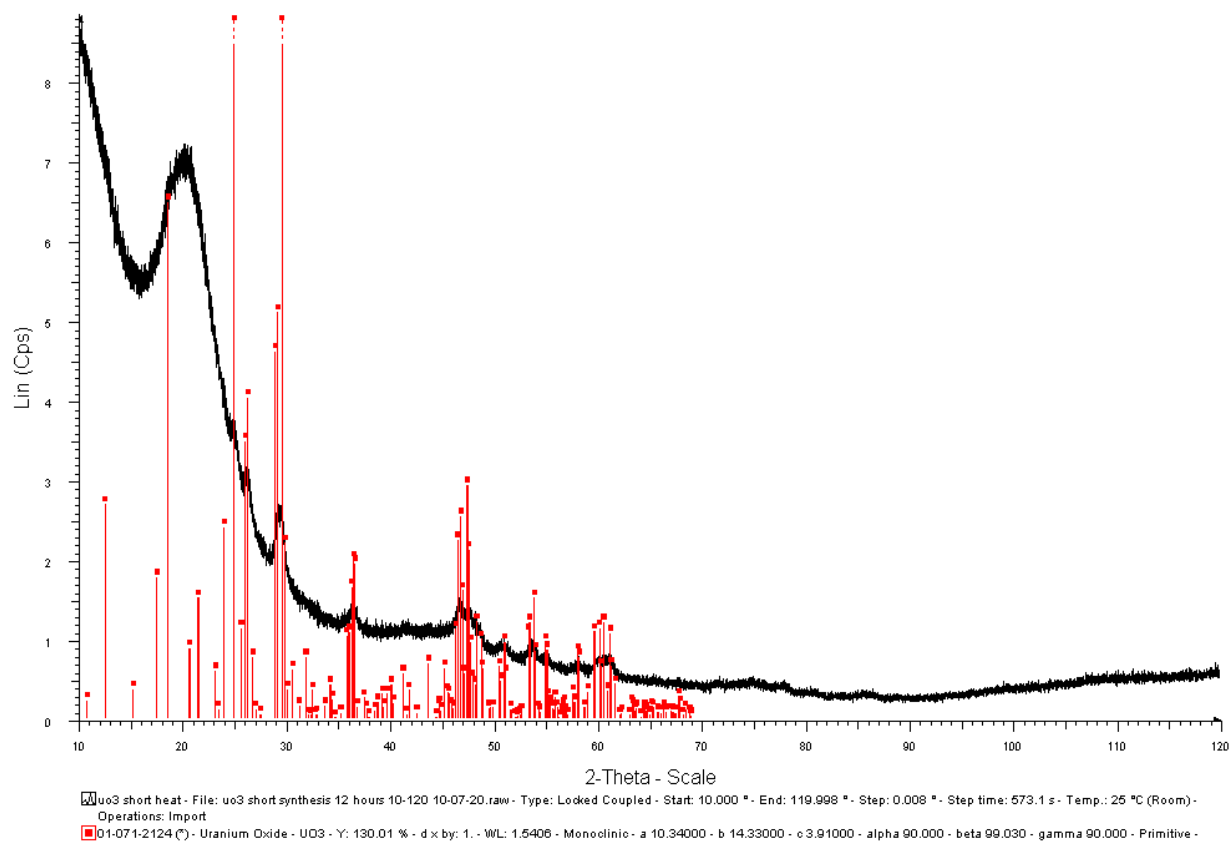


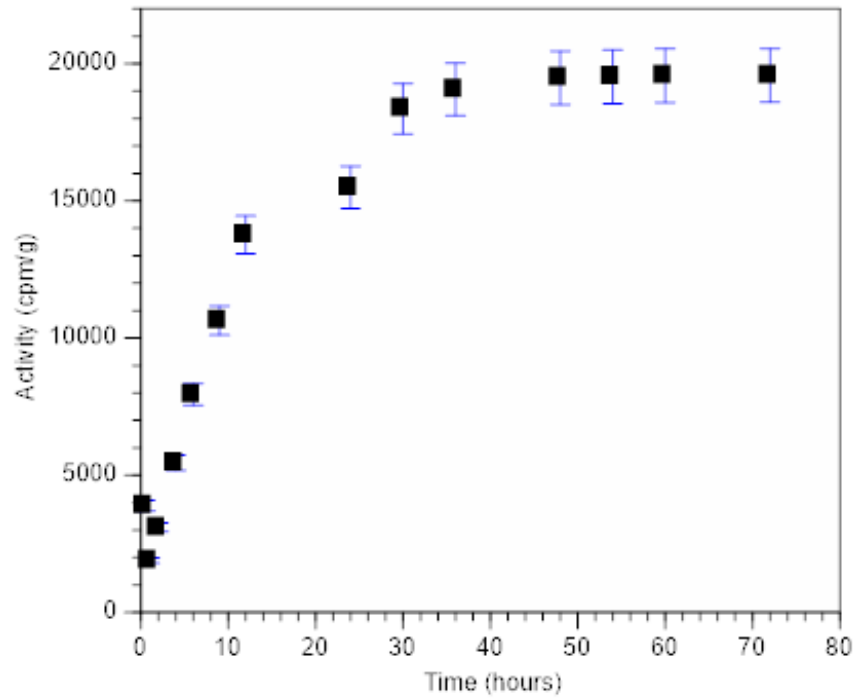
Figure 32: PXRD pattern of synthesized  $\text{UO}_3$ , with the matching pattern of  $\text{UO}_3$ .

#### 5.4 LSC

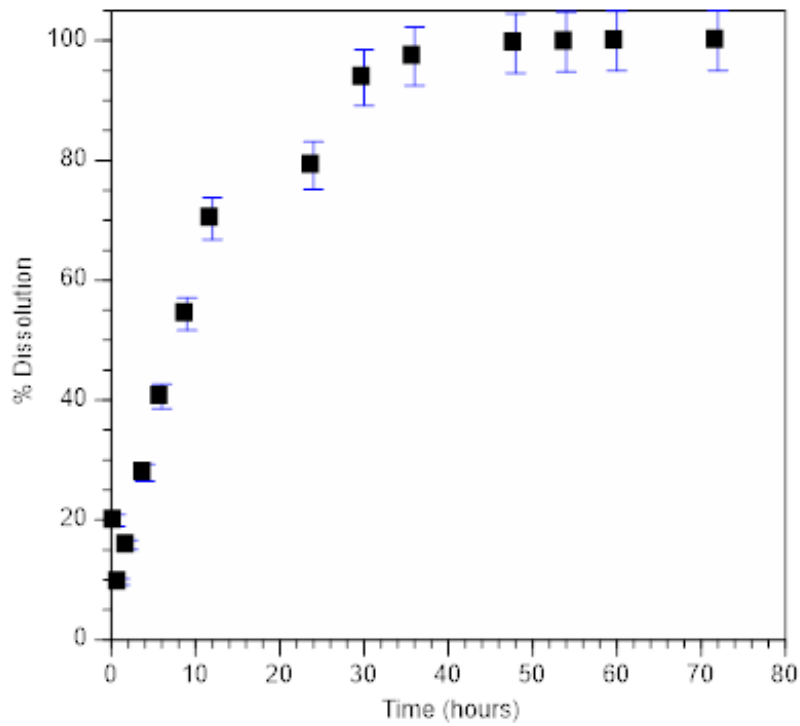
A sample of  $\text{UO}_3$  synthesized as described above for a 0.0247 M final uranyl concentration was dissolved in the IL. The sample appeared fully dissolved at 60 hours (clear yellow solution, with no undissolved material remaining). Aliquots were removed as described and prepared for LSC analysis. The resulting figure 33 (33a showing the dissolution over time in activity and 33b showing the dissolution over time as % dissolved) shows that the sample was fully dissolved between 30 and 40 hours from the start of the dissolution, consistent with visual observation. The graph shows the activity in counts per minute per gram of each sample over the

elapsed time from the start of the dissolution. The data shows saturation at around 36 hours, however the solution was still cloudy at this time (though no undissolved material remained in solution, the sample did not appear clear as other samples did).

The same data from figure 33 showing the activity over time is also represented in figure 34, which shows the best fit trendline matched to the data, a second order polynomial. Taking the derivative of the equation of the trendline provides a rate of dissolution, and the slope of that line provides a rate constant. The higher than expected activity in the 0.5 h aliquot is likely due to an undissolved particle that was not removed by centrifugation. The lower activity aliquot at 24 hours is likely a sampling error, where the volume dispensed was not fully incorporated into the vial. For  $\text{UO}_3$  the equation  $y = -6.6082x^2 + 678.45x + 3373.5$  provides a rate constant of -13.2. This is the slowest of the three reactions, because this dissolution is a chemical reaction, not simply oxidation. This chemical dissolution is slower, since the ozone flow has no affect (compared to the other two compounds, where the ozone is being constantly produced and bubbled through solution). Though this reaction rate is only an estimate it indicates that most of the dissolution is happening in the first 24 hours, with full dissolution occurring by approximately 30 hours, although this leaves the solution in a cloudy state that inhibits visual identification of final dissolution.



33a.



33b

Figure 33: Dissolution over time of  $UO_3$  in IL, a) activity in counts per minute per gram of sample and b) % of sample dissolved.

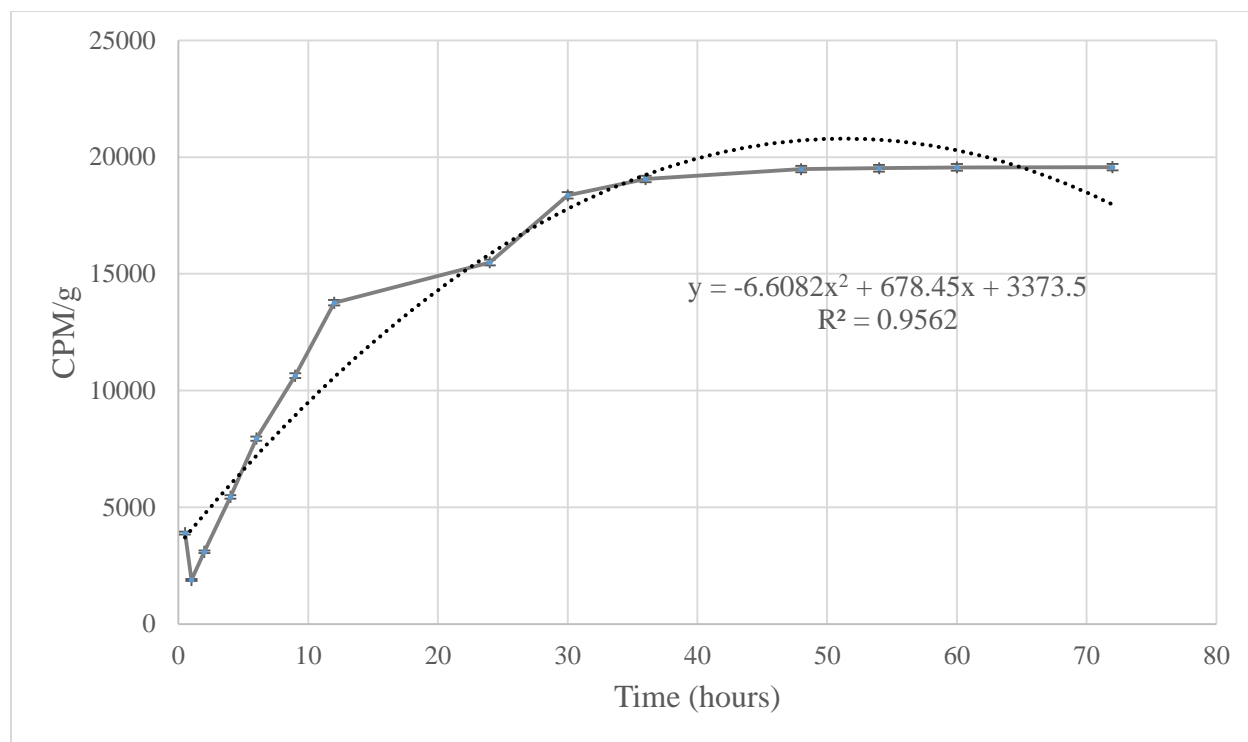


Figure 34: The dissolution of  $\text{UO}_3$  showing the rate of reaction.

### 5.5 UV-Visible spectroscopy

The final species in solution of an ozone-dissolved sample is uranyl,  $\text{UO}_2^{2+}$ . This species has a characteristic UV-Vis spectrum with a five banded peak, seen in Figure 35b) with peaks at 468 nm, 453 nm, 439 nm, 425 nm, and 414 nm. The electron transition representing each of these bands is the same as discussed previously in chapter 3. As done previously, the molar absorptivity coefficient was calculated using equation 2.14 with the peak intensity at 453 nm. First, the spectrum was normalized to the baseline, then the peak height was used as the absorbance value  $A$ . The solution concentration was 0.0247 M and the cell pathlength was the standard 1 cm. This resulted in the molar absorptivity coefficient  $\epsilon$  of 16.19. This is a larger value than those calculated for the  $\text{U}_3\text{O}_8$  and  $\text{UO}_2$  samples. This provides a qualitative

identification of uranyl in the sample. The intensity of the band also correlates with the concentration of the sample, but can be influenced by matrix effects.

By comparison, Figure 35a) shows an entirely different structure centered at ~420 nm inconsistent with U(VI) uranyl in IL but consistent with U(VI) uranyl in an aqueous environment.<sup>7</sup> A different peak was used for the molar absorptivity coefficient as there was no resolved peak at 453 nm. Using the same method at the highest intensity peak of 419 nm, the calculated molar absorptivity coefficient is 0.92, which is much smaller than any other sample. However, this sample is in an aqueous micro-environment, which affects both the normal absorbance intensity and can cause peak shifting. For reference, background samples of the IL that were exposed to ozone 35b) and not exposed to ozone 35a) were subtracted from the spectra.



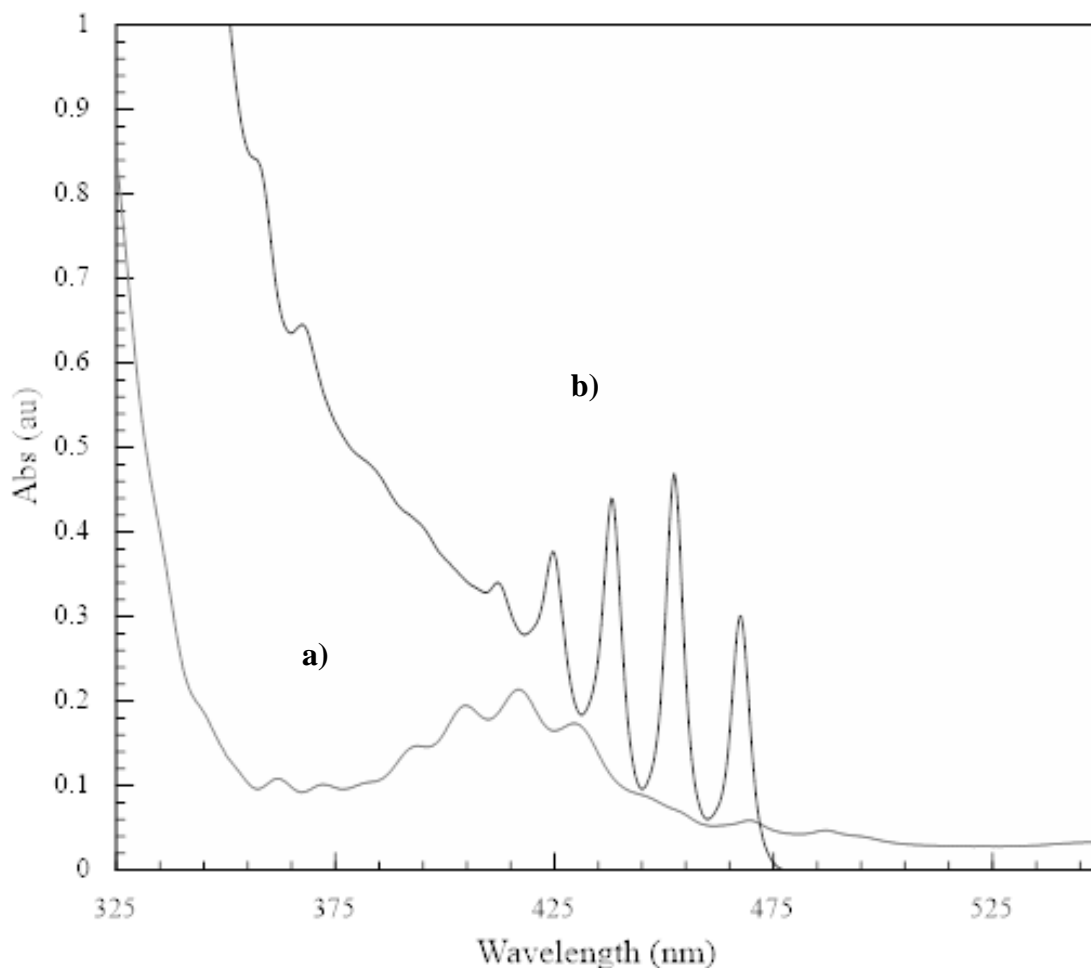


Figure 35: UV-Vis spectrum of dissolved  $\text{UO}_3$  sample showing a)  $\text{UO}_3$  dissolved without ozone in IL forming uranyl ( $\text{UO}_2^{2+}$ ) showing peak suppression from added water and HTFSI, and b)  $\text{UO}_3$  dissolved with ozone in neat IL forming uranyl ( $\text{UO}_2^{2+}$ ) with no peak suppression. Both spectra are background subtracted with the respective IL.

For comparison, the ozonated  $\text{UO}_3$  sample was analyzed by UV-Vis before and after performing electrochemical analysis. The resulting spectrum in figure 36 shows a) the sample before electrochemical analysis and b) the same sample after electrochemical analysis. The same peak resolution method used before (taking the normalized absorbance of the peak at 453 nm) for both samples. It was found that although the sample after electrochemical analysis had a

higher baseline (likely due to the changes in the IL from oxidation/reduction) the peak height was smaller. Using the same molar absorptivity coefficient from before, the value of the new concentration for the sample after electrochemical deposition was found to be 0.0179 M, a 27.5% reduction from the 0.0247 M starting concentration. Though this method is imprecise, where error could come from matrix effects, this peak height reduction does indicate a reduction in concentration after deposition is performed.

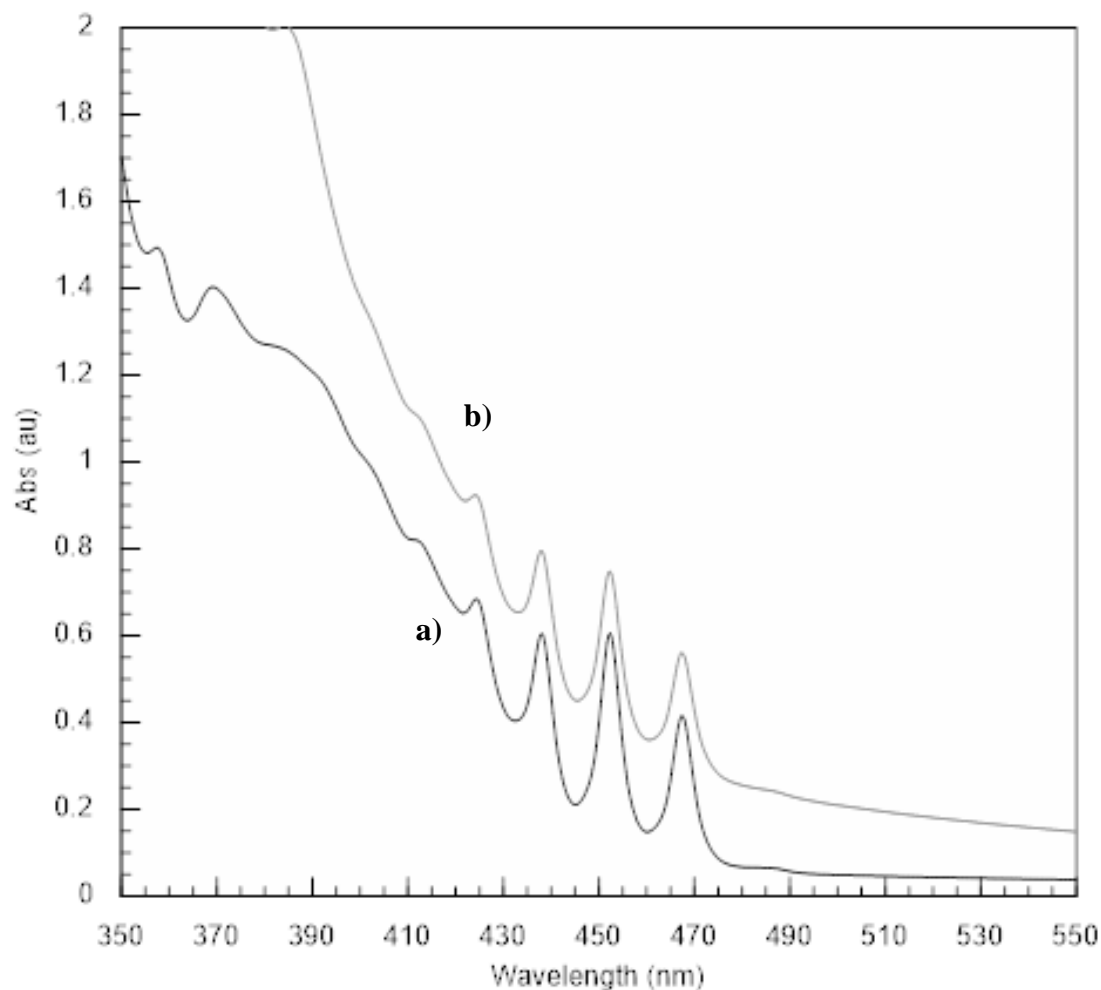


Figure 36: UV-Vis spectrum of  $\text{UO}_3$  sample both prior to electrochemical analysis (a) and after electrochemical analysis (b).

## 5.6 Electrochemical Analysis

As shown from the UV-Vis spectroscopy, the species once fully dissolved in solution is uranyl ( $\text{UO}_2^{2+}$ ). An exploration of this solution using cyclic voltammetry shows the redox reactions occurring in the sample, as shown in Fig 37-40. Each sample was analyzed using a three electrode cell, with a platinum sheet counter electrode, a gold mesh working electrode, and a silver wire/silver chloride (Ag/AgCl) reference electrode. The reference electrode was calibrated using 5 mM ferrocene, and then adjusted to the aqueous Ag/AgCl reference, a total shift of +0.536 V. The scan rate of 10 mV/s was selected to ensure the data collection was sensitive to the signal. The initial scan direction was positive, and multiple consecutive scans were performed until stasis was achieved. The ozonated sample seen in figure 37 was dried under vacuum to remove residual water. The acid/water sample without ozone seen in figure 38 was analyzed with no drying to study the complexation as-is in solution.

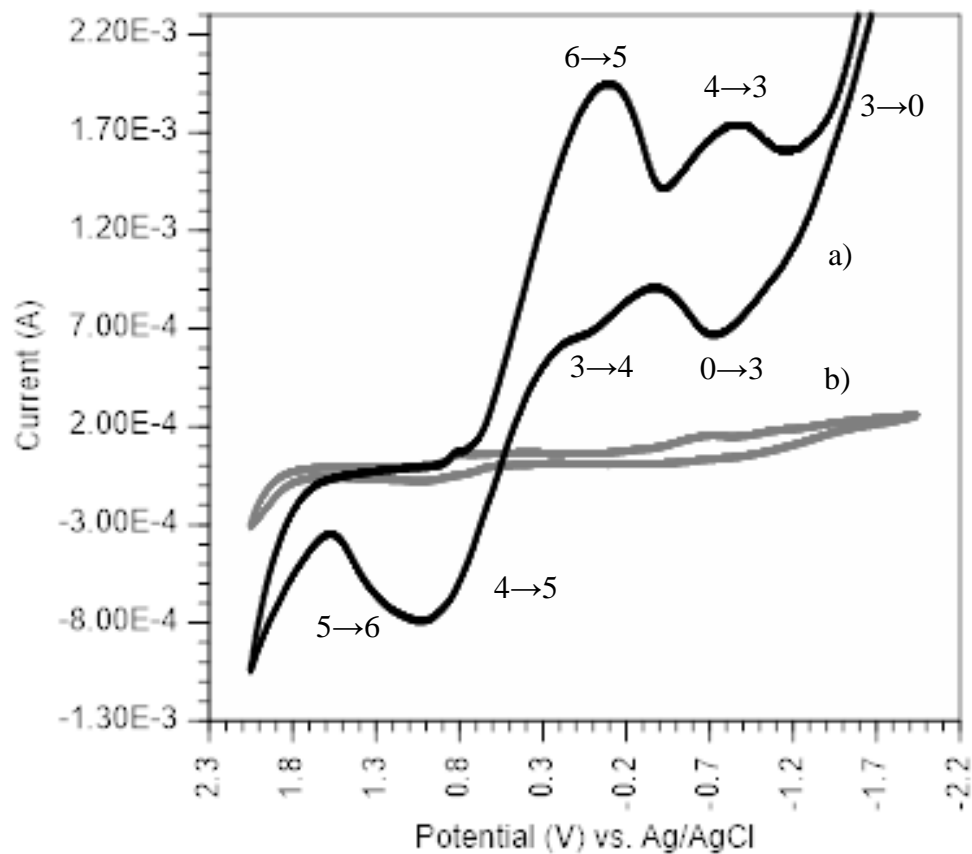


Figure 37: Cyclic voltammetry of uranyl from dissolved  $\text{UO}_3$  sample in IL where a) is a sample dissolved with ozone and b) is a blank IL sample.

Figure 37 shows the quasi-reversible reduction of  $\text{UO}_2^{2+}$  to  $\text{UO}_2$  at the surface of the gold mesh electrode. This peak is seen at -0.1 V vs Ag/AgCl. A second reduction step at -0.870 V vs Ag/AgCl, where the  $\text{UO}_2^+$  is reduced to  $\text{UO}_2$  (s). This reduction of U(VI) to U(V), an unstable transition state, and then to U(IV), a stable solid deposit, is the expected two-electron transfer reaction. The oxidation of the multiple species in solution is observed at +1.1 V vs Ag/AgCl, and may reflect both the release of  $\text{UO}_2$  (s) off the electrode surface and the oxidation of  $\text{UO}_2^+$  back to  $\text{UO}_2^{2+}$ .

Figure 38 shows the single step reduction step occurs at  $-0.870\text{ V}$  vs Ag/AgCl, where the  $\text{UO}_2^{2+}$  is reduced to U(IV) in the non-ozonated sample followed by deposition at the electrode with competing hydrogen evolution at  $-1.5\text{ V}$ . This growth and the subsequent reverse oxidation is not seen in the ozonated sample. In fact, the non-ozonated sample had visible deposition on the electrode surface after cyclic voltammetry was complete, as opposed to the microscopic nucleation sites that deposit from the ozonated sample. This also contributed to the much smaller oxidation peak at  $+0.6\text{ V}$  compared to the ozone dissolution sample, which had quasi-reversible reduction steps. The graph also shows hydrolysis at the electrode surface from the acid and high water content, which was not seen in the ozonated sample, with oxygen evolution at  $+1.0\text{ V}$  and hydrogen evolution at  $-1.5\text{ V}$ .

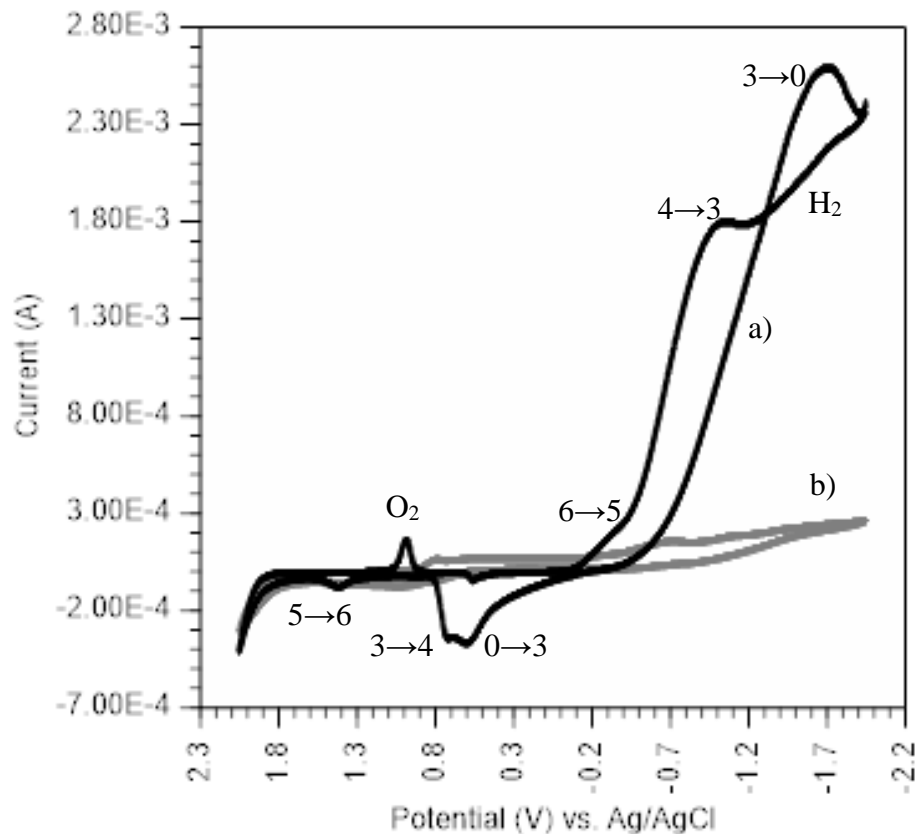


Figure 38: showing the oxidation and reduction peaks of the uranyl species in solution where a) shows the ozone dissolved sample and b) shows the non-ozone sample.

The cyclic voltammetry shown in figures 37 and 38 represent a mid-range of the potential window available for exploration. When the potential window is expanded, the quasi-reversible electron transitions seen can become quasi- and non-reversible reduction on the electrode. In figures 39 and 40, the potential window was expanded to -2.5 V vs. Ag/AgCl. By driving the solution to more negative potentials, more of the solution reduced to  $\text{UO}_3$  (s) and deposited irreversibly at the electrode surface. This results in large reduction peaks with little to no oxidation peaks.

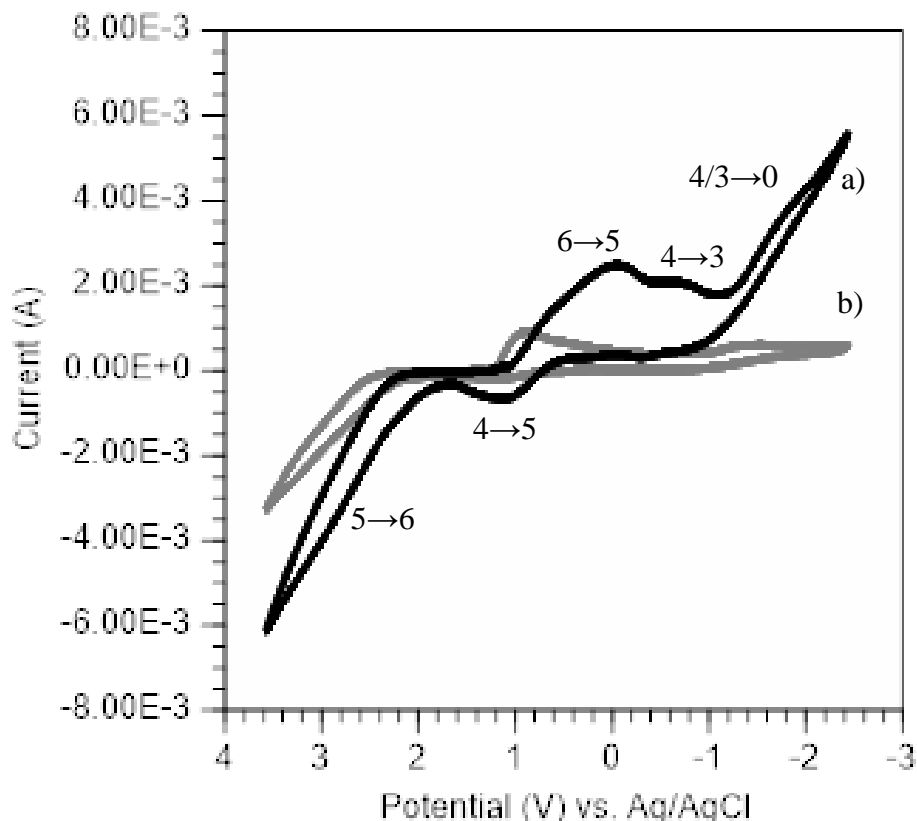


Figure 39: Reduction of uranyl due to the expanded electrochemical potential window with a) ozonated IL sample and b) the blank IL sample.

The large and overlapping peaks from +0.2 V to -1.0 V contain multiple species transitions. The two major transitions are shown on the graph, but the U(V) to U(IV) electron transfer is likely to be conflated in that range. Since peak area (charge) is proportional to the amount of species in solution undergoing that transition, the very large reductions peaks compared to the much smaller oxidation peaks show a solution that is driving to deposition and not reversing. This process is seen to an even stronger effect in figure 40, which shows total reduction peak overlap with no reverse oxidation. This resulted in deposition on the electrode surface not seen in any other sample.

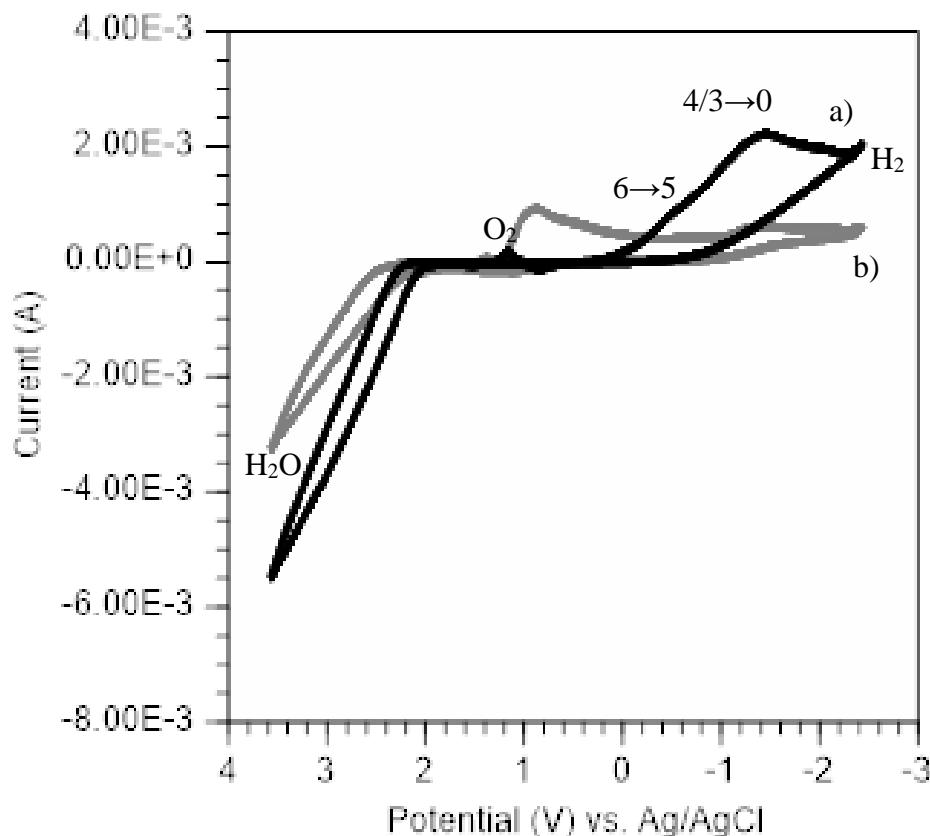


Figure 40: a) shows the complete reduction in solution of the uranyl species in the non-ozonated sample and b) shows the blank IL background in gray.

### 5.7 SEM/EDX

Scanning electron microscopy is an electron scatter imaging technique that can be used in conjunction with EDX to semi-quantitatively determine the elemental composition of a sample. SEM analysis was used to image multiple UO<sub>3</sub> samples, including standard and synthesized materials. The UO<sub>3</sub> standard is shown in figures 41-43, with the uranium oxide deposit shown in figures 44-46. The deposit analyzed using scanning electron microscopy (SEM) and energy dispersive X-ray spectroscopy (EDX) was prepared from a 25 mM uranyl in IL solution. The technique used was pulse deposition, with varying pulses of negative and positive potentials



applied to the gold mesh electrode. The major peaks found in the  $\text{UO}_2$  standard belong to uranium (U), oxygen (O), and carbon (C). The same peaks are found in the uranium oxide deposit, as well as a sulfur (S) and fluorine (F) peak which was a remnant of the IL and gold (Au) from the gold mesh electrode. The carbon peak is reduced in the uranium standard sample relative to the deposit sample as expected, since the standard covers the carbon tape while the deposit on the gold mesh electrode leaves some of the carbon tape revealed. The uranium and oxygen peaks in the deposit show a clear signal, indicating that the sample is uranium oxide recovered successfully from the ionic liquid.

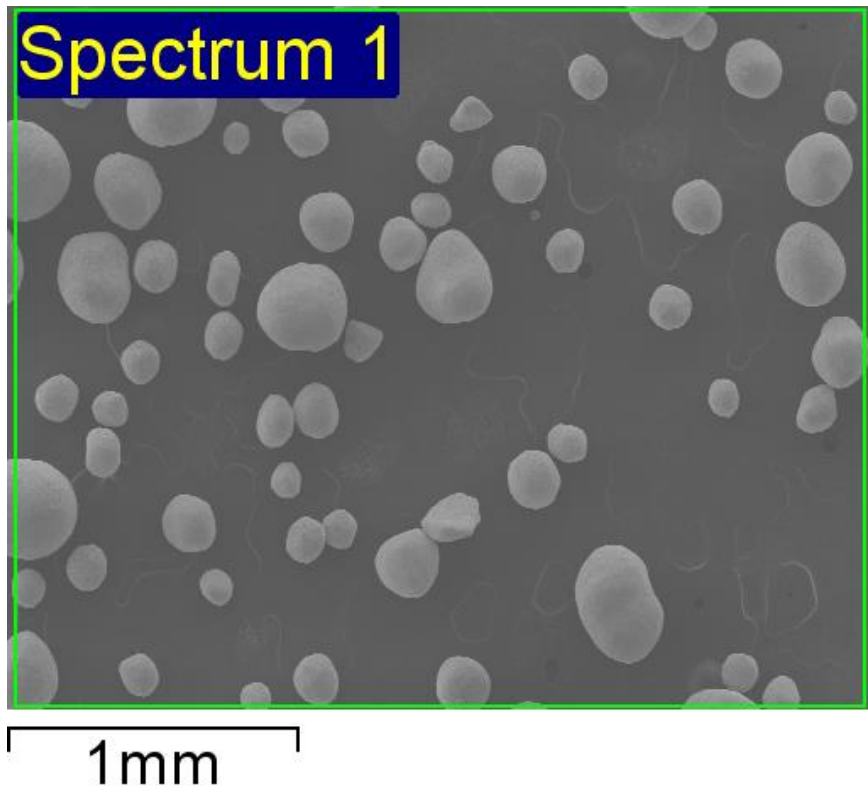


Figure 41:  $\text{UO}_3$  standard material SEM image at 35x magnification.

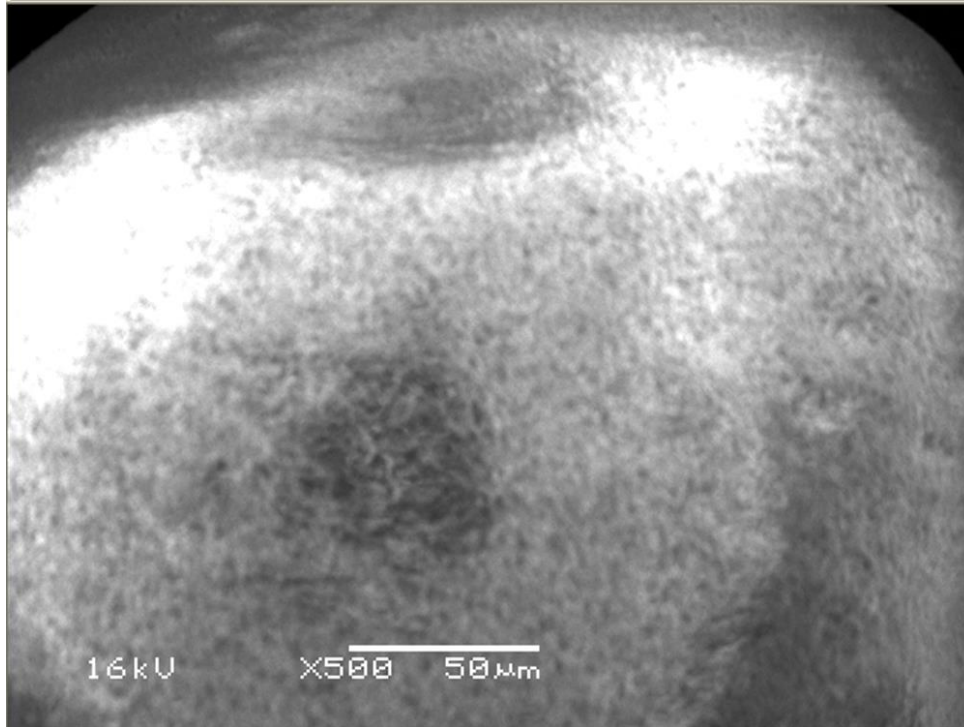


Figure 42: The same standard  $\text{UO}_3$  material shown at 500x magnification.

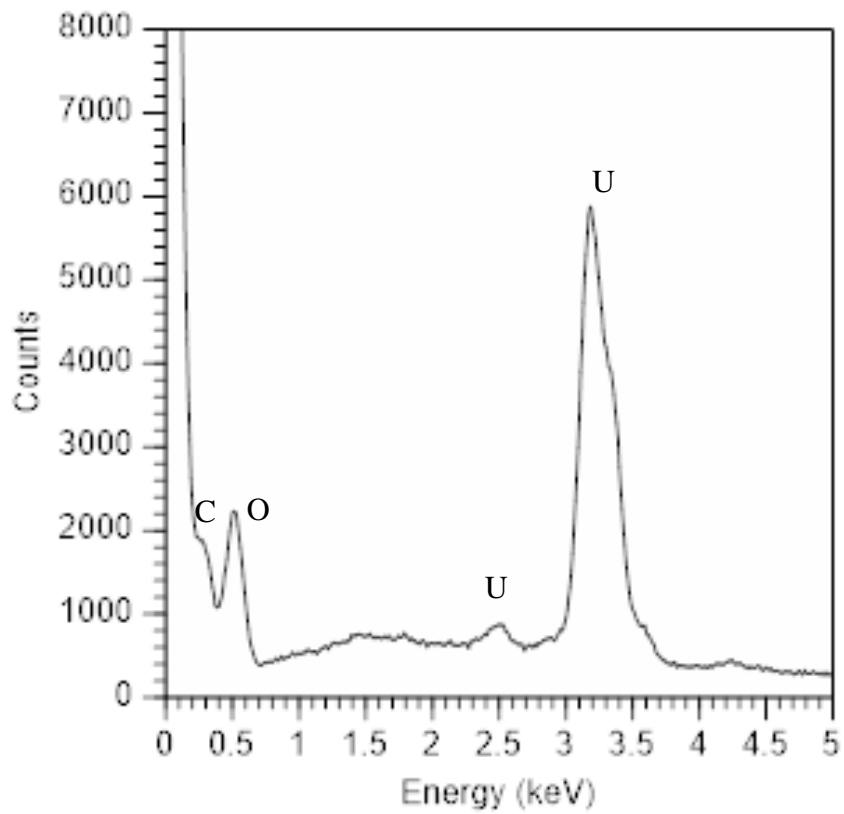


Figure 43: EDX of  $\text{UO}_3$  standard material at 16 kV beam energy and 500x magnification.

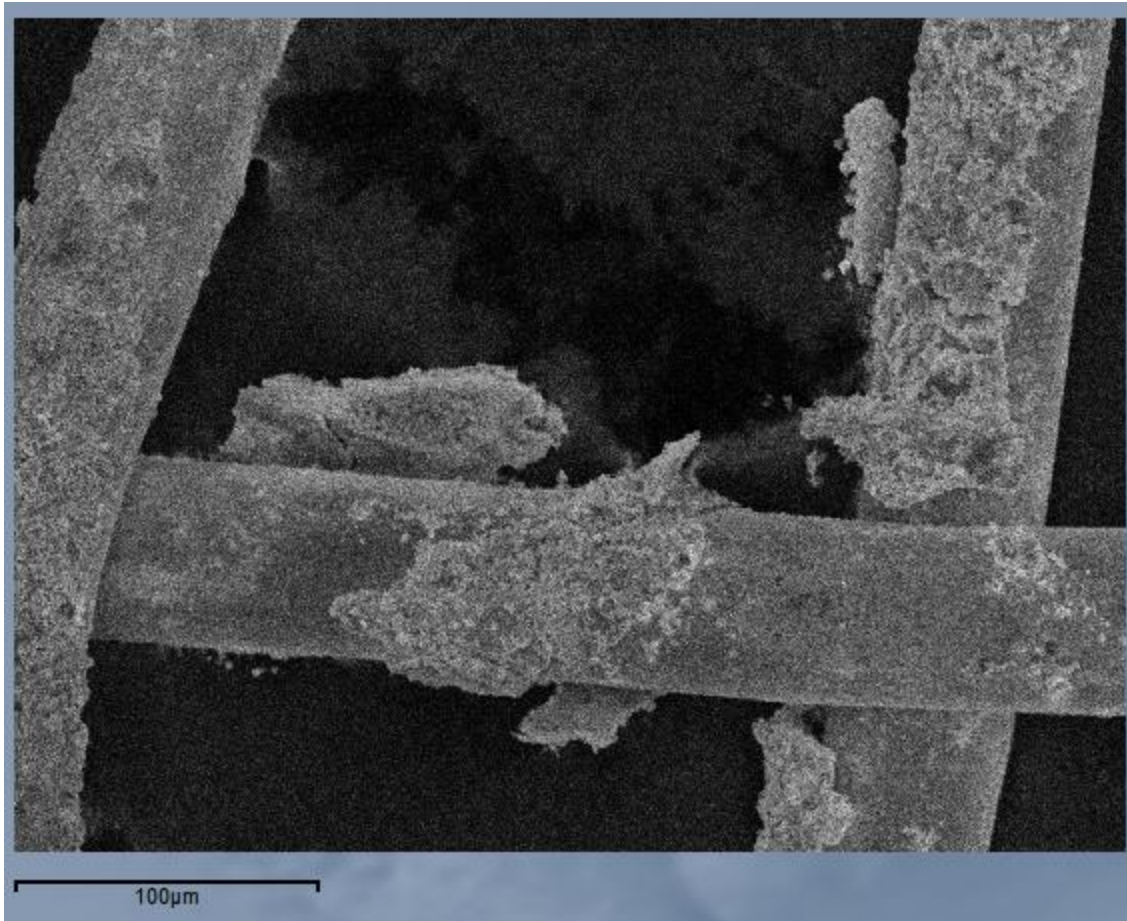


Figure 44: SEM image of UO<sub>3</sub> deposit on gold mesh electrode at 15 kv beam energy and 250x magnification.

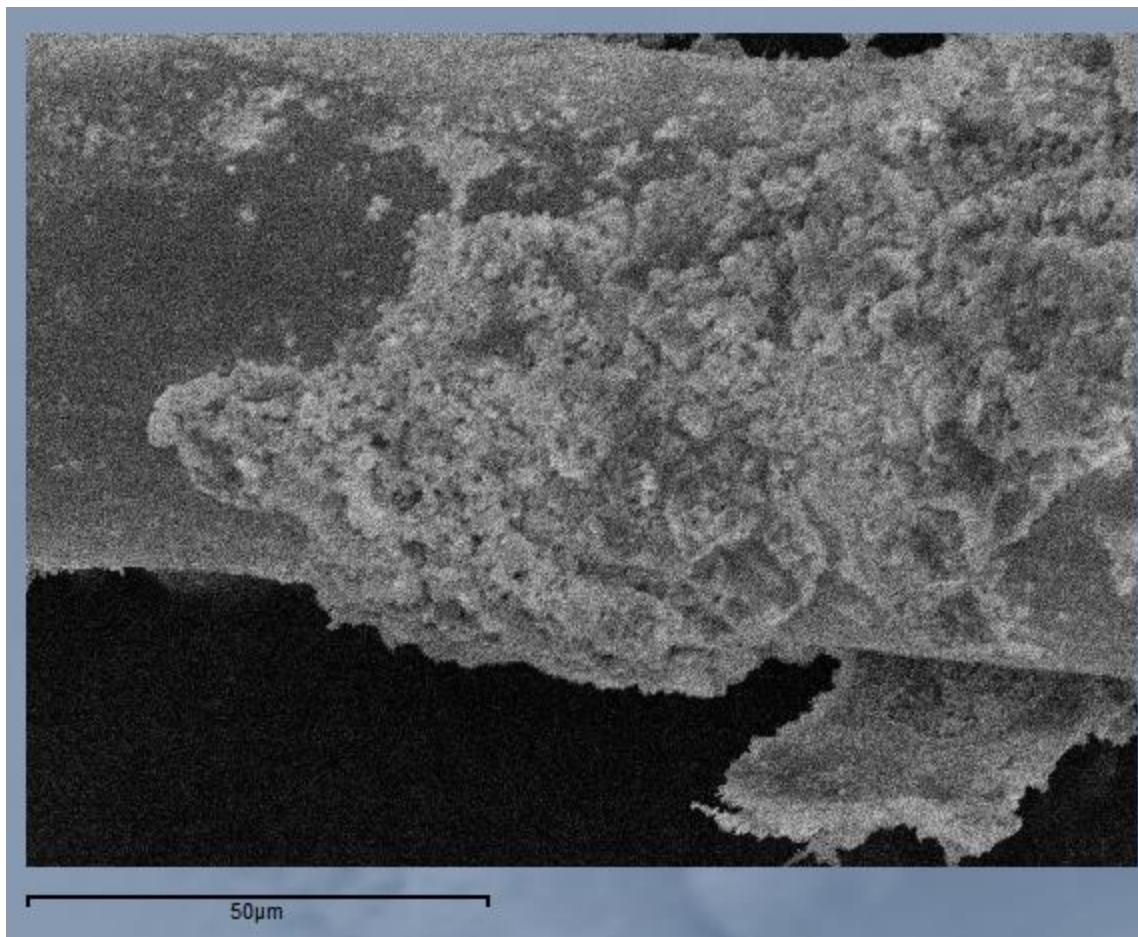


Figure 45: SEM image of UO<sub>3</sub> deposit on gold mesh electrode at 15 kv beam energy and 500x magnification.

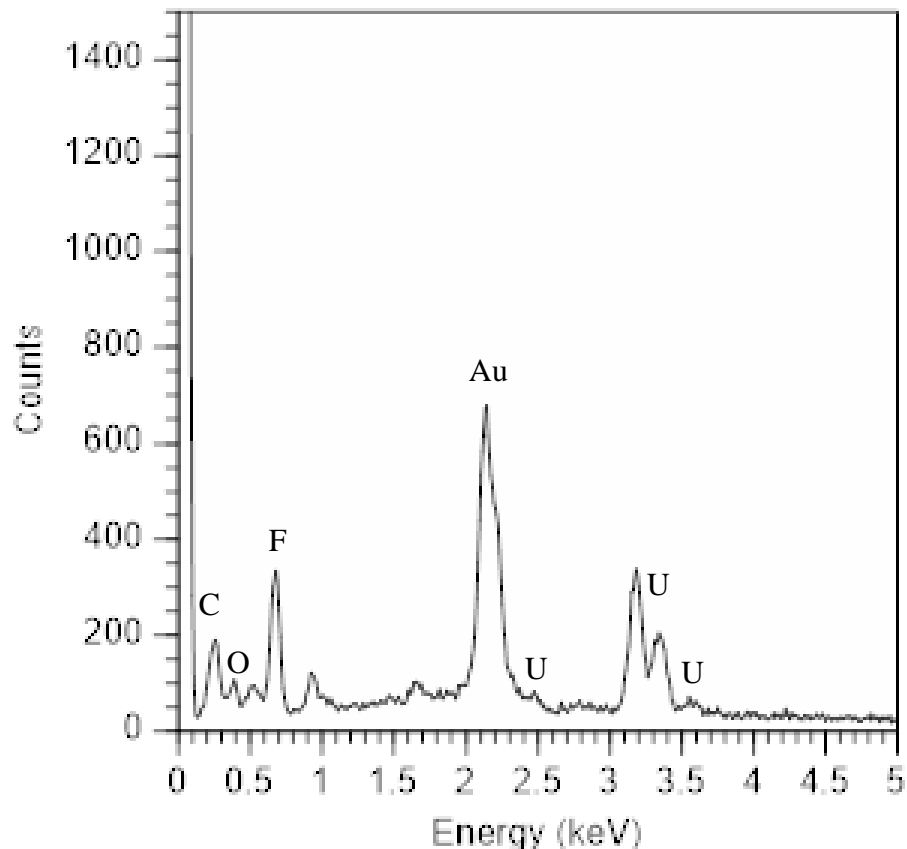


Figure 46: EDX spectrum of UO<sub>3</sub> deposit on gold mesh electrode at 15 kv beam energy and 250x magnification. Fluorine peak indicates the presence of IL still on the electrode.

## 5.8 Conclusion

The dissolution and recovery of synthesized UO<sub>3</sub> was explored in n-trimethyl-n-butylammonium bis(trifluoromethanesulfonyl)imide ionic liquid. The synthesis was successful, with the final mass recorded as 0.3431g UO<sub>3</sub> which was a 85.76% recovery. PXRD confirmed the material was monoclinic UO<sub>3</sub> which is the beta phase compound. Dissolution was successful with ozone at 24.7 mM and was monitored by liquid scintillation counting with a rate constant of -13.2. Dissolution was successful at 25 mM without the presence of ozone, although the non-ozonated sample required HTFSI acid and water saturated IL to dissolve. Fully dissolved samples were analyzed by UV-Visible spectroscopy (with a molar absorptivity coefficient of

16.19). UV-Vis spectra of the same  $\text{UO}_3$  sample both before and after electrochemical deposition showed a reduced concentration even with an increased baseline. This showed that deposition at the electrode resulted in a 27.5% reduction of concentration in solution. Cyclic voltammetry indicates that the solution would undergo electron transitions to the reduced solid state, though reversibility depended on the matrix conditions and the electrochemical window studied. Both spectroscopic and electrochemical techniques suggest the species in solution is uranyl,  $\text{UO}_2^{2+}$ . Although the sample dissolved without ozone showed interference from hydrolysis, that sample as deposited easily at the electrode surface. Deposition was performed and black dendritic deposits were collected. SEM/EDX analysis shows amorphous uranium oxide deposits. The most likely identity of these deposits is  $\text{UO}_2$  based on the species in solution.

## Chapter 6: Conclusions

With a demonstrated need for exploration of uranium oxide study in the field of nuclear waste and storage, this dissertation proposes a novel path of study. It has been shown that ionic solvents are well suited for actinide ion extraction and dissolution; liquid fuel use, transportation, and storage; and electrochemical study and recovery. The ionic liquid n-trimethyl-n-butylammonium bis(trifluoromethanesulfonyl)imide [Me<sub>3</sub>NnBu][TFSI] is suitable for the direct dissolution and electrochemical recovery of uranium oxides with oxidizing gas generated from compressed air. In exploring this chemical pathway of a full range of uranium oxide compounds, comparisons to modern nuclear fuel cycle processes can be made and evaluated, thus adding knowledge to the field. The work of this dissertation shows the viability of a standard procedure for in-situ dissolution and recovery of any uranium oxide used in the nuclear fuel cycle.

This dissertation discusses the synthesis of uranium oxides and the characterization methodologies used to dissolve, analyze, and recover the compounds. First, the uranium oxides (U<sub>3</sub>O<sub>8</sub>, UO<sub>2</sub>, and UO<sub>3</sub>) were synthesized with a tracing spike of <sup>233</sup>U to increase the activity of the samples and characterized with powder X-ray diffraction. The uranium oxides were then dissolved directly into the ionic liquid solvent with ozone generated from compressed air, with the exception of UO<sub>3</sub>, which was also dissolved in a non-ozonated IL sample with water and acid. Each sample was then analyzed with UV-vis spectroscopy, liquid scintillation counting, and cyclic voltammetry. Then electrochemical deposition was performed, and deposits were analyzed by scanning electron microscopy and energy dispersive X-ray spectroscopy.

First, the dissolution and recovery of synthesized U<sub>3</sub>O<sub>8</sub> in was explored in n-trimethyl-n-butylammonium bis(trifluoromethanesulfonyl)imide ionic liquid. The synthesis was successful, with the final mass recorded as 0.3959 g of U<sub>3</sub>O<sub>8</sub>, a 74.69% recovery. PXRD confirmed the

material was alpha phase  $U_3O_8$ . Dissolution was successful at both 27 mM and 0.94 M concentrations, and in the presence of water and acid [HTFSI]. Dissolution was monitored by liquid scintillation counting with a rate constant of -80.9, and fully dissolved samples were analyzed by UV-Visible spectroscopy (with a molar absorptivity coefficient of 14.56) and cyclic voltammetry. Cyclic voltammetry indicates that even in the presence of water and/or HTFSI the uranyl species in solution would undergo electron transitions to the reduced solid state, though reversibility depended on the matrix conditions. Both spectroscopic and electrochemical techniques suggest the species in solution is uranyl,  $UO_2^{2+}$ . Deposition was performed and black dendritic deposits were collected. SEM/EDX analysis shows amorphous uranium oxide deposits, results that match PXRD analysis. The most likely identity of these deposits is  $UO_2$  based on the species in solution.

Second, the dissolution and recovery of synthesized  $UO_2$  was explored in n-trimethyl-n-butylammonium bis(trifluoromethanesulfonyl)imide ionic liquid. The synthesis was successful, with the final mass recorded as 0.7604g  $UO_2$  which was a 78.24% yield. PXRD confirmed the material was face-centered cubic uraninite ( $UO_2$ ), the only phase of this compound. Dissolution was successful at 25 mM and was monitored by liquid scintillation counting with a rate constant of -58.5, and fully dissolved samples were analyzed by UV-Visible spectroscopy (with a molar absorptivity coefficient of 13.11) and cyclic voltammetry. Cyclic voltammetry indicates that the solution would undergo electron transitions to the reduced solid state, though reversibility depended on the matrix conditions and the electrochemical window studied. Both spectroscopic and electrochemical techniques suggest the species in solution is uranyl,  $UO_2^{2+}$ . Deposition was performed and black dendritic deposits were collected. SEM/EDX analysis shows amorphous



uranium oxide deposits. The most likely identity of these deposits is  $\text{UO}_2$  based on the species in solution.

Finally, the dissolution and recovery of synthesized  $\text{UO}_3$  was explored in n-trimethyl-n-butylammonium bis(trifluoromethanesulfonyl)imide ionic liquid. The synthesis was successful, with the final mass recorded as 0.3431 g  $\text{UO}_3$  which was a 85.76% recovery. PXRD confirmed the material was monoclinic  $\text{UO}_3$  which is the beta phase compound. Dissolution was successful with ozone at 24.7 mM and was monitored by liquid scintillation counting with a rate constant of -13.2. Dissolution was successful at 25 mM without the presence of ozone, although the non-ozonated sample required HTFSI acid and water saturated IL to dissolve. Fully dissolved samples were analyzed by UV-Visible spectroscopy (with a molar absorptivity coefficient of 16.19). UV-Vis spectra of the same  $\text{UO}_3$  sample both before and after electrochemical deposition showed a reduced concentration even with an increased baseline. This showed that deposition at the electrode resulted in a 27.5% reduction of concentration in solution. Cyclic voltammetry indicates that the solution would undergo electron transitions to the reduced solid state, though reversibility depended on the matrix conditions and the electrochemical window studied. Both spectroscopic and electrochemical techniques suggest the species in solution is uranyl,  $\text{UO}_2^{2+}$ . Although the sample dissolved without ozone showed interference from hydrolysis, that sample as deposited easily at the electrode surface. Deposition was performed and black dendritic deposits were collected. SEM/EDX analysis shows amorphous uranium oxide deposits. The most likely identity of these deposits is  $\text{UO}_2$  based on the species in solution.

The reproducibility of the explored ozone dissolution process, which resulted in consistent spectroscopic, electrochemical, and microscopic analysis regardless of starting material, shows a viable procedure for the reuse and recovery of nuclear “waste” materials such

as spent fuel and depleted uranium discarded from enrichment. To expand on this work, further exploration of the chemical dissolution of  $\text{UO}_3$  could be pursued. Further exploration of the ideal parameters for deposition could prove advantageous for electrochemical analysis. Additionally, the process of ozone dissolution in IL can be applied to other actinides or lanthanides, specifically plutonium oxide materials.

## References

- <sup>1</sup> Uranium dioxide | UO<sub>2</sub> - PubChem <https://pubchem.ncbi.nlm.nih.gov/compound/Uranium-dioxide#section=Experimental-Properties> (accessed May 6, 2020).
- <sup>2</sup> 1344-58-7 CAS MSDS (URANIUM(VI) OXIDE) Melting Point Boiling Point Density CAS Chemical Properties [https://www.chemicalbook.com/ChemicalProductProperty\\_US\\_CB6362445.aspx](https://www.chemicalbook.com/ChemicalProductProperty_US_CB6362445.aspx) (accessed May 6, 2020).
- <sup>3</sup> Thein, S. M.; Bereolos, P. J. *Thermal Stabilization of 233 UO<sub>2</sub>, 233 UO<sub>3</sub>, and 233 U<sub>3</sub>O<sub>8</sub>*.
- <sup>4</sup> King, H. M. Uraninite. <https://geology.com/minerals/uraninite.shtml>.
- <sup>5</sup> Table of Nuclides <http://atom.kaeri.re.kr/nuchart/> (accessed May 13, 2020).
- <sup>6</sup> USNRC. Stages of the Nuclear Fuel Cycle. <https://www.nrc.gov/materials/fuel-cycle-fac/stages-fuel-cycle.html>
- <sup>7</sup> USNRC. MODULE 1.0: OVERVIEW OF THE NUCLEAR FUEL CYCLE. <https://www.nrc.gov/docs/ML1204/ML12045A003.pdf>
- <sup>8</sup> DOE. Spent Nuclear Fuel and High Level Radioactive Waste Inventory Report.
- <sup>9</sup> <https://www.world-nuclear.org/information-library/facts-and-figures/uranium-production-figures.aspx>
- <sup>10</sup> Uranium. 2003
- <sup>11</sup> U.S. nuclear industry - U.S. Energy Information Administration (EIA) <https://www.eia.gov/energyexplained/nuclear/us-nuclear-industry.php> (accessed May 4, 2020). <https://www.eia.gov/energyexplained/nuclear/us-nuclear-industry.php> (accessed May 4, 2020).
- <sup>12</sup> What's the Lifespan for a Nuclear Reactor? Much Longer Than You Might Think | Department of Energy <https://www.energy.gov/ne/articles/whats-lifespan-nuclear-reactor-much-longer-you-might-think> (accessed May 4, 2020).
- <sup>13</sup> Hewlett, R. G.; Anderson, O. E. *The New World, 1939/1946, A History of The United States Atomic Energy Commission, Volume I*, The Pennsylvania State University Press, University Park, Pennsylvania, 1962; 1939.
- <sup>14</sup> Nuclear Waste <https://www.nei.org/fundamentals/nuclear-waste> (accessed May 4, 2020).
- <sup>15</sup> Used Nuclear Fuel <https://www.nei.org/advocacy/make-regulations-smarter/used-nuclear-fuel> (accessed May 4, 2020).
- <sup>16</sup> Starks, J. B. *The PUREX Process*; E. I. du Pont de Nemours & Company, 1977.
- <sup>17</sup> Paiva, A. P.; Malik, P. *Recent Advances on the Chemistry of Solvent Extraction Applied to the Reprocessing of Spent Nuclear Fuels and Radioactive Wastes*; **2004**; Vol. 261.
- <sup>18</sup> Gill, M.; Livens, F.; Peakman, A. Nuclear Fission. In *Future Energy: Improved, Sustainable and Clean Options for our Planet*; Elsevier Inc., **2013**; pp 181–198.
- <sup>19</sup> Oak Ridge National Laboratory. Molten Salt Chemistry Workshop; 2017.
- <sup>20</sup> Gupta, N. K. Ionic Liquids for TRansUranic Extraction (TRUEX)—Recent Developments in Nuclear Waste Management: A Review. *Journal of Molecular Liquids*. Elsevier B.V. November 1, **2018**, pp 72–91.
- <sup>21</sup> Mishra, B.; Olson, D. L. Molten Salt Applications in Materials Processing. *Journal of Physics and Chemistry of Solids* **66**, **2005**, 396–401.
- <sup>22</sup> Archimede Solar Energy [http://www.archimedesolarenergy.it/molten\\_salt.htm](http://www.archimedesolarenergy.it/molten_salt.htm) (accessed May 12, 2020).

- <sup>23</sup> What is Molten Salt? <http://moltensalt.org/whatIsMoltenSalt.html> (accessed May 13, 2020).
- <sup>24</sup> Ignatiev, V. V.; Kormilitsyn, M. V.; Kormilitsyna, L. A.; Semchenkov, Y. M.; Fedorov, Y. S.; Feinberg, O. S.; Kryukov, O. V.; Khaperskaya, A. V. MOLTEN-SALT REACTOR FOR NUCLEAR FUEL CYCLE CLOSURE ON ALL ACTINIDES. *At. Énergiya* **2019**, *125* (5), 251–255.
- <sup>25</sup> Molten Salt Reactors - World Nuclear Association <https://www.world-nuclear.org/information-library/current-and-future-generation/molten-salt-reactors.aspx> (accessed May 13, 2020).
- <sup>26</sup> Seddon, K. R.; Stark, A.; Torres, M. J. Influence of Chloride, Water, and Organic Solvents on the Physical Properties of Ionic Liquids. In *Pure and Applied Chemistry*; Walter de Gruyter GmbH, 2000; Vol. 72, pp 2275–2287. <https://doi.org/10.1351/pac200072122275>.
- <sup>27</sup> Murali Krishna, G.; Suneesh, A. S.; Kumaresan, R.; Venkatesan, K. A.; Antony, M. P. Dissolution of U 3 O 8 in 1-Butyl-3-Methylimidazolium Chloride and Spectroscopic and Electrochemical Behavior of U(VI) in the Resultant Solution. *J. Electroanal. Chem.* **2017**, *795*, 51–58.
- <sup>28</sup> Cocalia, V. A.; Gutowski, K. E.; Rogers, R. D. The Coordination Chemistry of Actinides in Ionic Liquids: A Review of Experiment and Simulation. *Coordination Chemistry Reviews*. April 2006, pp 755–764.
- <sup>29</sup> Mohapatra, P. K. Actinide Ion Extraction Using Room Temperature Ionic Liquids: Opportunities and Challenges for Nuclear Fuel Cycle Applications. *Dalt. Trans.* **2017**, *46*, 1730.
- <sup>30</sup> Vasudeva Rao, P. R.; Venkatesan, K. A.; Rout, A.; Srinivasan, T. G.; Nagarajan, & K. Potential Applications of Room Temperature Ionic Liquids for Fission Products and Actinide Separation. *Sep. Sci. Technol.* **2012**, *47* (2), 204–222.
- <sup>31</sup> Chiappe, C.; Malvaldi, M.; Melai, B.; Fantini, S.; Bardi, U.; Caporali, S. An Unusual Common Ion Effect Promotes Dissolution of Metal Salts in Room-Temperature Ionic Liquids: A Strategy to Obtain Ionic Liquids Having Organic–Inorganic Mixed Cations. *Green Chem.* **2010**, *12* (1), 77–80.
- <sup>32</sup> Pereiro, A. B.; Araújo, J. M. M.; Oliveira, F. S.; Esperança, J. M. S. S.; Canongia Lopes, J. N.; Marrucho, I. M.; Rebelo, L. P. N. Solubility of Inorganic Salts in Pure Ionic Liquids. *J. Chem. Thermodyn.* **2012**, *55*, 29–36.
- <sup>33</sup> Murali Krishna, G.; Suneesh, A. S.; Kumaresan, R.; Venkatesan, K. A.; Antony, M. P. Dissolution of U 3 O 8 in 1-Butyl-3-Methylimidazolium Chloride and Spectroscopic and Electrochemical Behavior of U(VI) in the Resultant Solution. *J. Electroanal. Chem.* **2017**, *795*, 51–58.
- <sup>34</sup> Binnemans, K. Lanthanides and Actinides in Ionic Liquids. **2007**.
- <sup>35</sup> Pemberton, W. J.; Droessler, J. E.; Kinyanjui, J. M.; Czerwinski, K. R.; Hatchett, D. W. Electrochimica Acta Electrochemistry of Soluble UO 2 2+ from the Direct Dissolution of UO 2 CO 3 in Acidic Ionic Liquid Containing Water. *Electrochim. Acta* **2013**, *93*, 264–271.
- <sup>36</sup> Bard, A. J.; Parsons, R.; Jordan, J. *Standard Potentials in Aqueous Solution*; IUPAC, 1985.
- <sup>37</sup> Droessler, J. E. *DIRECT DISSOLUTION AND ELECTROCHEMICAL INVESTIGATION OF CERIUM AND URANIUM IN IONIC LIQUID*; 2016.
- <sup>38</sup> Long, K.; Goff, G.; Runde, W.; Unusual redox stability of neptunium in the ionic liquid [Hbet][Tf2N]. *ChemComm Chemical Communications.* **2014**, *50*, 7766.
- <sup>39</sup> Sweet, L.; Henager, C. J.; Hu, S.; Johnson, T.; Meier, D.; Peper, S.; Schwantes, J. Investigation of Uranium Polymorphs. **2011**, No. August.

- <sup>40</sup> Alfaro, P. O.; Torres, J. H.; Thiele, F. P. Reduction Kinetics of Uranium Trioxide to Uranium Dioxide Using Hydrogen. *World J. Nucl. Sci. Technol.* **2015**, *5*, 149–156.  
<https://doi.org/10.4236/wjnst.2015.53015>.
- <sup>41</sup> Ball, M. C.; Birkett, C. R. G.; Brown, D. S.; Jaycock, M. J. The Thermal Decomposition of Ammonium Diuranate. *J. inorg. nucl. Chem.* **1974**, *36* (stage 1), 1527–1529.
- <sup>42</sup> Huang, C. T.; Kuo, M. S.; Tyen, J. G.; Shieh, M. C. US5139709A - Process for Converting Uranyl Compounds to UO<sub>2</sub> via ADU.
- <sup>43</sup> Chang, M. B.; Wu, S. Experimental Study on Ozone Synthesis via Dielectric Barrier Discharges, *Ozone Science and Engineering*. *19* (1997) 241-254.
- <sup>44</sup> Ozone Solutions. OZV-8 : Ozone from Dry Air or Oxygen <https://ozonesolutions.com/ozv-8/> (accessed Apr 14, 2021).
- <sup>45</sup> Yuan, D.; Xie, S.; Ding, C.; Lin, F.; He, Y.; Wang, Z.; Cen, K. The Benefits of Small Quantities of Nitrogen in the Oxygen Feed to Ozone Generators, *Ozone Science and Engineering*. *40* (2018) 313-320.
- <sup>46</sup> Sehested, K.; Corflitz, H.; Holcman, J.; Fischer, C. H.; Hart, E. J. The Primary Reaction in the Decomposition of Ozone in Acidic Aqueous Solutions. *Environ. Sci. Technol.* *25* (1991) 1589-1596.
- <sup>47</sup> Ershov, B. J. Characteristics of ozone as an oxidant for actinides in alkaline solutions and the mechanism of possible reactions. *Journal of Radioanalytical and Nuclear Chemistry* *317* (2018) 1059–1064.
- <sup>48</sup> Billard, I.; Gaillard, C.; Hennig, C. Dissolution of UO<sub>2</sub>, UO<sub>3</sub> and of Some Lanthanide Oxides in BumimTf2N: Effect of Acid and Water and Formation of UO<sub>2</sub>(NO<sub>3</sub>)<sub>3</sub>-. *Dalt. Trans.* **2007**, *2* (37), 4214–4221.
- <sup>49</sup> Gayer, K. H.; Leider, H. The Solubility of Uranium Trioxide, UO<sub>3</sub>-H<sub>2</sub>O, in Solutions of Sodium Hydroxide and Perchloric Acid at 25°. *J. Am. Chem. Soc.* **1955**, *77* (6), 1448–1450.
- <sup>50</sup> Skoog, D. A.; Holler, F. J.; Crouch, S. R. *Principles of Instrumental Analysis*; 2007.  
[https://doi.org/10.1016/s0003-2670\(00\)84936-3](https://doi.org/10.1016/s0003-2670(00)84936-3).
- <sup>51</sup> Agilent. *Unrivaled. Precise. Consistent. Agilent Cary 4000/5000/6000i Series UV-VIS-NIR Spectrophotometers*.
- <sup>52</sup> Knoll, G. F. *Radiation Detection and Measurement*; John Wiley & Sons, Ltd, 2010.
- <sup>53</sup> Bard, A. J.; Faulkner, L. R. *Electrochemical Methods: Fundamentals and Applications*; John Wiley & Sons, Ltd, 2001.
- <sup>54</sup> Saheb, A.; Janata, J.; Josowicz, M. Reference Electrode for Ionic Liquids. *Electroanalysis* **2006**, *18* (4), 405–409.
- <sup>55</sup> Saheb, A.; Janata, J.; Josowicz, M. Reference Electrode for Ionic Liquids, *Electroanalysis* *18* (2006) 405-409.
- <sup>56</sup> Bard, A. J.; Parsons, R.; Jordan, J. *Standard Potentials in Aqueous Solution*; IUPAC, 1985.
- <sup>57</sup> Zhang, Q.; Wang, Q.; Zhang, S.; Xingmeil, J.; Zhang, X. Electrodeposition in Ionic Liquids. *Chem Phys Chem* **2016**, *17*, 335–351.
- <sup>58</sup> Starks, J. B. *The PUREX Process*; E. I. du Pont de Nemours & Company, 1977.
- <sup>59</sup> Paiva, A. P.; Malik, P. *Recent Advances on the Chemistry of Solvent Extraction Applied to the Reprocessing of Spent Nuclear Fuels and Radioactive Wastes*; 2004; Vol. 261.
- <sup>60</sup> Oak Ridge National Laboratory. Molten Salt Chemistry Workshop; 2017.
- <sup>61</sup> Gupta, N. K. Ionic Liquids for TRansUranic Extraction (TRUEX)—Recent Developments in Nuclear Waste Management: A Review. *Journal of Molecular Liquids*. Elsevier B.V. November 1, 2018, pp 72–91.

- <sup>62</sup> Smetana, V.; Kelley, S. P.; Titi, H. M.; Hou, X.; Tang, S. F.; Mudring, A. V.; Rogers, R. D. Synthesis of Anhydrous Acetates for the Components of Nuclear Fuel Recycling in Dialkylimidazolium Acetate Ionic Liquids. *Inorg. Chem.* **2020**, *59* (1), 818–828.
- <sup>63</sup> Asanuma, N.; Harada, M.; Yasuike, Y.; Nogami, M.; Suzuki, K.; Ikeda, Y. Electrochemical Properties of Uranyl Ion in Ionic Liquids as Media for Pyrochemical Reprocessing. *J. Nucl. Sci. Technol.* **2007**, *44* (3), 368–372.
- <sup>64</sup> Ansari, S. A.; Mohapatra, P. K.; Chen, L.; Yuan, L.; Feng, W. Complexation of Actinides with Phosphine Oxide Functionalized Pillar[5]Arenes: Extraction and Spectroscopic Studies. *Eur. J. Inorg. Chem.* **2018**, *2018* (36), 4022–4030.
- <sup>65</sup> Giridhar, P.; Venkatesan, K. A.; Subramaniam, S.; Srinivasan, T. G.; Vasudeva Rao, P. R. Extraction of Uranium (VI) by 1.1 M Tri-n-Butylphosphate/Ionic Liquid and the Feasibility of Recovery by Direct Electrodeposition from Organic Phase. *J. Alloys Compd.* **2008**, *448* (1–2), 104–108.
- <sup>66</sup> Gujar, R. B.; Ansari, S. A.; Goswami, D.; Mohapatra, P. K. Role of TBP on the Extraction of Trivalent F-Cations with CMPO Dissolved in a Room Temperature Ionic Liquid. *Sep. Sci. Technol.* **2019**, *54* (9), 1443–1452.
- <sup>67</sup> Chang, M. B.; Wu, S. Experimental Study on Ozone Synthesis via Dielectric Barrier Discharges, *Ozone Science and Engineering*. 19 (1997) 241-254.
- <sup>68</sup> Yuan, D.; Xie, S.; Ding, C.; Lin, F.; He, Y.; Wang, Z.; Cen, K. The Benefits of Small Quantities of Nitrogen in the Oxygen Feed to Ozone Generators, *Ozone Science and Engineering*. 40 (2018) 313-320.
- <sup>69</sup> Sehested, K.; Corflten, H.; Holcman, J.; Fischer, C. H.; Hart, E. J. The Primary Reaction in the Decomposition of Ozone in Acidic Aqueous Solutions. *Environ. Sel. Technol.* **25** (1991) 1589-1596.
- <sup>70</sup> Ershov, B. J. Characteristics of ozone as an oxidant for actinides in alkaline solutions and the mechanism of possible reactions. *Journal of Radioanalytical and Nuclear Chemistry* **317** (2018) 1059–1064.
- <sup>71</sup> De Souza, A. R.; Mahlmann, C.M.; Muzart, J.L.; Speller, C.V. Influence of nitrogen on the oxygen dissociation in a DC discharge. *J. Phys. D: Appl. Phys.* **26** (1993) 2164-2167.
- <sup>72</sup> Allen, G. C.; Holmes, N. R. A Mechanism for the UO<sub>2</sub> to UO<sub>2</sub>SO<sub>4</sub> Phase Transformation. *J. Nucl. Mater.* **1995**, *223*, 231–237.
- <sup>73</sup> V. V. Syt'ko and D. S. Umreiko. SPECTROSCOPIC STRUCTURE OF (REWEW) PROPERTIES AND URANYL COMPLEX ELECTRONIC COMPOUNDS. *J. Appl. Spectrosc.* **1998**, *65* (6), 818–831.
- <sup>74</sup> Fujino, T.; Grenthe, I.; Droz, J.; Buck, E. C.; Schmitt, T. E. A.; Wolf, S. F. URANIUM \*; 1948.
- <sup>75</sup> Baker, R. J. New Reactivity of the Uranyl (VI) Ion. *Chem. Eur. J.* **2012**, *18* (Vi), 16258–16271.
- <sup>76</sup> Droessler, J. E.; Czerwinski, K. R.; Hatchett, D. W. Electrochemical Measurement of Gold Oxide Reduction and Methods for Acid Neutralization and Minimization of Water in Wet Ionic Liquid. *Electroanalysis* **2014**, *26*, 2631-2638.
- <sup>77</sup> Glazoff, M. V.; Van Rooyen, I. J.; Coryell, B. D.; Parga, C. J. Comparison of Nuclear Fuels for TREAT: UO<sub>2</sub> vs U<sub>3</sub>O<sub>8</sub>; **2016**.
- <sup>78</sup> Starks, J. B. *The PUREX Process*; E. I. du Pont de Nemours & Company, 1977.
- <sup>79</sup> Paiva, A. P.; Malik, P. *Recent Advances on the Chemistry of Solvent Extraction Applied to the Reprocessing of Spent Nuclear Fuels and Radioactive Wastes*; 2004; Vol. 261.

- <sup>80</sup> Oak Ridge National Laboratory. Molten Salt Chemistry Workshop; 2017.
- <sup>81</sup> Gupta, N. K. Ionic Liquids for TRansUranic Extraction (TRUEX)—Recent Developments in Nuclear Waste Management: A Review. *Journal of Molecular Liquids*. Elsevier B.V. **November 1, 2018**, pp 72–91.
- <sup>82</sup> Marc, P.; Magnaldo, A.; Vaudano, A.; Delahaye, T.; Schaer, É. Dissolution of Uranium Dioxide in Nitric Acid Media: What Do We Know? *EPJ Nucl. Sci. Technol.* **2017**, 3, 13.
- <sup>83</sup> Freiderich, J. W.; Wanigasekara, E.; Sun, X. G.; Meisner, R. A.; Meyer, H. M.; Luo, H.; Delmau, L. H.; Dai, S.; Moyer, B. A. Direct Electrodeposition of UO<sub>2</sub> from Uranyl Bis(Trifluoromethanesulfonyl)Imide Dissolved in 1-Ethyl-3-Methylimidazolium Bis(Trifluoromethanesulfonyl)Imide Room Temperature Ionic Liquid System. *Electrochim. Acta* **2014**, 115, 630–638.
- <sup>84</sup> Tan, X. F.; Yuan, L. Y.; Nie, C. M.; Lui, K.; Chai, Z. F.; Shi, W. Q. Electrochemical Behavior of Uranyl in Ionic Liquid 1-Butyl-3-Methylimidazolium Chloride Mixture with Water. *J. Radioanal. Nucl. Chem.* **2014**, 302 (1), 281–288.
- <sup>85</sup> A. R. Beketov; Strekalovskii, V. N.; Vlasov, V. G. THE STUDY OF THE STRUCTURE OF GAMMA URANIUM TRIOXIDE. *Zhurnal Strukt. Khimii* **1965**, 6 (1), 164.
- <sup>86</sup> Gayer, K. H.; Leider, H. The Solubility of Uranium Trioxide, UO<sub>3</sub>-H<sub>2</sub>O, in Solutions of Sodium Hydroxide and Perchloric Acid at 25°. *J. Am. Chem. Soc.* **1955**, 77 (6), 1448–1450.
- <sup>87</sup> Oak Ridge National Laboratory. Molten Salt Chemistry Workshop; 2017.
- <sup>88</sup> Gupta, N. K. Ionic Liquids for TRansUranic Extraction (TRUEX)—Recent Developments in Nuclear Waste Management: A Review. *Journal of Molecular Liquids*. Elsevier B.V. **November 1, 2018**, pp 72–91.
- <sup>89</sup> Starks, J. B. *The PUREX Process*; E. I. du Pont de Nemours & Company, **1977**.
- <sup>90</sup> Paiva, A. P.; Malik, P. *Recent Advances on the Chemistry of Solvent Extraction Applied to the Reprocessing of Spent Nuclear Fuels and Radioactive Wastes*; **2004**; Vol. 261.
- <sup>91</sup> Wanigasekara, E.; Freiderich, J. W.; Sun, X. G.; Meisner, R. A.; Luo, H.; Delmau, L. H.; Dai, S.; Moyer, B. A. Tandem Dissolution of UO<sub>3</sub> in Amide-Based Acidic Ionic Liquid and: In Situ Electrodeposition of UO<sub>2</sub> with Regeneration of the Ionic Liquid: A Closed Cycle. *Dalt. Trans.* **2016**, 45 (25), 10151–10154.
- <sup>92</sup> Billard, I.; Gaillard, C.; Hennig, C. Dissolution of UO<sub>2</sub>, UO<sub>3</sub> and of Some Lanthanide Oxides in BumimTf2N: Effect of Acid and Water and Formation of UO<sub>2</sub>(NO<sub>3</sub>)<sub>3</sub>-. *Dalt. Trans.* **2007**, 2 (37), 4214–4221.

## Curriculum Vitae

Katherine Luebke (Formerly Katherine Thornock)

Department of Radiochemistry  
University of Nevada, Las Vegas  
Email: katluebke18@gmail.com

### Current Education

Ph.D. in Radiochemistry: University of Nevada, Las Vegas; Las Vegas, Nevada; Department of Radiochemistry; Commenced August 2015; Graduated May 2022

*Relevant Coursework:* Nuclear Physics, Radiochemistry, Radiation Detection with Laboratory, Nuclear Forensics

### Previous Education

Bachelor of Science in Chemistry, ACS Professional Emphasis: Boise State University; Boise, Idaho; Department of Chemistry and Biochemistry; Graduated May 2014

*Relevant Coursework:* Advanced Instrumental Analysis, Spectroscopy Identification, Physical Chemistry with Laboratory, Inorganic Chemistry

### Research and Instrument Experience

University of Nevada, Las Vegas, 2015-Present

#### *Graduate Assistant*

Assisted and led on projects of electrochemical deposition of uranium in ionic liquid. Current work is in dissolution and electrochemical deposition of  $UF_6$  and  $U_3O_8$  in ionic liquid. Taught gas chromatography, mass spectrometry, UV-VIS spectroscopy, and AA spectroscopy for undergraduate analytical and chemistry courses. Additional experience in ICP, liquid scintillation, and cyclic voltammetry.

Los Alamos National Laboratory, Los Alamos, New Mexico, 2019

#### *Graduate Student Intern*

Created and measured calibration standards for gamma detection.

Los Alamos National Laboratory, Los Alamos, New Mexico, 2017

#### *Graduate Student Intern*

Assisted research team with measurement of low energy x-rays and calibration of a silicon drift detector.

Boise State University, 2010-2014

#### *Undergraduate Researcher*



Led on electrical field separation of proteins in non-polar solutions. Developed and wrote the standard operating procedure for RAMAN spectrometer. Additional experience in NMR and IR.

#### Presentations

Luebke, K. (October 2018) *Speciation and Recovery of Uranium from Ionic Liquids for Nuclear Forensics*. Nuclear Science and Security Consortium Workshop: Livermore, California.

Thornock, K. (June 2018) *Electrochemical Recovery of Uranium from UF<sub>6</sub> in Ionic Liquids*. UPR 2018: Ann Arbor, Michigan.

Thornock, K. (April 2018) *Application of Silicon Drift Detector to Nuclear Forensics*. Poster presentation, MARC XI: Kona, Hawaii.

Thornock, K. (November 2017) *Electrochemical Separation of Uranium from UF<sub>6</sub> in Ionic Liquids*. Oral presentation, Hunter College Symposium on Radiometals: New York, New York.

Thornock, K. (September 2017) *Application of Silicon Drift Detector to Nuclear Forensics*. Oral presentation, Nuclear Science and Security Consortium Workshop: Berkeley, California.

Thornock, K. (June 2017) *Electrochemical Separation of Uranium from UF<sub>6</sub> in Ionic Liquids*. Oral presentation, University Program Review: Walnut Creek, California.

Thornock, K. (June 2016) *Electrochemical Recovery of Actinides in Ionic Liquid*. Poster Presentation given at the UITI 2016 Program and Technical Review Meeting, Raleigh, North Carolina.

Thornock, K. (March 2016) *Proposed Research: Electrochemical Recovery of Actinides in Ionic Liquid*. Poster Presentation given at the ANS Student Conference 2016, Madison, Wisconsin.

#### Honors and Awards

3<sup>rd</sup> Place Winner, Rebel Grad Slam 3 Minute Thesis competition, 2021

Best Poster Award, University Program Review, University of Michigan, 2018

Certificate of Completion, "School of Nukes," Los Alamos National Laboratory, 2017.

Honors Scholar, Boise State University Honors College, 2014.

Student Research Initiative Fellowship, Boise State University, 2013.

## Affiliations

American Nuclear Society (ANS)

## Teaching Experience

Quantitative Analysis, Fall 2020, University of Nevada, Las Vegas, Department of Chemistry, Las Vegas, Nevada

Quantitative Analysis, Fall 2018, University of Nevada, Las Vegas, Department of Chemistry, Las Vegas, Nevada

Instrumental Analysis, Spring 2018, University of Nevada, Las Vegas, Department of Chemistry, Las Vegas, Nevada

Quantitative Analysis, Fall 2016, University of Nevada, Las Vegas, Department of Chemistry, Las Vegas, Nevada

Instrumental Analysis, Spring 2016, University of Nevada, Las Vegas, Department of Chemistry, Las Vegas, Nevada

Quantitative Analysis, Fall 2015, University of Nevada, Las Vegas, Department of Chemistry, Las Vegas, Nevada

First Year Seminar, Fall 2013, Boise State University, Honors College, Boise, Idaho